UNIVERSITY OF HULL

SCHOOL OF BIOLOGICAL AND MARINE SCIENCE

The biological and physical controls on phytoplankton blooms off the north-east coast of the UK

By

Dan Hill

BSc Marine Biology

May 2024

A thesis submitted in fulfillment of the requirements for the degree of

MSc (by Research) Biological Science

Supervisor: Professor Rodney Forster

Contents

Acknowledgments:

Thank you for reading this thesis. I have a lot of people to thank who have enabled me to complete this research. First and foremost, I am deeply grateful to my supervisor, Professor Rodney Forster for his invaluable advice, encouragement and continuous support during my masters research. I also extend my sincere thanks and gratitude to Eleanor Adamson and The Fishmongers' company for funding the research and my tuition fees.

Special thanks also go out to:

Joe Redfern and the Whitby lobster fishing community for their continued support with the collection of weekly/bi weekly water samples.

Nick Meaton, Environment Agency and the RV Humber Guardian crew for providing the opportunity to board their vessel for data collection, and for also collecting water samples on my behalf.

CEFAS for the opportunity to join them on the Spring Nephrops survey which unfortunately I had to withdraw from due to COVID just before departure. However, they were kind enough to undertake water sampling on my behalf which provided me with a great dataset of offshore water samples.

NERC-FSF loan equipment pool and Robbie Ramsey for the loan of the multispectral radiometer and the training/setup guidance for the use of the instrument.

Dr Julie Hope for supplying water sampling and filtration equipment.

Linda McGillivary for proofreading this thesis.

Abstract:

The North Sea is a highly productive temperate coastal shelf sea which contains important fisheries that provides protein to the global market. This study investigated the biological and physical controls on the different spring bloom events in North East coastal waters of the UK in 2022. The study area is situated off the north-east coast of the UK where three distinct hydrodynamic zones were observed. The zones were derived from utilising bathymetry and mixed layer depths, where an inshore / offshore stratified and a permanently mixed zone were outlined. This study uses a range of data collected *in situ*, remotely sensed data and modelling to assess the physical and biological controls (phytoplankton growth and grazing rates) on varying phytoplankton bloom phenology and primary production in differing hydrodynamic regions along the north-east coast in 2022. Observations showed a north-south gradient whereby increased phytoplankton biomass (blooming) was initiated earliest in stratified waters in the northern latitudes, with delayed blooming in the permanently mixed southern latitudes of the study area. The key drivers in determining temporal and spatial distribution of blooming events were dictated by the onset of stratification and varying light attenuation. Stratification was modelled and estimated to be greatest in the inshore / offshore stratified regions, with significant stratification occurring for approximately 169 days commencing in early spring. This correlated to significant phytoplankton blooms at the initial stages of stratification formation in late March, where high concentration of nutrients and reduced light attenuation, helped facilitate phytoplankton growth. Prolonged stratification within these zones enabled blooming in late Autumn. The permanently mixed region experienced delayed phytoplankton growth, with the initiation of the bloom phase beginning in early June. Blooms correlated to neap-spring tidal cycles where stratification formation occurred on the neap phase of the tidal cycle. The neap phase resulted in lower current speeds, facilitating short periods of stratification formation and potentially aiding in the reduction of light attenuation, enhancing phytoplankton growth in summer and autumn.

List of figures

List of tables

Abbreviations

Abbreviation	Definition
CDOM	Coloured dissolved organic matter
CHL	Chlorophyll
CHL-a	Chlorophyll a
CTD	Conductivity, temperature and depth instrument
DO	Dissolved oxygen
EA	Environment agency
FNU	Formazin Nephelometric Unit
GPP	Gross primary production
IS	Inshore partially stratified zone
kd	Light attenuation
MLD	Mixed layer depth
NAP	Non algal-particles
NPP	Net primary production
OCR	Seabird OCR-507 Multispectral Ocean Colour Radiometer
OS	Offshore stratified zone
PAR	Photosynthetically active radiation
PM	Permanently mixed zone
R	Reflectance ratio
RFU	Relative fluorescence unit
S2P3	Shelf Sea Physics and Primary Production
SCM	Subsurface chlorophyll maximum
SPM	Suspended particulate matter
SST	Sea surface temperature

Section 1- Introduction

Temperate shelf seas are perceived to be highly productive ecosystems that account for 10-15% of total ocean productivity (Muller-Karger et al., 2005). This is due to their characteristics of nutrient-rich waters with multiple sources of organic carbon (Sharples et al., 2019; Alvera-Azcárate et al., 2021). Ocean productivity is characterised by the rapid production of organic compounds by phytoplankton (Cloern, 1996), which are single celled algae suspended in the water column. Phytoplankton are photoautotrophic microorganisms that receive energy and nutrients by utilising sunlight to convert inorganic compounds into organic substances (Sigman and Hain, 2012). There are many different groups of phytoplankton, but the two key phytoplankton groups that dominate the North Sea are dinoflagellates and diatoms (Johns & Reid, 2001). According to Sigman and Hain (2012), variations in light intensity, temperature, stratification, availability of inorganic compounds, grazing pressure, and the presence of essential nutrients such as nitrogen, phosphorus, and silicon can drive variations in the growth of phytoplankton and primary production (Xu et al., 2020). This study aims to investigate the physical and biological controls on phytoplankton blooms in the North East coast of the United Kingdom, resulting in a greater understanding of the coastal water processes in this greatly understudied region.

Phytoplankton blooms in aquatic systems are characterised by a rapid increase in algal biomass (Cloern, 1996) resulting from the onset of stratification and increasing light after the winter solstice (Dimitry et al., 2012). Increased algal biomass during blooming periods results in gross primary production exceeding phytoplankton losses from grazing, sinking and respiration within spring blooming periods resulting in a positive net primary production (Opdal et al., 2019). The duration and intensity of blooming events are dictated by nutrient availability which can be altered by vertical mixing of the water column through upwellings, tides, waves and storm conditions (Sharples et al., 2006). These conditions enable the convergence of nutrient-rich water from the seabed and surface waters. This process replenishes the nutrient-depleted surface water after blooming events, as well as the water column in autumn and through the winter. The process thereby fuels primary production and phytoplankton growth (Nicholson et al., 2016). The spring bloom in a shelf sea region has the potential – often within as little as a 1- to 2-week period – to contribute as much as one-third of the total annual primary production (Townsend et al., 1994). Gaining insight into the factors that contribute to the inter-annual variability in the timing and magnitude of spring blooms is a key concept for understanding ecosystem variability and dynamics on a broader scale (Sharples et al., 2006). Spring blooms are substantial suppliers of organic matter to all levels of the marine food web, providing an important organic fuel for pelagic and benthic communities (Xu et al., 2020). The timing of blooming

events is thought to have significant impact on the energy transfer to higher trophic levels within the marine food web, for example bloom timing can affect the success of copepods which subsequently, alongside phytoplankton, form the diets of larval fish (Sharples et al., 2006; Capuzzo et al., 2017; Di Pane et al., 2023; Semmouri et al., 2023; Tilstone et al., 2023). Lack of suitable prey greatly reduces the survival rate of juvenile fish, making bloom timing a pivotal role in ecosystem dynamics (Marshak & Link, 2021). This concept of synchronisation and misalignment between the timing of bloom events and larval development can be interpreted as the 'match-mismatch' hypothesis (Cushing, 1990).

The distribution of phytoplankton groups varies based on conditions that best suit their adaptability and characteristics. The two main phyla of phytoplankton present in the North Sea, namely diatoms and dinoflagellates (Johns & Reid, 2001), have very different conditions which they thrive under. Diatoms require silicon to grow and often occur in nutrient-rich, turbid coastal waters because of their rapid growth rates and tolerance to low irradiance (Pan et al., 2016). They occur in turbulent regions because of their very limited ability to control their buoyancy, resulting in the phytoplankton being circulated via currents and mixing into the high irradiance surface waters. In contrast, dinoflagellates are less sensitive to nutrients due in part to their ability to consume other algae (e.g. mixotrophy; Litchman, 2007). This results in these species becoming dominant in more oligotrophic waters (Litchman & Klausmeier, 2008). Some genera of dinoflagellates, in particular certain *Gymnodiniaceae* can produce various harmful toxins which can result in a multitude of seafood poising syndromes (Wang, 2008). If these species of phytoplankton bloom (causing Harmful Algal Blooms), it can have drastic consequences to crab, lobster and shellfish fisheries stocks within the surrounding vicinity (Karlson et al., 2021) with devastating social-economic consequences. Understanding the causes of phytoplankton blooming events for the North East coast of the UK is important to help mitigate or predict potential Harmful Algal Blooms (HABs) in the future. The underlying physical, chemical and biological processes which are thought to structure shallow shelf seas, and control phytoplankton blooms, are described below.

Stratification:

Stratification refers to the layering of water masses with different properties which restrict vertical mixing of the water column. Water can become stratified through differences in temperature, salinity and density (Sharples et al., 2006). The most recognised type of stratification in temperate shelf seas, beyond the reach of freshwater sources, is thermal stratification. This is regulated by the interplay between two forces: the stratifying impact of solar irradiance at the surface, and the countervailing mixing effects driven by tidal currents, surface wind stress, and convective overturning (Sharples et al., 2006). In strong tidally mixed areas, the onset of stratification can be delayed whilst solar irradiance increases to levels where heat supply can outweigh the mixing of the water column (Zhao et al., 2019).

It is thought that, within these high tidal mixing areas, meteorological forcing can be the driver of inducing stratification. This is caused by the additional mixing forces on the water column, alongside the persistent tidal 'background' mixing (Sharples et al., 2006; Zhao et al., 2019).

Colder waters are believed to have higher productivity when compared to temperate and tropical regions due to reduced formations of thermoclines and pycnoclines (Shimoto and Matsumura, 1992), which results in reduced density and temperature gradients, enabling greater vertical mixing of nutrients from deeper depths to the sea surface (Shimoto and Matsumura, 1992). Ocean currents and storm conditions promote water column mixing, which subsequently causes the breakdown of stratification and the recycling of nutrients from depth, allowing secondary blooms in late summer to form when sea surface temperature and light irradiance is greatest (Nicholson et al., 2016). Phytoplankton growth in temperate seas frequently relies on water column stability which stems from the onset of spring stratification, providing a well-lit, highly productive surface water layer in which phytoplankton are constrained (Opdal et al., 2019).

Nutrients:

The Redfield ratio is a concept used to describe the ratio of carbon, nitrogen and phosphorous in phytoplankton biomass. The biomass is built with a C:N:P stoichiometric ratio of 106:16:1 which is an important concept in understanding biogeochemical cycles in the ocean (Redfield, 1958). Alterations in this ratio can determine changes in phytoplankton compositions (Xu et al., 2020). The Redfield ratio concept has been extended to include silicon, given its significance on diatom growth, which is especially key for the North Sea (Sharp, 2001). The revised ratio for balanced diatom growth including silicon is 106:16:1:16 (C:N:P:Si) because the average Si/N ratio for small and large diatoms closely resembling a 1:1 ratio (Sharp, 2001). The ratio of dissolved nitrogen and phosphorus is 16:1 throughout the water column and it is thought that phytoplankton impose this ratio on the deep ocean, owing to the similarity to the ratio of phytoplankton biomass (Sigman and Hain,2012).

Nitrogen, which is commonly found in the form of nitrate (NO_3^-) is converted into an essential component for amino acid formation and subsequently protein synthesis (Malone et al., 2016). Nitrate availability post-bloom can be a limiting factor in phytoplankton growth in coastal waters (Malone et al., 2016). If nitrate is limiting in the environment, nitrite (NO_2^-) will be used as a source of nitrogen to synthesize cellular components, however in high quantities this can be toxic and harmful to phytoplankton and aquatic organisms (Pozzobon et al., 2021). Ammonia can also be a source of nitrogen for some species of phytoplankton in areas where ammonia is the dominating nutrient (Fouilland et al., 2007). It primarily undergoes nitrification which converts ammonia into a commonly used nitrogen form of NO_2^- or NO_3^- (Brockmann et al., 1990). Ammonia is produced by the breakdown of organic matter and by excretion of nitrogenous waste from marine organisms (Domingues et al.,

2011). Ammonia levels increase post bloom, after large quantities of phytoplankton decompose. Phosphorus found in the form of phosphate (PO_3^{2-}), is a mineral that is essential for DNA and RNA replication, energy transfers and photosynthesis (Filippelli, 2008). It is a vital component in the formation of adenosine triphosphate (ATP) and chlorophyll (Wang et al., 2011). The availability of phosphate can greatly influence phytoplankton dynamics as the mineral is depleted during and after blooming events (Moll, 1998). It is present in the marine environment through geological and geochemical processes, alongside anthropogenic nutrient enrichment (Filippelli, 2008). Phosphorus supply in the North Sea is declining (van Beusekom et al., 2019) thanks to improvements in detergent and fertiliser removal from waste water treatment (Filippelli, 2008). Silicon is an essential component for diatom growth and is found in plentiful supply in the Earth's crust. It is fundamental in the production of cell walls and hard parts, alongside being used as a proxy for phytoplankton composition due to only being required by diatom species (Brown et al., 2003; Oehler et al., 2015). The abundance of silica is reduced after a spring bloom comprising large quantities of diatoms (Desmit et al., 2019). Finally, iron is found in trace amounts within phytoplankton biomass, but is used in the production of chlorophyll and enzymes (Martin and Fitzwater, 1988).

Anthropogenic nitrogen and phosphorus input from surface run off and riverine discharge enrich coastal waters which subsequently impacts phytoplankton dynamics and composition (Rabalais et al., 2009). An unbalanced de-eutrophication has occurred since the 1980s, resulting in the N:P Redfield ratio being greatly exceeded. The ratio has become significantly more unbalanced by reason of riverine inputs having increased nitrogen load relative to phosphate (Garnier et al., 2010; Grizzetti et al., 2011). This can cause potentially drastic changes in nearshore coastal phytoplankton communities and productivity (Brauer et al., 2012), with potential consequences for the entire food web which could disrupt ecosystem dynamics (Philippart et al., 2007). Nutrient depletion can be a key factor in the termination of blooming events, suggesting that nutrients can be a key driver in the variation of phytoplankton biomass.

Light:

At any specified wavelength at any given time, light approximately diminishes exponentially with depth, which is dictated by the optical properties of the water column (Wang et al., 2010). An essential optical characteristic of seawater is the spectral absorption coefficient ($a(\lambda)$, m^{-1}). This coefficient is commonly classified into four distinct components, as described by Kirk in 2000. The four components are as follows: $a(\lambda) = a_W(\lambda) + a_{ph}(\lambda) + a_{NAP}(\lambda) + a_{CDOM}(\lambda)$ with '$a(\lambda)$' being total absorption and the remaining components account for the spectral absorption coefficients of pure seawater(W), phytoplankton (ph), non-algal particles (NAP) and colour dissolved organic matter (CDOM). (Wang et al., 2010). The quantities of the 3 constituents other than pure seawater(W) – sea water that is absent

from dissolved or suspended particulate material - are variable, resulting in the spectral absorption coefficient of seawater being highly variable on temporal and spatial time scales (Babin, 2003; Wei et al., 2023). In addition to variable absorption coefficients, there are also fluctuations in backscattering coefficients caused by differing concentrations of light-scattering material (chiefly, suspended sediments). Together, absorption and scattering interact to determine the remote sensing reflectance spectra recorded from satellites (Cannizzaro & Carder, 2006). Overall increased light attenuation can impact productivity of the water column by hindering available photosynthetically active radiation (PAR) to photosynthesising algal cells (Opdal et al., 2019).

In the presence of phytoplankton blooms, light absorption can rapidly increase as algal cell density increases (Barocio-León et al., 2008; Wang et al., 2010). The subsequent spectral shift towards particular wavelengths (preferential absorption of blue part of the spectrum for chlorophyll-a) that are not absorbed by the algal cells, allows chlorophyll concentrations to be estimated from satellite. Satellite observations help to track blooming events in size and magnitude, when *in situ* measurements are not available (Wang et al., 2010). Phytoplankton comprise of photosynthetic pigments that absorb wavelengths of light and transfer the energy to the photosystems. North Sea Phytoplankton communities mainly comprise chlorophyll-a as their majority photosynthetic pigment. Chlorophyll-a tends to absorb wavelengths of light within the blue and red ends of the spectrum (Kirk, 2000; Roy et al., 2011). Depending on phytoplankton density, a self-shading effect can occur (Zhao et al., 2019), causing a upper limit to the maximum output of primary production in the case of very high biomass. Within coastal regions and estuaries, the spectral absorption coefficients of the constituents colour dissolved organic matter (CDOM) and non-algal particles (NAP) have significantly greater weighting in terms of overall spectral absorption coefficient of seawater (Babin, 2003; Wang et al., 2010). With elevated suspended particulate matter (SPM) and increased CDOM from riverine run offs of humic matter, absorption coefficients for these ‘case 2 water’ regions can drastically increase (Kirk, 2000; Kowalczuk et al., 2010).Case 2 waters are regions that are situated in coastal and inland areas and have water properties that contain CDOM and NAP (Matsushita et al., 2012). CDOM tends to impart a yellow-brown colour to the water which follows trends in decreasing CDOM with distance from the land and away from inland discharge (Kirk, 2000; Kowalczuk et al., 2010). CDOM can have major consequences in absorption within the blue end of the spectrum. Whilst SPM absorption is low, scattering by SPM is high, and this increases the pathlength for absorption. Within productive offshore regions away from riverine run offs, phytoplankton detritus can make up a large composition of SPM. In coastal and estuarine areas, SPM is comprised of a large proportion of sediments and humic materials (Kirk, 2000). There are also significant trends of elevated NAP around areas of river discharge or highly mixed regions where the resuspension of settled sediment particles is common (Cloern,

1987; Pan et al., 2016). Pure seawater has the most significant light absorption, increasing from 550 nm onwards and peaking within the red wavelength bands (Kirk, 2000) . Estimations of light attenuation serve as valuable indicators of the overall ecosystem health, vigour, and consequently, its ecosystem functional capacity (Tett et al. 2007).

Temperature and light play key roles in regulating physiological processes affecting enzyme activity, which has a significant effect on nutrient uptake by phytoplankton (Chen et al., 2015), resulting in overall consequences to bloom duration, magnitude and maximum photosynthetic efficiency. If the mixed layer depth is deeper than the 1% euphotic depth, dispersion and dilution of phytoplankton biomass can reduce the cellular exposure to available PAR, thereby limiting photosynthetic potential and decreasing overall productivity (Opdal et al., 2019).

Phytoplankton bloom modelling:

Phytoplankton bloom modelling is used as a tool to understand the complex dynamics of blooming events and their response to fluctuations in environmental parameters. Models use mathematical frameworks to simulate the growth, distribution, and behaviour of phytoplankton communities within a range of oceanographic settings (open oceans to coastal shelf seas for example). These models integrate a variety of variables, including nutrient availability, light attenuation, temperature, currents and tides, as well as biological parameters such a predator prey interactions to simulate the spatiotemporal dynamics of bloom formations. By encompassing biological and physical mechanisms inherent in phytoplankton ecology, including photosynthesis, nutrient, and trophic interactions, these models offer provide insights into the drivers governing bloom dynamics and their ecological repercussions. Through phytoplankton bloom modelling outputs, the underlying mechanisms governing these events can be used to access the wider implications on the marine ecosystems.

S2P3 O2 Model

A coastal shelf seas model developed by Sharples (2012), is a 1- dimensional model that was used in this thesis to simulate phytoplankton blooming events on a one year time scale. This model predicts the phytoplankton biomass distribution throughout the water column on a vertical plane. It also calculates primary production on varying time scales which range from hourly to yearly. Temporal and spatial patterns in nutrient and dissolved oxygen concentrations from the direct relationship with blooming events can also be simulated. The model requires various data sources which included hourly meteorological observations. Time (days), wind velocity x-component (m s-1), wind velocity y-component (m s-1), air temperature (°C), air pressure (mbar), relative humidity (%), radiation (W m-2), cloud cover (%), were necessary (Appendix 5), alongside parameter adjustments for water column mixing, tidal constituents, friction, turbulence and vertical attenuation coefficient for

Photosynthetically Active Radiation PAR (m-1), (Appendix 2 & 3). Dissolved inorganic nitrogen, temperature, and heat distribution were also considered in determining the primary production outputs from the model

The North Sea:

With its semi-enclosed temperate shelf sea environment, the North Sea is a highly productive region (Skogen and Moll, 2000). The interplay of bathymetry, tidal mixing and prominent seasonal winds creates a dynamic setting that decisively shapes the regional patterns and seasonal trends observed in primary production (Fouilland et al., 2007). The North Sea can be divided into two primary zones: the southern North Sea which is shallow and characterised by highly mixed water column conditions, and the northern North Sea which is deeper, and seasonally stratified with evidence of subsurface chlorophyll maximums in summer (Charnock et al., 2012; Sharples et al., 2006). In the southern North Sea, tidal forces and wind action play a dominant role in mixing of the water column, making this area vertically homogeneous throughout the year (Charnock et al., 2012). There are also increased industrial and agricultural activities in this area, thereby fuelling more intense blooms (Desmit et al., 2019; Alvera-Azcárate et al., 2021). The deeper waters of the northern North Sea remain mixed during winter attributable to wind influence, but transition to stratified waters in spring and summer because of intensified solar heating and reduced wind mixing. The productivity of the water column in the northern region is influenced by the stratification that occurs during summer (Sharples et al., 2006). A study by Capuzzo et al., 2017 observed a significant decline in primary production for the North Sea in recent decades as a consequence of sea surface warming and reduced riverine nutrient inputs. Reduced nutrient concentration in riverine inputs was thought to be attributed to stricter agricultural policies reducing nitrogen and phosphorus entering the North Sea. In the 1990s, primary production was estimated at approximately 100–150 × $10^{\wedge 12}$ gC/year and has declined to approximately 50-100 × $10^{\wedge 12}$ g C/year since the early 2000s. This resulted in a statistically significant decline($r^2 = 0.673$, $p < .0001$) in average annual abundance in small copepods between 1990 and 2013 (~5000 small copepods per m^{-3} to 2000 m^{-3} respectively; Capuzzo et al., 2017).

Within the central and southern parts of the North Sea, there has been a deterioration of water clarity whereby water has become less clear over the second half of the 20th century. The average Secchi disk depth decreased between 25% to 75% when comparing pre 1950 data to post 1950 Secchi disk depths. This has resulted in changes in energy flux through the marine food web with reduced light penetration to depth (Capuzzo et al., 2015). The main causes purportedly driving a decline in water clarity are increased concentrations of suspended sediment through changes in sea-bed community, weather patterns, decreased estuarine sediment sinks and increased erosion of coastlines (Capuzzo et al., 2015). With predicted increases in severe weather events through climate change (Groß et al.,

2022), the likelihood of increased sedimentation is set to continue, providing future consequences in water clarity which could have detrimental impacts on phytoplankton biomass and fishery production. The North-east coastal region drains large areas of agricultural lands, resulting in nutrient enrichment and increases in dissolved organic matter to the rivers and estuaries (Burson et al., 2016). This pressure has seen coastal areas experience 'coastal darkening' which can further result in an increase in light attenuation and a reduction in water clarity for this region (Dupont and Aksnes, 2013).

Over the past few decades, there has been a notable rise in average sea surface temperature (SST) in the North Sea (Kirby et al., 2008), with a recorded increase of approximately 1.6°C from 1988 to 2014 (Desmit et al., 2019). An Increase in number of warmer days in summer and a decrease in extremely cold days in winter, are responsible for the decadal increases in sea surface temperatures within the North Sea. Two long term SST datasets from Helgoland off the German Bight (Offshore, open water) and Sylt –situated in shallow coastal waters in the Wadden Sea – show almost identical trends despite the two sites being hydrographically different. Both sites observed SST trends of a ~ 0.3°C / decade increase in temperatures. These increasing temperatures have heavily impacted on the stratification regime, alongside disrupting the physiology of phytoplankton through enhanced phytoplankton cell division (Desmit et al., 2019). However, productivity can decrease when the temperature exceeds the photosynthetic optimum due to elevation of cell respiration (Desmit et al., 2019).

Research gaps and importance:

There has been no research to my knowledge on the timing of spring blooms and the controls thereof within the North-east coastal region of the North Sea, which makes this project crucial in understanding the overall productivity in this area. It is an important area for small scale, inshore fisheries, with particular focus on lobster and crab catches. The Humber region alone employs the greatest number of workers throughout British fisheries with approximately 5,546 full time equivalent roles in the sector (Uberoi et al., 2022). Additionally, there was a mass crustacean die-off event that occurred in 2021, with no solid evidence on the potential causes. A suggested cause of the die-off event was harmful algal blooms (*Sealife mortality off the North East Coast - Committees - UK parliament,* 2022; DEFRA, 2023) which are known to have had drastic consequences to ecosystem health. This study therefore aims to help understand the broader context of phytoplankton dynamics in this area, which could help with determining the possible cause to mass crustacean die-offs. A study from Edwards et al., (2006) suggested the North Sea could be an area where HABs may be increasing, but further evidence is required in order to establish if this is the case. .

In addition, there are no primary production estimates along the North East coast. Primary production estimates would be a crucial value which could be used to understand whether productivity is high enough to support the North-east fisheries as well as the abundant marine wildlife such as seabirds,

seals and cetaceans. Understanding the nature of change at the base of the marine food web is critical in understanding the effects of climate change for the small scale, inshore lobster and crab fisheries on the North-east coast of the UK (Spence et al., 2022). As we see global temperatures increase, alongside more extreme weather events and patterns which could disrupt nutrient cycling from depth and the formation of stratification, there will be consequences for phytoplankton dynamics and productivity (Opdal et al., 2019). It has been observed that spring phenology within oceans around the world have advanced under climate change conditions as a result of alterations in hydrographic properties in recent years (Lindemann & St. John, 2014). This could have further consequences on primary production outputs, specifically within this study area of the North Sea, whereby increasing sea surface temperatures could heavily alter blooming events in this region.

Many endeavours have been made to quantify primary production for the entire North Sea alongside regionalised efforts for northern and southern North Sea estimations (Skogen et al., 1995; Varela et al., 1995; Moll, 1998; Skogen and Moll, 2000; Van Beusekom and Diel-Christiansen, 2009; van Leeuwen et al., 2012). These studies take into consideration a significantly larger research area than this study, and also have a main focus on offshore primary production. A study from Zhao et al., 2019 investigated the tidal impacts on primary production, with Sharples et al., 2006 studying the timing and effects of stratification on productivity in the north-western region of the North Sea. In addition, a study looking at the effects of water clarity and light on bloom timing (Opdal et al., 2019) alongside multiple papers on the effects of changing nutrients loads (Brockmann et al., 1990; Skogen et al., 2004) have all contributed to building a picture of the overall causes of change in spring bloom timing and magnitude in the North Sea. However, the majority of studies provide approaches at low resolution on a decadal or multiyear time scale. A summary of the keys North Sea studies that relate to the same topic of this thesis are outlined in Table 1. This study provides a holistic approach towards understanding the multi-faceted causes of spring blooms for the North-east coast at a smaller spatial scale, providing a broader overview for productivity in this region.

Table 1 Summary of the Key North sea studies that relate to phytoplankton blooming

Topic	Location	Study
Offshore primary production estimates	North Sea	Skogen et al., 1995 Varela et al., 1995 Moll, 1998 Skogen and Moll, 2000 Van Beusekom and Diel-Christiansen, 2009 van Leeuwen et al., 2012
Tidal impacts on primary production	North Sea	Zhao et al., 2019
Timing and effects of stratification on productivity	North-western North Sea	Sharples et al., 2006
Effects of water clarity and light on bloom timing	North Sea	Opdal et al., 2019
Effects of changing nutrient loads on phytoplankton blooming	North Sea	Brockmann et al., 1990 Skogen et al., 2004

Carbon sequestration in marine sediments, also known as 'blue carbon' is also fundamental to oceanic processes, and can have fundamental impacts on climate change and atmospheric conditions (Lovelock and Duarte, 2019), and is yet to be studied for this research site. Decreasing / increasing productivity through climate change or annual variations can alter carbon sequestration. The findings of this study could help play a pivotal role in understanding the carbon uptake of the region which can then be applied on larger scales.

Aims and objectives:

This study follows on from a previous undergraduate study, which used a 1-dimensional model to estimate primary production on the North-east coast from remotely sensed data. It was identified that there was variability in timing and size of phytoplankton blooming events in this region.

The main aim of this thesis is to determine the variability in phytoplankton blooms on the North-east coast with reference to the physical and biological controls that dictate the variability in blooming events. A variety of *in situ* and remotely sensed data was used to track and analyse blooming events in 2022, alongside the use of 2 different models to help estimate primary production for different hydrodynamic regions within the study site. The objectives of the study are as follows:

1. To use *in situ* and remotely sensed data to track and assess the magnitude of phytoplankton blooming events on the North East coastal waters of the UK in 2022.
2. To incorporate site specific meteorological data and forcing parameters into a 1-dimensional model to try simulate blooming events observed from satellite data.
3. To compare primary production outputs from two different primary production models with each other and to compare the spatial and temporal model trends to in situ data.

Section 2- Materials and Methods:

To estimate marine productivity and phytoplankton biomass (chlorophyll a concentration), as well as understanding the timing and spatial distribution of the blooming events within the North Sea, sampling was undertaken between March 2022 to June 2022. The sampling period between March and June did not allow for a yearly time series of quantification of chlorophyll a for our sample area. To fill gaps within our data, the Environment Agency water quality program undertaken in the same region as our study area (archive available as open data under open government licence here https://environment.data.gov.uk/water-quality/view/landing) was used, and the EA chlorophyll extractions were combined with *our in situ* values to help with filling gaps for missing monthly data for the year of 2022. The EA sampling was undertaken along inshore areas of the North-east coast, with their cruise route going from Grimsby Dock to the River Tees. Both the EA data and our own were quantified in the same units (mg/m^3) and samples were analysed using the acetone extraction method which is outlined in 'Chlorophyll extraction and quantification' section of the methods. Remotely sensed data, alongside the use of CEFAS wavenet and smartbuoys were also used to fill gaps within our oceanographic datasets.

Study area:

Figure 1 depicts the 72 sample sites that were used for the collection of water samples, alongside the Cefas Wavenet buoys and their associated buoy names. The station 13 and J6 labels are the sites that were used for primary production modelling. Figure 2 shows the 11 sites that were used for the deployment of instrumentation on three separate cruises. The three one-day cruises were conducted on the 12th May 2022, 9th June 2022 and the 10th June 2022 . Samples from the Humber Estuary were excluded from the analysis in the subsequent results section because only one set of samples were collected in this region in early March. The site distribution spanned the North East coast of the UK with the southernmost site situated in the Humber Estuary (53° 35.2'N, -0° 4.1'W). The northernmost site was off the Northumbrian coast (55°27.1'N, 0°43.1'W) with the majority of sites being located within 12 nautical miles from the coast. Limited access to suitable charter vessels hindered the capability of reaching more offshore locations. Sea bed depth varied across the whole study site. The deepest site had a depth of 98m, and the shallowest was 2m within the Humber Estuary. The depth values for each site were derived from the GEBCO Bathymetric charts or with vessel depth sounders.

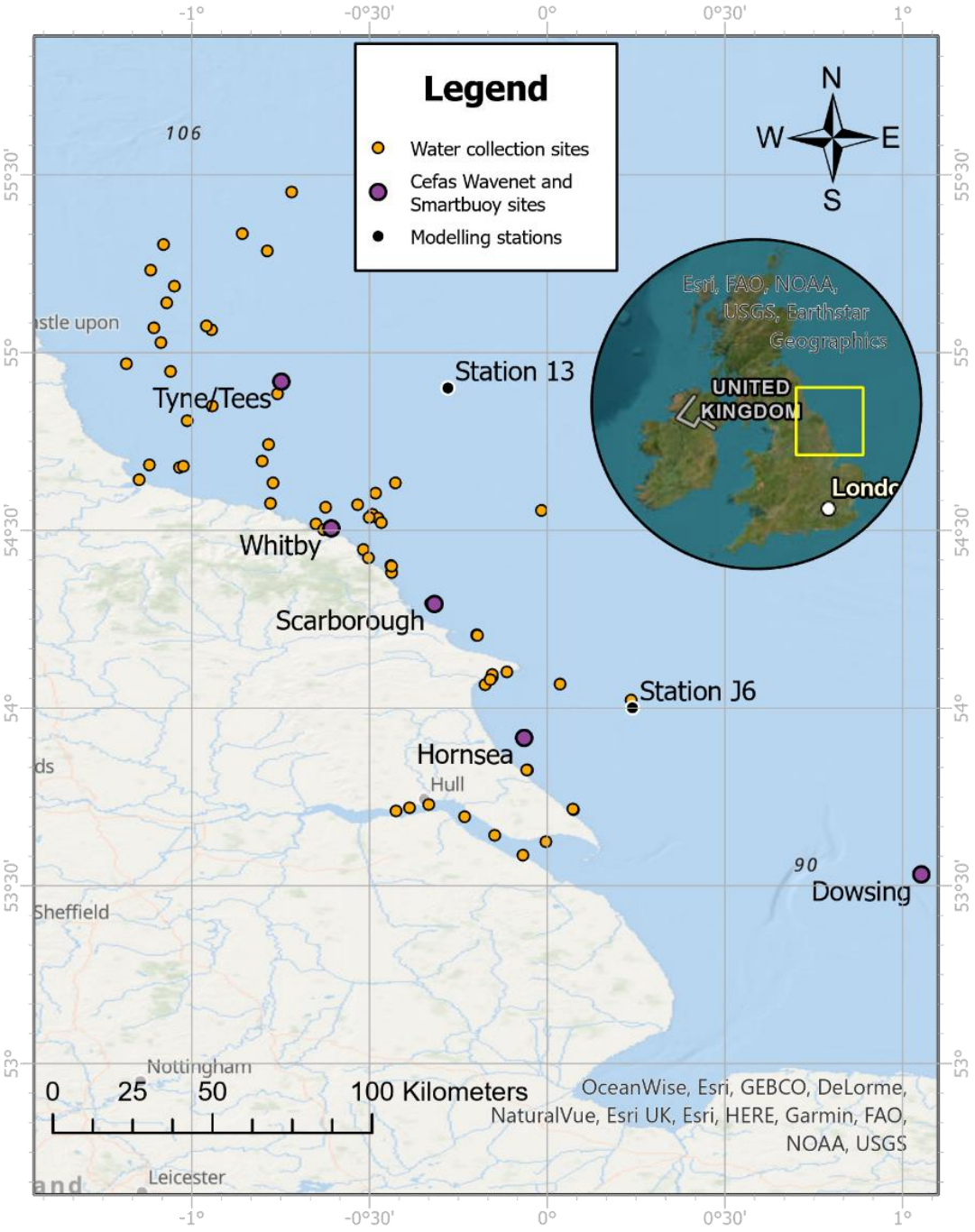

Figure 1. Map of the sample area and locations of sample sites. The Tyne/Tees, Whitby, Scarborough and Hornsea labels are the associated Cefas Smartbuoy names.

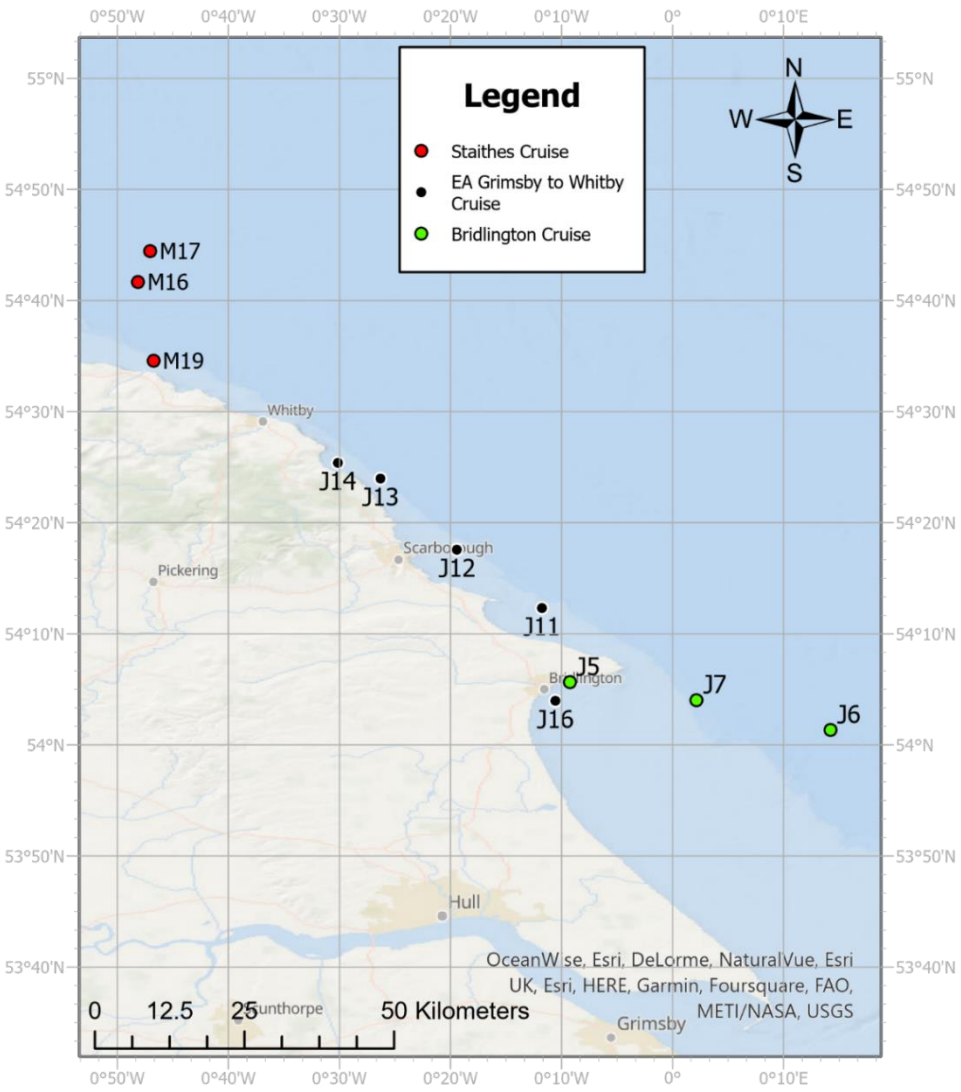

Figure 2. A map of the North East Coast of England displaying the three cruise days and their corresponding sample sites where in situ measurements were taken using CTDs and a multispectral radiometer.

Water sampling

Local fishing vessels and research vessels-of-opportunity were used to aid in sampling within the outlined study site. *Ad hoc* water sampling was completed by the lobster fishing fleet based in Whitby. Clean 25 litre canisters were dropped off to the vessel before departure, with subsequent collection of the sample on their return and transfer back to the laboratory in Hull. Weekly – biweekly water samples at a range of coastal and offshore sample sites around the Whitby vicinity were obtained by this means. Samples were also collected onboard the Environment Agency (EA) research vessel '*RV Humber Guardian*'. Two inshore cruise routes along the coast from Grimsby to Whitby, were used for water collection and deployment of the agency's Conductivity, temperature and depth instrument (CTD) and a multispectral radiometer (Figure 2). One-day boat charters with *RV Huntress* from the Holderness Fishing Industry Group (Bridlington), as well as *All our Sons* from Real Staithes Wildlife

Watching (Staithes), provided an opportunity for further *in situ* measurements. These consisted of water sample collection as well as deployment of instrumentation for water column structure and optical property analysis. Finally, 16 water samples were filtered and collected from the *RV Cefas Endeavour* during a 10-day Spring survey of the decapod *Nephrops* off the north-east coast. This survey was of significant help in providing a greater scope into the chlorophyll dynamics at more offshore locations, which the smaller vessels of opportunity could not reach.

Water sample collection:

Water samples were taken using two different methods. With every water sample collected, the container and the collection equipment were rinsed several times with water from that site. This reduced contaminants left previously in the containers and bucket. Deck hoses were rinsed and left running for 1 minute prior to collection to ensure no residual water was in the hose, and to flush any buildup of contaminants. On the Environment Agency vessel, water samples were collected using a bucket whereas the rest of the water samples were collected from a high-pressure deck hose which pumped water straight from the sea surface layer into the corresponding water container. 'A minimum of 5l was collected for each sample, which was subsequently used for chlorophyll a (CHL a) filtration and water quality analysis which included taking measurements for turbidity using a turbidity meter, and using a YSI EXO 2 CTD placed in a bucket with the water sample to measure salinity, dissolved oxygen and, conductivity. Samples were also prepared for nutrient analysis which was sent to a contractor for subsequent analysis of nutrient concentrations.

Sample transportation and storage:

Samples collected were left in shaded areas for the duration of the voyage before being left in a dark fridge, for no more than 24 hours, until they could be collected. They were returned to the lab and placed in the fridge without further exposure to light. Samples were analysed within 48 hours from arriving in the lab - helping to reduce the chances of chlorophyll degradation.

Sample analysis:

Filtration

To filter water the standard method described in (Knefelkamp et al, 2007; Roy et al., 2011) was used. Figure 3 shows an example of the filtration set up used. Before each sample was filtered, forceps were used to place 47 mm Whatman GF/F filter paper in between the 100ml filtration flask (annotation B in Figure 3) and the filter cup (label A in Figure 3). In subdued light conditions, each water sample bottle was inverted several times to create a homogenous mixture and poured into the filtration cup. A stand-alone vacuum pump was used to draw the water through the filter paper (annotation C in Figure 3). The vacuum pressure was held at 0.4 bar which reduced mechanical stress and cell lysis as a result of excessive pressure (Roy et al., 2011). Water was continuously filtered for 10 minutes with the total volume of water filtered being recorded after the 10 minute timer went off. This method was chosen due to varying levels of organic matter in samples effecting sample filtration rate, resulting in some samples filtering greater volumes of water in a quicker time than highly turbid samples. Filtering for 10 minutes would also reduce the exposure of chlorophyll to ambient lighting and high temperatures, and preventing filter paper saturation (Richardson and Pickney,2004; Wasmund et al., 2006), which ultimately could lead to an underestimation of chlorophyll a. Immediately after filtration, filter papers were blotted dry (Wasmund et al., 2006) and rolled with the algae facing inwards and placed into 15 ml test tubes. Subsequently, tubes were wrapped in foil and placed in a -20°C freezer and left frozen for a maximum of 3 months to ensure the degradation of chlorophyll on the filter papers was kept to a minimum (Wasmund et al, 2006).

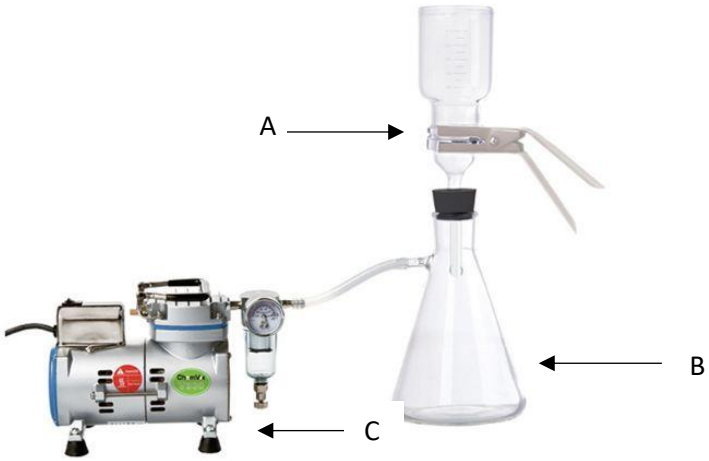

Figure 3. Example of the filtration set up used A) 47 mm Whatman GF/F filter paper, B) 1000 ml filtration flask and C) stand-alone vacuum pump (Gaia Science , 2024).

Chlorophyll extraction and quantification

To extract chlorophyll a the standard method described in (Wasmund et al., 2006) was used. 5ml of the acetone dilution was added to each sample test tube to ensure that the filter paper was fully submerged and the algae completely exposed to the acetone. The filter papers were then subjected to 15 minutes in an ultrasonic bath on ice, before being transferred into a fridge and left for 24 hours to allow the extraction process to begin (Wasmund et al., 2006). To quantify the concentration of chlorophyll a,b and c pigments , each sample was run on a single beam Jenway 7151 spectrophotometer. The acetone solution was pipetted into a clean cuvette (3500 µl Hellma UV 6030 quartz cuvette) and placed into the spectrophotometer for analysis. The settings for the spectrophotometer were set to a 350 to 750 nm wavelength range with an interval of 2 nm. Absorbance was then recorded and the data exported to Excel for each corresponding wavelength. A blank acetone sample was run, both prior to sampling on the spectrophotometer and after every 8 samples, in order to confirm that there was no deviation in baseline absorbance after repeated spectrophotometer use, and to ensure that variability in baseline absorbance levels was low. To quantify the concentration of Chlorophyll a , b and c (g m^{-3}) in a 90% acetone solution, a trichroic formulae was used from Ritchie (2008).

$$\text{CHL a} = -0.3319\ (\text{A}_{630} - \text{Average A}_{720}\text{:A}_{750}) - 1.7485\ (\text{A}_{647} - \text{Average A}_{720}\text{:A}_{750}) + 11.9442\ (\text{A}_{664} - \text{Average A}_{720}\text{:A}_{750}) \quad (\pm 0.0020) \quad (1a)$$

$$CHL\ b = -1.2825\ (A_{630} - Average\ A_{720}\text{:}A_{750}) - 19.8839\ (A_{647} - Average\ A_{720}\text{:}A_{750}) - 4.8860\ (A_{664} - Average\ A_{720}\text{:}A_{750}) \quad (\pm 0.0076) \quad (1b)$$

$$\text{CHL c} = 23.5902\ (\text{A}_{630} - \text{Average A}_{720}\text{:A}_{750}) - 7.8516\ (\text{A}_{647} - \text{Average A}_{720}\text{:A}_{750}) - 1.5214\ (\text{A}_{664} - \text{Average A}_{720}\text{:A}_{750}) \quad (\pm 0.0075) \quad (1c)$$

The inherent values – the constant values associated with each specific chlorophyll pigment and their absorbance wavelength that are not changed when determining chlorophyll a, b and c - were derived from Ritchie (2008). The constant's were derived from 1,748 spectrophotometric readings in order to derive more accurate equations for the determination of chlorophylls a, b and c. Absorbance (A) was measured at the wavelengths 630, 647 and 664nm which coincide with chl red peaks (Qy) of known CHL and phytoplankton solutions. The 95% confidence limits can be taken as the lower detection limit for CHLs from multiple organisms. The average of A720 – 750 was deducted from the Qy peaks of 630, 647 and 664 nm to offset the variability in baseline levels on account of potential artefacts increasing absorbance in spectrophotometric scans. Qy peaks at 691 were taken out of the original Ritchie (2008) equations due to the absence of CHL d in phytoplankton communities within the North Sea.

A conversion from the acetone concentration of CHL (µg/ml) to seawater concentration of CHL (mg/m^3 seawater) was completed using the following equation:

$$Chl = acetone\ concentration\ of\ chl \times Volume\ acetone \times (1000/sample\ volume\ filtered)$$

This equation is interchangeable and can be used with the three different CHL pigments being analysed.

Phytoplankton photosynthetic activity: fast repetition rate fluorometry

In addition to measuring chlorophyll using the acetone extraction method, chlorophyll fluorescence was also used as a secondary method to quantifying chlorophyll a concentration using active fluorescence. Using a fast repetition rate fluorometer (Fastact lab system 2; Chelsea Instruments, London, UK), a distilled water blank, a seawater sample blank and an unfiltered sample were measured. To confidently decipher fluorescence measurements, corrections need to be made to offset instrument noise, signal quality and electronic offsets (Suggett et al., 2006). A distilled water blank was run prior to sampling and at the end, as well as after every 8 samples run in a batch. The blank helped determine that the variable fluorescence signal maintained a low baseline level throughout sampling. Instrument blanks can regularly vary because of factors such as instrument temperature, cuvette transparency and atmospheric conditions (Suggett et al., 2006). For the sample blank, a small volume of each sample was filtered through GF/F Whatman 25 mm filter papers. These blanks were required to correct for any fluorescence signal from coloured dissolved organic matter (CDOM) or CHL detritus. The two blanks in conjunction with an unfiltered live sample, provided a corrected overall fluorescence signal for CHL in each sample. The outputs for the Fast Act system are shown in Table 2.

Table 2. Parameters and definitions from FRRF output.

Parameter	Definition
CHL	Chlorophyll concentration
Fo	Minimum fluorescence in darkness
F'	Steady state fluorescence at any point
Fm	Maximum fluorescence in darkness
Fm'	Maximum fluorescence under actinic light
Fv/Fm	Maximum photochemical efficiency
Fq'/Fm'	Photochemical efficiency under actinic light
PAR x Fq'/Fm'	Primary production

Optical properties of the water column:

Multispectral radiometer:

A Seabird OCR-507 Multispectral Ocean Colour Radiometer (OCR) was used to measure optical properties of samples taken from locations shown in Figure 2. The setup is shown in Figure 4. The mounting positions of both OCRs covered both downwelling (E_d) and upwelling (E_u) irradiance (abels A and B in Figure 4). A dive computer and a mini CTD were also attached to the board and used to log time and depth. The rope used for the OCR deployment was marked at 1 m intervals, allowing a backup procedure for the estimation of depth of the instrument. The OCR was set to a, 250 ms sample rate with a pre-warm up flush of 5 s and a sampling delay of 10 s from when the logger activation plug was in place (Label E in Figure 4). During each cast, surface photosynthetically active radiation (PAR) was measured using a hand-held irradiance sensor to detect fluctuations in surface incident flux caused by drifting clouds (Kirk, 2000). As a result of not having any logging capabilities on the surface PAR sensor, video recordings of the sensor display were used. The video was also used for regular depth call outs based on estimations from the marked rope being used; aiding in subsequent matching-up of depth recorded from the dive watch / CTD with the recordings from the OCRs. The OCR was lowered through the water by hand and the descent rate was controlled and kept consistent for all casts by using a 'one hand over the other' method for both the downwards and upwards casts.

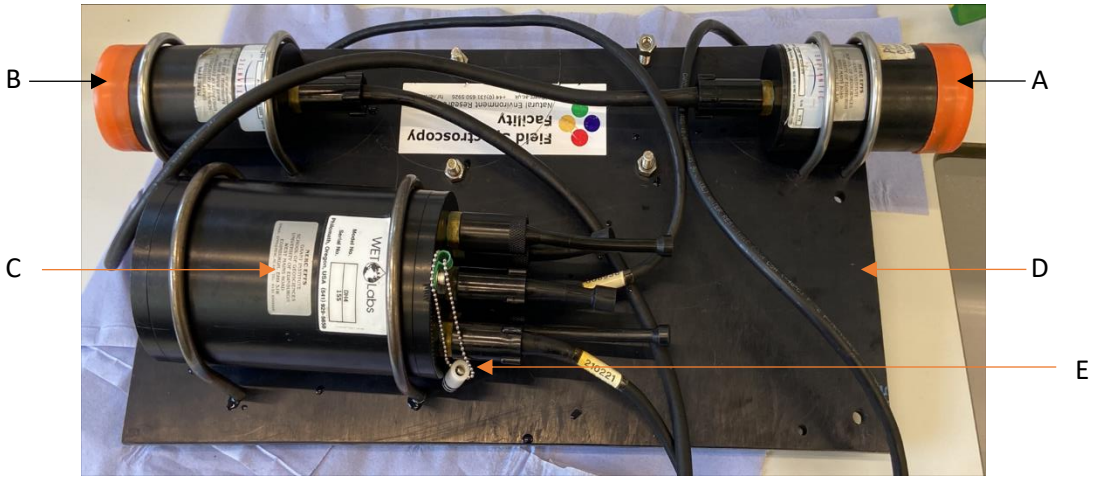

Figure 4. The Seabird OCR-507 Multispectral Ocean Colour Radiometer setup, A) Seven wavelength channel downwelling OCR, B)) Seven wavelength channel upwelling OCR, C) Data logger, D) Mini CTD and dive watch found on the reverse of the backboard, E) logger activation plug

Raw OCR data preparation:

The sample rate of the OCR was set to 250 ms while depth was recorded on the CTD and dive watch at 1 s intervals. To allow an accurate matchup between the multiple instruments, the time intervals of the OCRs were rounded to the nearest whole second. An average was taken for each E_0 value recorded within the 1 s interval for each of the seven wavelength channels.

Surface PAR was recorded to offset variations in E_0 (PAR irradiance at the surface) arising from changes in surface incident flux. Surface PAR was matched against the corresponding underwater spectral readings. Each cast was corrected for varying surface light using the following formula:

$$Corrected\ underwater\ irradiance\ with\ surface\ PAR = Ed(Z)\ \times \frac{Mean\ PAR\ for\ the\ Cast}{Surface\ PAR\ at\ Ed(Z)}$$

With $E_d(z)$ representing the downward irradiance (E_d) at a specific depth in meters (z) within the water column. Every cast was corrected using surface PAR, apart from deployments on the Grimsby to Whitby cruise. Only one person was available for deployment, resulting in no video being taken of the surface PAR sensor. However, during these casts, light conditions were steady with no cloud cover, resulting in minimal surface light variability.

Estimation of depth

The OCR casts at Staithes and the Grimsby to Whitby sites relied on depth being measured by a dive watch. Data was stored internally on the watch and then extracted using the dive profile software. The procedure of estimating depth based off the dive watch measurements and the 1 m interval marked deployment rope is shown in the schematic diagram below.

A)

Time (secs)	Depth (m)
1	1
2	
3	
4	
5	
6	
7	
8	
9	
10	2.3
11	
12	
13	
14	
15	
16	
17	
18	
19	
20	2.4
21	
22	
23	
24	
25	
26	
27	
28	
29	
30	3
31	
32	

B)

Time (secs)	PAR (from video of handheld sensor	Call outs based off the marked 1m interval OCR rope
1	543	Event
2	539.8	
3	536.6	
4	533.4	
5	530.2	
6	527.0	
7	527.2	at 2m
8	527.4	still at 2m
9	527.6	
10	527.8	
11	528.0	
12	528.8	hold
13	531.6	
14	532.8	
15	534	
16	532.0	
17	534.8	
18	537.6	
19	540.4	
20	543.2	
21	546.0	
22	530	
23	532.25	go down to 3m
24	530.5	
25	533.725	
26	539.0	
27	541.2	
28	543.4	
29	545.6	yes at 3m
30	547.8	
31	550.0	hold
32	550.6	

C)

Time (secs)	PAR (from video of handheld sensor	Call outs based off the marked 1m interval OCR rope	Depth (m)
1	543	Event	1
2	539.8		
3	536.6		
4	533.4		
5	530.2		
6	527.0		
7	527.2	at 2m	
8	527.4	still at 2m	
9	527.6		
10	527.8		2.3
11	528.0		
12	528.8	hold	
13	531.6		
14	532.8		
15	534		
16	532.0		
17	534.8		
18	537.6		
19	540.4		
20	543.2		2.4
21	546.0		
22	530		
23	532.25	go down to 3m	
24	530.5		
25	533.725		
26	539.0		
27	541.2		
28	543.4		
29	545.6	yes at 3m	
30	547.8		3
31	550.0	hold	
32	550.6		

D)

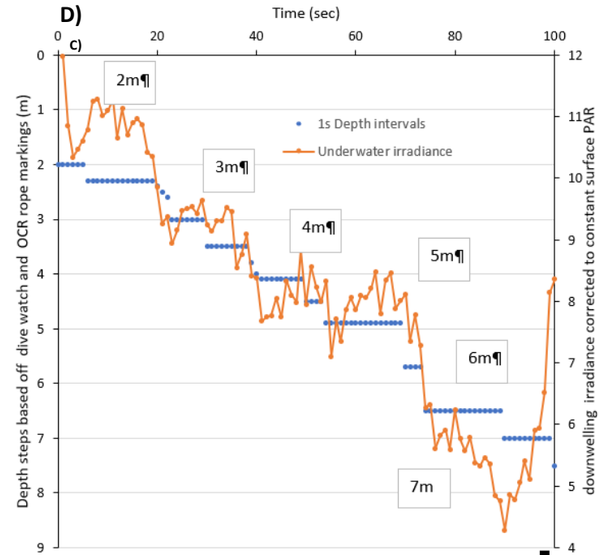

E)

C) Time (secs)	PAR (from video of handheld sensor	interval OCR rope	Depth (m)	Depth_1 second
1	543	Event	1	1
2	539.8			1.25
3	536.6			1.5
4	533.4			1.75
5	530.2			2
6	527.0			2
7	527.2	at 2m		2
8	527.4	still at 2m		2
9	527.6			2
10	527.8		2.3	2.3
11	528.0			2.3
12	528.8	hold		2.3
13	531.6			2.3
14	532.8			2.3
15	534			2.3
16	532.0			2.3
17	534.8			2.3
18	537.6			2.3
19	540.4			2.3
20	543.2		2.4	2.4
21	546.0			2.4
22	530			2.4
23	532.25	go down to 3m		2.4
24	530.5			2.5
25	533.725			2.6
26	539.0			2.7
27	541.2			2.8
28	543.4			2.9
29	545.6	yes at 3m		3
30	547.8		3	3
31	550.0	hold		3
32	550.6			3

A)

The dive watch was water activated and had a sample rate of 10 seconds. Depth data was manually entered at 10 sec intervals on a 1-second interval timeline

B)

Surface PAR readings and depth call outs (depth call outs based off estimations from the 1m interval marked deployment rope) from the video taken of the handheld par sensor display were also placed on a 1-second interval timeline.

C)

The dive watch data was overlayed against the already inputted surface PAR and depth call outs for the corresponding cast. When overlapping the dive watch data, the dive watch depths were matched against the key call outs of estimated depth from the rope, ensuring the timings of surface PAR and depth were aligned. The cast profile at the Staithes deployments consisted of lowering the OCRs by 1 m intervals, followed by a ~10 sec hold at each interval. This would aid in matching depth to the underwater irradiance given the clearly defined depths against which matching was possible

D)

To ensure accuracy in estimated depths between the 10-second sample rate on the watch, underwater irradiance for a single channel was plotted against time on a scatter plot, with depth being overlayed on the graph as a new series. Using the graph, the start and end time of each holding station could then be derived

E)

The estimated depths from the video, alongside recorded dive watch depths allowed an estimated depth to be derived for each second alongside the depths of each holding station. The estimated depths between the holding depth steps were a combination of recorded dive watch depths and adding in the unknown depths with either an increasing/ decreasing depth based on the assumption of a steady rate of descent/ascent

On some casts at Staithes and on the Grimsby to Whitby cruise, the OCR rig experienced current drift, meaning the cast was not completely vertical nor at precisely at the assumed depth. The rig would be at a shallower depth than expected at holding stations as it drifted away from the vertical drop. To correct for the actual depth of the holding station, the ratio of the maximum depth (Assumed depth from the amount of rope used) divided by the recorded dive watch depth was used. This ratio was then applied for the whole cast where dive watch depth did not match assumed depth.

During the Bridlington cruise, depth call outs based on estimated depth from the markers on the OCR rope were used, as no other option was available. Ultimately, it was assumed that the depth call outs were accurate, and a 1 second depth interval was derived based off the known amount of rope used and steady descent rate being the same for the whole cast. The derived 1-second interval depths were matched against irradiance profiles. This matching process can be seen in Appendix 1. There was minimal to no drift in the OCR rig, helping to improve the reliability of accuracy in estimated depths derived.

Underwater irradiance attenuation calculations (K_d):

Light attenuation (K_d) was calculated for each site, and for individual downward and upwards casts, by using the logarithmic rate of change in irradiance with depth. Underwater spectral irradiance after correction with surface PAR was used to calculate the natural logarithm of irradiance for each wavelength channel. An estimate of total underwater irradiance at each depth (similar to PAR) was estimated by taking the sum of the ln $E_d(z)$ for all 7 wavelength channels. K_d was then finally derived for each wavelength channel using the 'LINEST' function in Excel. Only depth ranges that were known with confidence were used. The LINEST calculation was placed into an array displaying values described in appendix 2 and repeated for each wavelength band with the slope value (Mn) being the K_d output. R^2 provided evidence on how good a fit depth was with irradiance. Low R^2 values were discounted and K_d was not taken for these sections of the cast. Additionally, 1% depth (depth in which 1% of all light reaches) was measured for each wavelength using the following formula.

$$1\%\ depth = LN(100)/Kd$$

LN represents the natural logarithm function with Kd standing for light attenuation.

Reflectance ratio:

A reflectance ratio (R) was calculated by dividing the corrected upwelling underwater irradiance by the corrected downwelling measurement. An average was then taken for the first 5m of each cast at each wavelength for the reflectance ratio value. This derived R_5 for each wavelength channel which was plotted for each site and used to compare reflectance values for different regions.

Remote sensing:

Copernicus Marine Service data were used to supplement our in situ datasets (marine.copernicus.eu). Daily and monthly averages for chlorophyll a (CHL), Mixed Layer Depth (MLD), sea surface temperature (SST) and Suspended Particulate Matter (SPM) were downloaded for the study area. A full list of all the data used can be found in Table 3.

Table 3. List of Copernicus products used.

Name	ID	Parameter	DOI
Global Ocean OSTIA Sea Surface Temperature and Sea Ice Analysis	SST_GLO_SST_L4_NRT_OBSERVATIONS_010_001	Sea surface temperature (SST)	https://doi.org/10.48670/moi-00165
Atlantic- European North West Shelf-Ocean Physics Reanalysis	NWSHELF_MULTIYEAR_PHY_004_009	Mixed layer depth (MLD)	https://doi.org/10.48670/moi-00059
Atlantic - European North West Shelf - Ocean Physics Analysis and Forecast	NORTHWESTSHELF_ANALYSIS_FORECAST_PHY_004_013	Temperature, Salinity	https://doi.org/10.48670/moi-00054
Global Ocean Colour (Copernicus-GlobColour), Bio-Geo-Chemical, L3 (daily) from Satellite Observations (Near Real Time)	OCEANCOLOUR_GLO_BGC_L3_NRT_009_101	Suspended particulate matter (SPM)	https://doi.org/10.48670/moi-00278
North Atlantic Ocean Colour Plankton, Reflectance, Transparency and Optics L3 NRT daily observations	OCEANCOLOUR_ATL_BGC_L3_NRT_009_111	Chlorophyll-a, Gap-free chlorophyll-a (CHL a)	https://doi.org/10.48670/moi-00284

All remote sensing data were processed and analysed using ArcGIS PRO 10.2.0. CHL data used is based on ocean colour-observing satellites and was downloaded at daily temporal scale (Table 3). CHL 10-day average figures were created using the raster aggregation tool in ArcGIS Pro to avoid tidal bias and allow for missing data attributed to cloud cover. Data from March to June were used to coincide with the spring bloom events in the study area (Sharples et al., 2006). CHL values were extracted from the remotely sensed data at the same site and on the same day as CHL was taken *in situ* and used to compare the two independent data sets. SST was downloaded as monthly averages (Table 3) to visualise changes from March to June. A 1°C contour polygon was used to display SST data to enable regions with significant temperature difference to be depicted. Longitude-depth plots for subsurface temperature were made from the *Atlantic - European North West Shelf - Ocean Physics Analysis and Forecast product* (Table 3), and displayed using Panopoly (https://www.giss.nasa.gov/tools/panoply/) for selected latitudes from north to south through the region. Mixed layer depth (MLD) .was obtained from a reanalysis hydrodynamic model (Table 3), which inputs available *in situ* data into the model. A monthly average was taken for the period of March to June to enable observations in MLD over varying temporal and spatial scales within the study area. Two figures were calculated which included MLD and then also a figure based on calculation for the percentage of the water column that was mixed. This second figure involved using the raster calculator function using the following formula.

$$\%\ of\ the\ water\ column\ that\ is\ mixed = \frac{Monthly\ averaged\ MLD}{Bathymetric\ depth} \times 100$$

This was used to help divide the north-east region into discrete, coherent hydrodynamic regions by using SST, MLD and sea bed depth. SPM was downloaded from colour-observing satellites at daily and monthly time scales (Table 3). SPM data was used to understand the changes in turbidity over time as well as being used for calculating the underwater light attenuation coefficient (K_d) using a linear regression equation published by Devlin et al., (2008). The linear relationship between K_d and SPM for coastal inshore regions allowed the extraction of the slope and intercept of the regression to be used within the following formula;

$$Light\ attenuation\ coefficient\ (Kd)\ =\ 0.039\ +\ 0.067\ x\ SPM$$

Daily SPM data was used as a comparison against *in situ* turbidity values to help verify the reliability of turbidity measurements being used. In addition, corresponding SPM data for each *in situ* underwater light recording was used to derive K_d and was used as a comparison between two light attenuation calculations. Finally, monthly SPM was used to understand the variation in turbidity over the course of one year. The satellite remote sensing and hydrodynamic model data were essential for filling gaps in data that could not be collected *in situ*, as well as being used as a comparison with *in situ* data to help

understand the reliability and validity of using remote sensing data for future chlorophyll projects. A table of all the remotely sensed data downloaded can be seen in Table 3.

Nutrients:

A 15 ml sample of water was filtered through a sterile 0.45 µm syringe filter and stored in sterile polypropylene tubes. The samples were stored at -20°C until silicate, nitrate and phosphate analysis was undertaken using a seal Analytical AutoAnalyser III. Samples were also analysed for nitrate, nitrite and ammonium, Dissolved inorganic nitrogen (DIN) was calculated through the sum of nitrates, nitrite and ammonium. To provide an annual estimation of nutrients, missing temporal data was extracted from the Environment Agency's water quality data (WIMS database, available under Open Government Licence https://environment.data.gov.uk/water-quality/view/landing) to reconstruct a yearly time series. This was needed to provide initial values of nitrate for phytoplankton growth modelling.

Physical water properties:

Multi-sensor probes:

To understand the physical and chemical properties of the water column a Valeport MIDAS CTD+ (Midas CTD PLUS - Valeport) and YSI Exo 2 CTD sonde were deployed (YSI EXO2 Multiparameter Water Quality Sonde | ysi.com). Different sensors were available on each instrument (Table 4). Measurements taken from both CTDs were oxygen, turbidity, conductivity, temperature, fluorescence and pressure. Two casts for each site were taken using two different CTDs to allow quality control on data output as well as calibration of instrumentation.

Table 4 List of the sensors on each of the different CTDs used

	CTD	
Sensors	**Valeport MIDAS CTD+**	**YSI EXO 2**
Turbidity (FNU)	☑	☑
Chlorophyll (RFU)	☑	☑
Calculated Density	☑	☒
Dissolved Oxygen (%)	☑	☑
PH	☑	☒
PAR	☑	☒
Pressure (PSI)	☑	☑
Temperature (°C)	☑	☑
Salinity (PSU)	☑	☑
Conductivity (µS/cm)	☑	☑
Redox (mV)	☑	☒

Cefas SmartBuoy and Wavenet data:

CEFAS automated 'SmartBuoys' and 'Wavenet' stations found within our sample area, were used to gather essential wave height and sea surface temperature (SST) data from a range of sites (Figure 1). Data was downloaded (Appendix 6) for 2022 and used to help understand the influence of sea state and sea surface temperature on blooming events in the North Sea. The temporal and spatial autocorrelation was accounted for by reducing SmartBuoy values from 30 minutes to daily and monthly averages. Data was sorted and averaged using the Pivot table function in Excel with wave height and SST being plotted against time.

Primary production modelling:

Two sites were chosen based on previous model runs that were undertaken for undergraduate projects. The sites J6 and site 13 (Figure 1 & Figure 10) were used, with site J6 coinciding with one of our *in situ* sampling sites where instrumentation was deployed.

One-dimensional S2P3 model:

The S2P3 0_2 model (Simpson and Sharples, 2012) was used to estimate primary production and observe annual trends in chlorophyll values alongside stratification. The model required various data sources which included hourly meteorological observations. Time (days), wind velocity x-component (m s^{-1}), wind velocity y-component (m s^{-1}), air temperature (°C), air pressure (mbar), relative humidity (%), radiation (W m^{-2}), cloud cover (%), were necessary (Appendix 5), alongside parameter adjustments for water column mixing, tidal constituents, friction, turbulence and vertical attenuation coefficient for Photosynthetically Active Radiation PAR (m^{-1}), (Appendix 2 & 3). Dissolved inorganic nitrogen, temperature, and heat distribution were also considered in determining the primary production outputs from the model. However, due to the unavailability of *in situ* data within our study area, parameters such as phytoplankton growth rates, grazing, plankton nutrient uptake, and vertical movement velocities remained at Celtic Sea default values used by Simpson and Sharples, 2012. The initialization files containing the parameters can be found in appendix 2 and 3. Meteorological parameters (Appendix 5) were gathered from ECMWF Reanalysis v5 (ERA5 dataset found at ECMWF Reanalysis v5 | ECMWF) dataset, where hourly data was obtained and conversion of units specified by the model were undertaken. All meteorological data was extracted directly from the ERA5 dataset, apart from relative humidity (RH). This was calculated based off dewpoint (D_p) and temperature (T) measurements using the following equation:

$$RH = 100 \times \{exp[17.625 \times D_p/(243.04 + D_p)]/exp[17.625 \times T/(243.04 + T)]\}.$$

Diffuse attenuation coefficient (K_d) derived from SPM, which was outlined by Devlin et al., (2008), was used as the vertical attenuation coefficient for PAR (m^{-1}). The model only allows one K_d value to be used, therefore an average K_d was taken from March-August to help limit increases in K_d averages as a result of high sediment load in winter months. The resolution of the model could be determined by the user by adjusting the depth cell parameters. To assess the reliability of model outputs, SST generated by the model was compared against remotely sensed SST, to check the reliability of meteorological data inputted.

Excel primary production model:

Hourly data for surface irradiance in the form of PAR, light attenuation, chlorophyll concentration and photosynthetic efficiency (Pbmax and alpha) were used to predict gross primary production (GPP) and net primary production (NPP) as developed by Cole and Cloern (1987) (Greenwood et al., 2011). Hourly PAR data was obtained from ERA5 datasets, with K_d being obtained through Devlin's SPM calculations. As no hourly remotely sensed SPM measurements were taken, daily SPM was used to calculate a daily K_d value which was input for each hour for 1 day. Daily chlorophyll values extracted from satellite gap free product (Table 3) to enable a full daily time series for the whole of 2022. Due to the absence of hourly chlorophyll estimations, a single daily chlorophyll value was input to each hourly cell for 1 day. A P_{bmax} of 6 and a 0.060 alpha value were used throughout the year, with these values being derived from previous research estimations for averaged values for the North Sea (Shaw & Purdie, 2001; Napoléon et al., 2014). Values entered into the model can be found in appendix 4.

Site description and sampling sites

Bathymetry and currents:

The bathymetry of the sample area, alongside the mixed layer depth was used to define different water bodies that represented the areas containing the sample sites. A mixture of inshore and offshore sample sites was derived based on a depth of 40m. Samples that were taken between the shore and 40m depth were defined as inshore, with any samples past the 40m depth contour being classified as offshore. The 40m contour shown in Figure 5 was approximately parallel to the coast at a distance of 15 km, stretching from the Northumberland coast down to Flamborough Head. The bathymetry beyond the 40m contour in this region is distinguished by a gently deepening gradient out towards the central North Sea. Below Flamborough Head and around/down to the Humber estuary is predominantly characterised by a shallow plateau extending towards the Dogger Bank, which has depths not exceeding 40m. However, within this area, there are a few sub-sea depressions with depths of up to 100m e.g. the Inner Silver Pit. The majority of samples are within the 40m contour with more

offshore samples in depths of 60m or less. Our deepest sample sites are situated off the Northumberland coast with depths up to 90m.

The currents in the North Sea shown in Figure 6 illustrates that the majority of water enters at the north from the Norwegian Sea and North Atlantic, flowing down towards the centre of the North Sea and then returning out towards Scandinavia. Additionally, a current propels water through the English Channel and up the southern region of the North Sea, along the northern European coast, towards the centre of the North Sea and the Scandinavian coast. Generally, water circulation is counter-clockwise (Baretta-Bekker et al., 2009). Within our study area, there are two major competing current directions. The Northumberland coast lies on a currents convergence zone where the currents are split between northerly and southerly currents. The area above Northumberland has northerly currents moving water into a small gyre off the coast of Scotland. Below Newcastle, the currents move in a southerly direction down towards the Humber estuary. A few undercurrents may redirect water back in to the centre of the North Sea.

Off the coast of Flamborough Head there is a frontal system (approximate location of the frontal system is shown by a purple line in Figure 6) which is characterised by a pronounced temperature gradient between the northern and southern waters. Flamborough front provides an effective barrier that isolates the northern and southern water masses, where little exchange between the two hydrodynamic regions occurs (Holligan, 1981; Eaton et al., 2003). However on the convergence zone of the two water masses, upwelling has been observed.

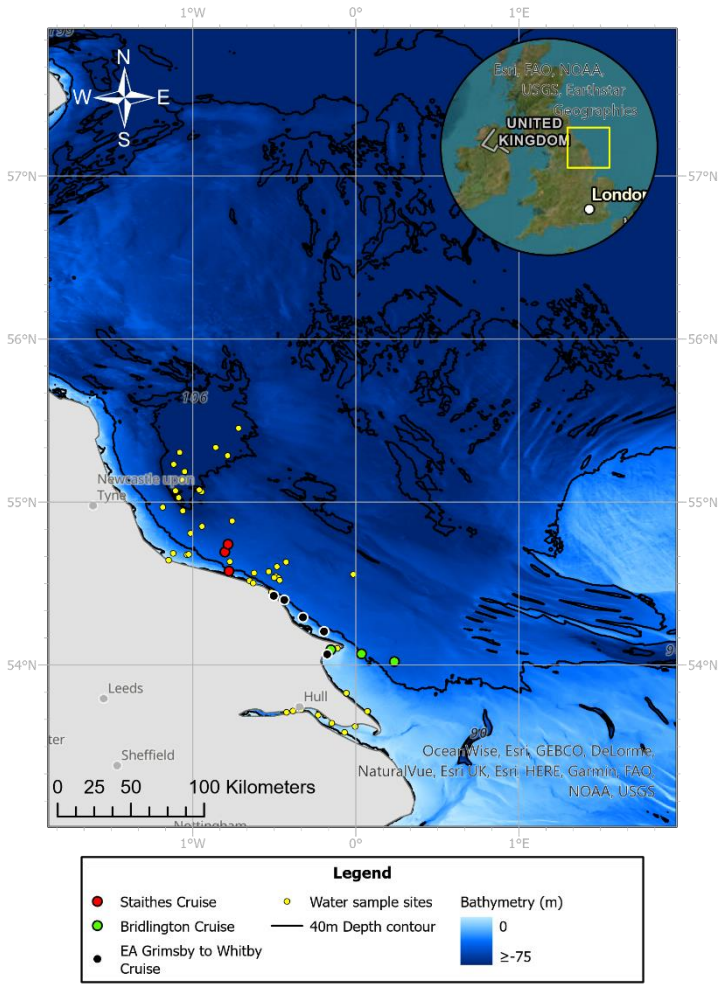

Figure 5. Bathymetry around the sample sites and the wider North Sea, with a 40 m depth contour added.

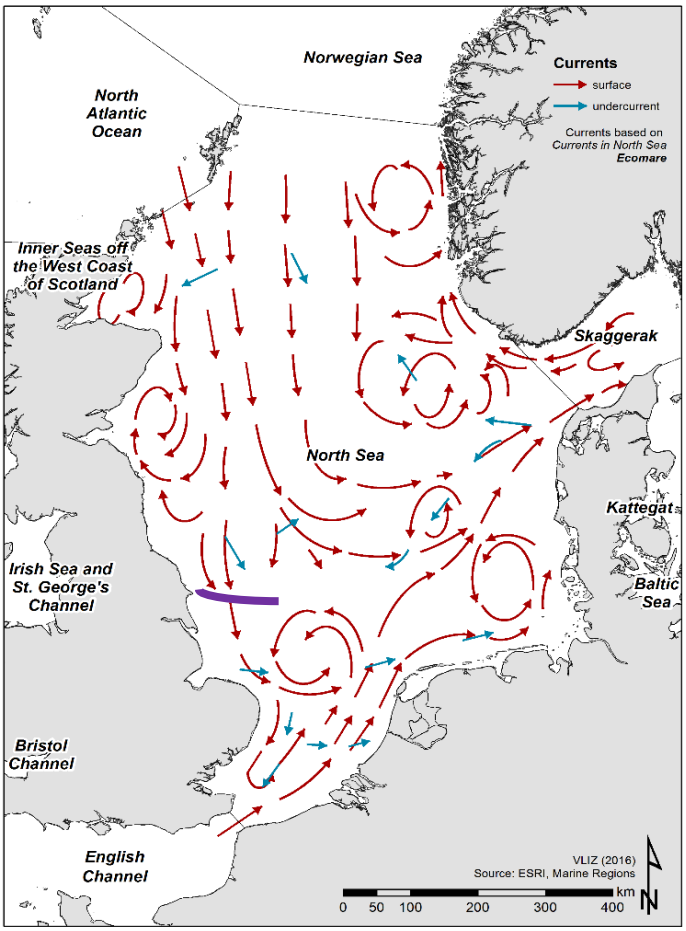

Figure 6. Currents in the North Sea (Nathalie, 2016). Purple line is the approximate location of the Flamborough front.

Wave height:

There was a north-south gradient in the monthly maximum significant wave height (the mean wave height (trough to crest) of the highest third of the waves), with the Tyne-Tees and Scarborough SmartBuoys recording the highest values (6.06m and 5.67m respectively), particularly in the autumn and winter (Figure 7). The Hornsea SmartBuoy showed lower significant wave heights for all months. The general trends for maximum significant wave height showed elevated height in the winter months with reduced and steady wave height during the months of May to August. November had the highest wave height for all buoys, with a maximum height of 6.06m at the Tyne-Tees buoy. June and July were the calmest months in terms of sea state with a maximum wave height of 2.33m recorded at the Tyne-Tees buoy in July. Of all the Cefas Wavenet and SmartBuoy stations, the Tyne-Tees site recorded the maximum highest waves for all months apart from February where the Dowsing saw the largest waves.

Figure 5 reveals that the month of April had the overall highest maximum wave height during the water collection and *in situ* measurements sampling period (March to June). There was an average

maximum wave height of 3.41m for April, when a mean was taken for all recordings. The highest maximum wave height recorded from all SmartBuoy locations was the Tyne-Tees buoy which had a maximum height of 4.11m, while the lowest maximum height was at Hornsea with a value of 2.12m in April. Whitby and the Tyne-Tees buoys saw the greatest decrease in maximum significant wave height between months.

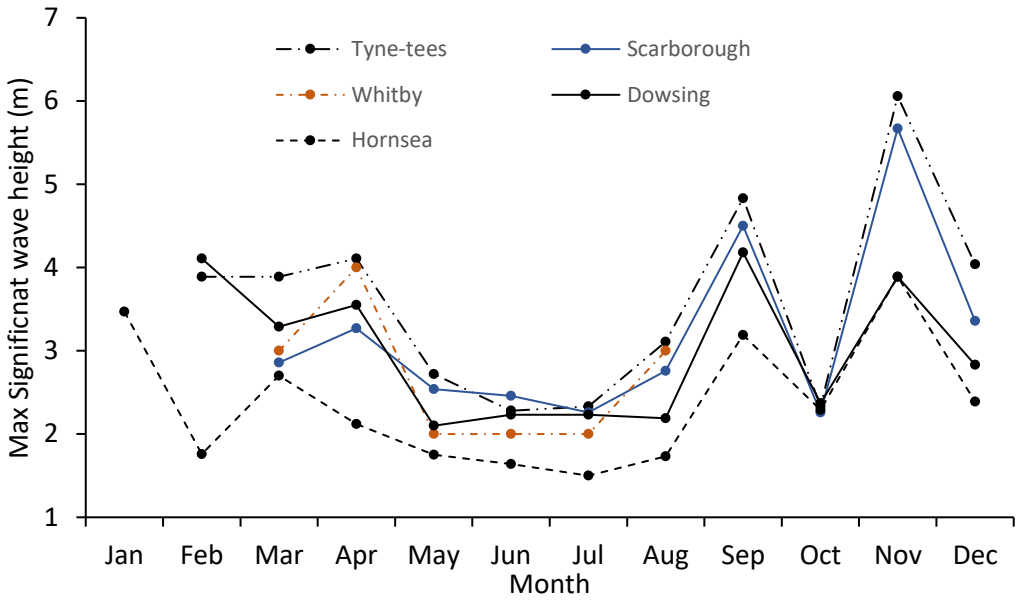

Figure 7. Monthly maximum significant wave height from CEFAS Wavenet and SmartBuoy sites on the north-east coast of the UK in 2022.

Section 3- Results:

Seasonal dynamics of physical oceanographic data:

Mixed layer depth (MLD):

Seasonal dynamics of the mixed layer depth (MLD) showed the water column in the majority of the North Sea to be completely mixed to the seabed in March (Figure 8A and Figure 9A). The central and northern North Sea (location found at map label ① in Figure 8) had an MLD ranging from 55-90m with 100% of the water column being mixed in shallower regions, and 70% mixing in the deepest areas (Figure 8 and Figure 9). The shallow plateau around the Humber and the Dogger Bank (map label ②), as well as the coastal zone from Flamborough to Whitby (SW of map label ③), showed that 80-100% of the water column, with an MLD ranging from 35-50m, was predominantly mixed to the seabed. However, this was not the case for the area around the cluster of offshore sample sites that are

situated north west of the Tyne-Tees CEFAS SmartBuoy (Map label ④). At this site there was early signs of the onset of stratification due to 25-40% of the water column being mixed. This location had the shallowest MLDs when compared to the rest of the North Sea, with values ranging between 19-40m.

In April, the beginning of stratification in northern parts of the North Sea (map label ①) was seen (Figure 8B and Figure 9B). It had a shoaling of the MLD from 55-90m to approximately 30-50m with an average of 47% of its water column being mixed and an average shoaling of the MLD by 37.5m. Our northernmost sites off the Northumberland coast (map label ④) had a shoaling of the MLD on average by 14m, resulting in a MLD of 19-25m in April for this area of our sample site. The percentage of the water column that was mixed in this stratified area decreased, resulting in percentage values ranging from 17-33%. This region where the formation of stratification was earliest, correlated with the deepest area of our sample sites shown in Figure 5. The rest of the inshore sample sites off the coast of Whitby down to the Humber Estuary (map label ② & ③), still had no signs of stratification formation in April.

In Figure 8C and Figure 9C, the regions of the central and northern North Sea (map label ①) became fully stratified with an average MLD depth of < 17.5m in May. This is approximately 22.5m shallower than in April. The percentage of the water column above the thermocline ranged from 15-20% in the central and northern areas of the North Sea. The areas around map label ④ remained stratified, with further shoaling of the MLD to <10.5m and with an average of 10% of the water column above the thermocline being mixed. For our inshore sites off the coast of Northumberland and Hartlepool (map label ⑤), there was a transition from a fully mixed water column in April with an MLD of <27 m to a partially stratified water body in May with an MLD of <19m. This was an 8m shoaling of the MLD at our northernmost inshore sites. However, areas very close to the shore still experienced high levels of mixing. The coastal region from Whitby to Flamborough (map label ③), and the shallow plateau in the southern North Sea (map label ②), remained fully mixed in May. The MLDs for these regions ranged from 30m to 45m with almost complete (75-100%) mixing of the water column. For this mixed region, significant wave height was greatest for the Scarborough Cefas SmartBuoy location when compared against all other SmartBuoy buoy data for that month, with the Dowsing site having the third highest significant wave height and Hornsea having the lowest (Figure 7). Increase in stratification could be correlated with significant wave height decreasing for all wave buoy locations when compared to the month of April.

The MLD in June (Figure 8D and Figure 9D) showed an increase in stratification for the main body of water in the North Sea (Map label ①) when compared with May. 13-18% of the surface water layer

was mixed, which gave an average MLD of <15m (Figure 8 and Figure 9). Our northernmost sample site region (Map label ④) remained relatively unchanged with 10% of the water column being mixed and with an average MLD of 10m. The sample sites off Flamborough Head, in particular the Bridlington survey sites (Map label ⑥), had a reduction in MLD from approximately 35m to 28m with the percentage of the water column that was mixed reducing by 14%. The remaining shallow plateau (Map label ②) around the Humber and the Whitby to Flamborough coast (Map label ③) still remained highly mixed. Offshore stratification was evident in a large proportion of the North Sea which could be associated with the lowest recorded maximum wave heights for the Tyne/Tees and Whitby buoy for the whole year in 2022. Significant wave height reduced to 2.23m and 2m for both the Tyne/Tees and Whitby wave rider buoys in May 2022 (Figure 7).

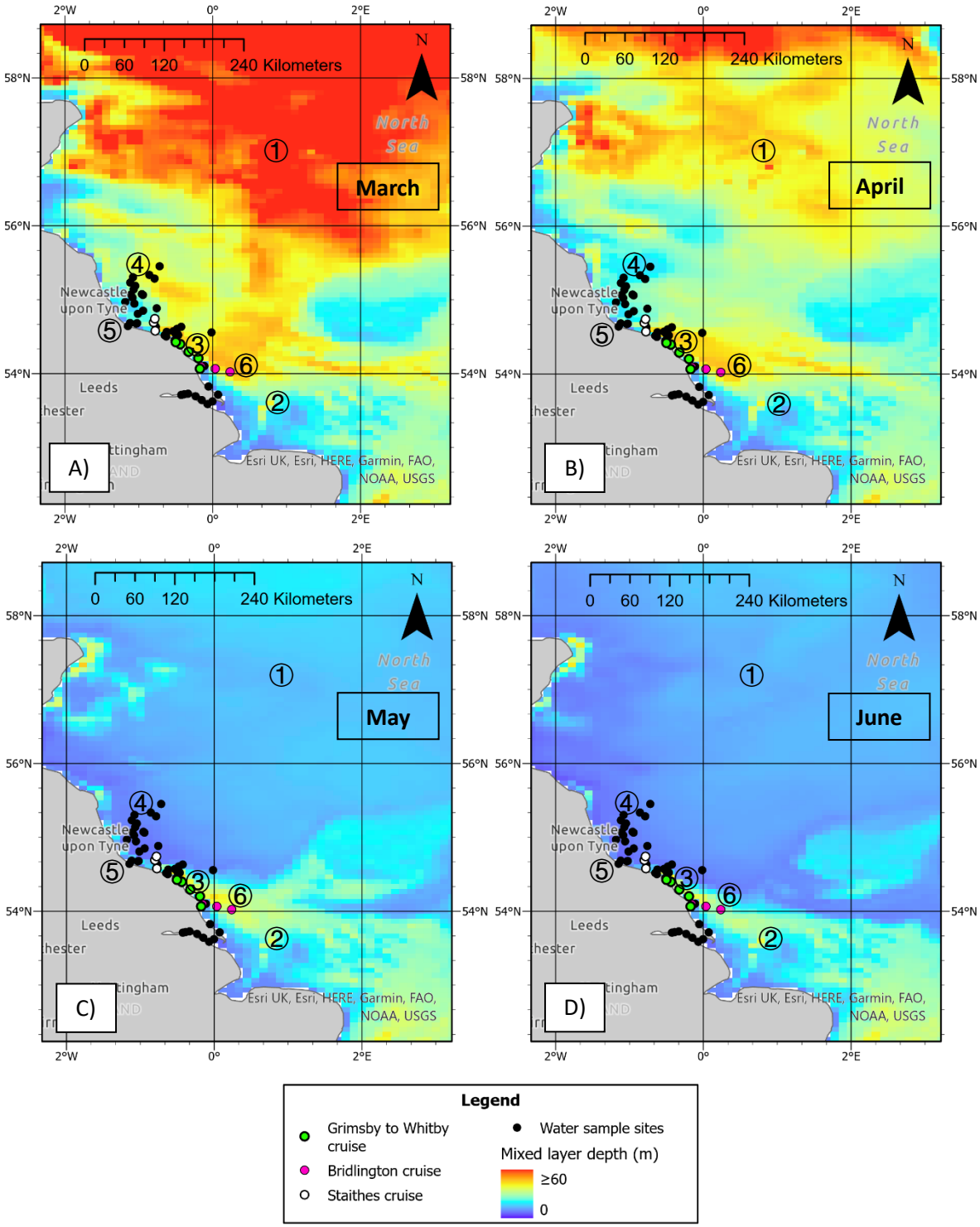

Figure 8. Monthly average mixed layer depth for the north east coast of the North Sea (A - March to D-June).

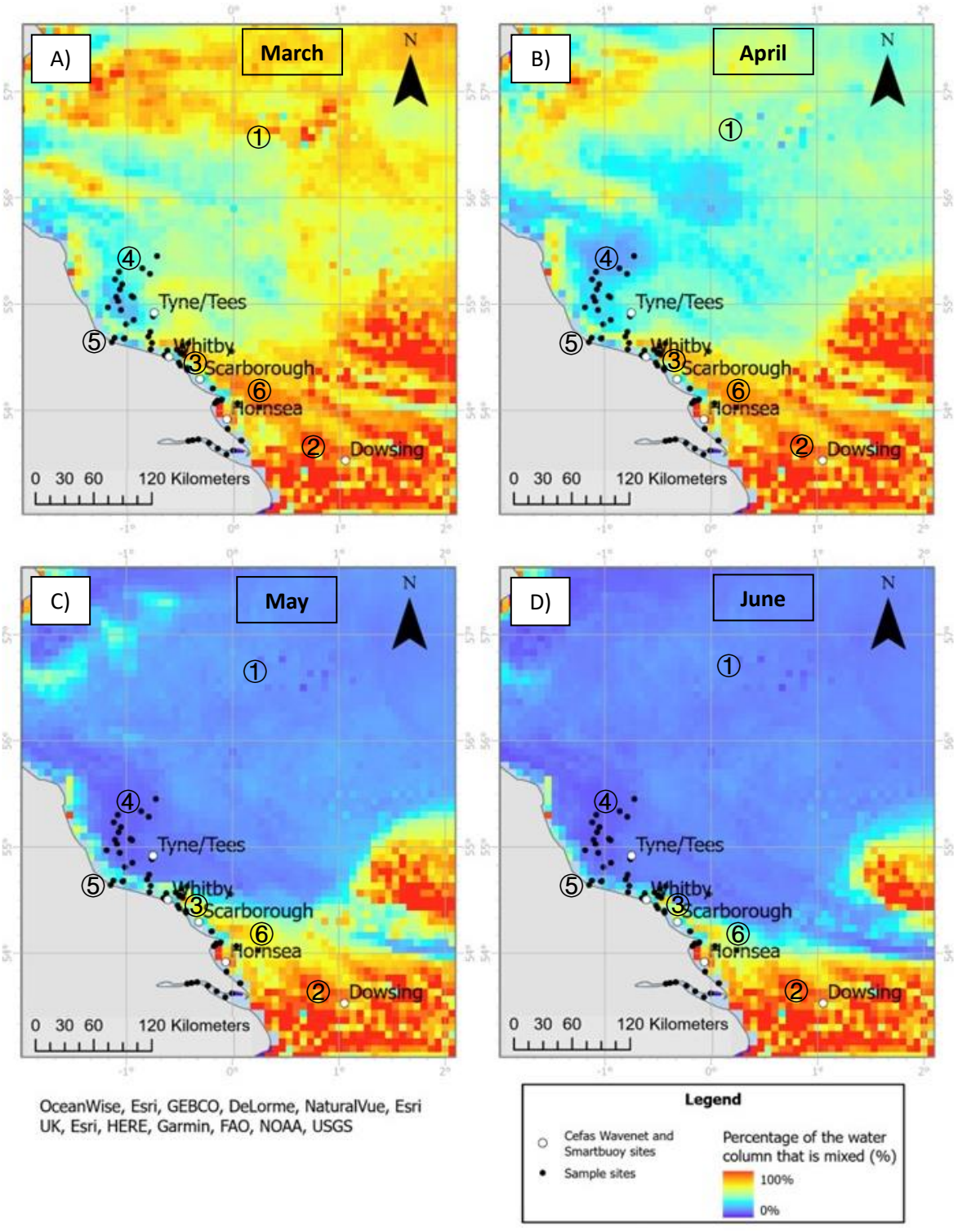

Figure 9. Percentage of the water column that is mixed for the Months of March (A) to June (D) in 2022.

Zoning of sample sites:

Water body types that encompassed our sample sites were delineated in Figure 10 by using MLD and bathymetry. Our sampling region was regionalised into three areas. Samples from the Humber Estuary were excluded from the analysis, and this area was not regionalised because only one set of samples was collected in this region in early March. The estuary was not revisited for sampling. The MLD map for May was chosen to depict the degree of mixing of water body regions, as this is the earliest month where areas of the North Sea became fully stratified. Three zones were delineated: An offshore seasonally stratified region (OS) encompassing all our offshore sites; an inshore partially stratified zone (IS) sample sites falling within the 40m depth contour and in a region where the water becomes partially stratified in summer month) and sites that were permanently mixed (PM) (Figure 10).

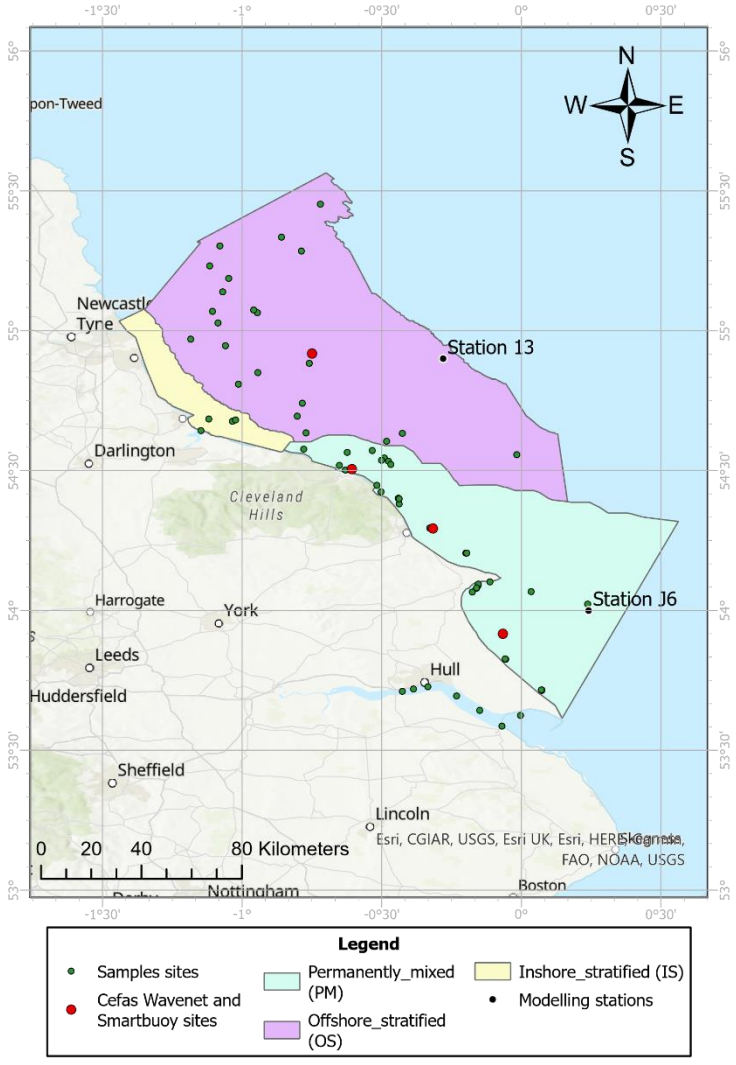

Figure 10. Defined zones based on MLD during stratified months and bathymetry.

An average depth for each area was derived (Table 5). The offshore stratified (OS) zone was deepest overall with the inshore stratified (IS) site being the shallowest. The IS zone was 44.22m shallower than the deepest region.

Table 5. Average depth for each zone in 2022.

Zone	Average Depth (M)
OS	67.79
IS	23.57
PM	39.58

The zones were also used to obtain average MLD for each month (Table 6) to understand which area had the greatest mixing alongside zones that are stratified. Using Table 6 and Figure 11 , OS had the overall lowest mixing (i.e. strongest stratification) each month when compared to the other sites. This region had only 13-14% of its water column stratified between the months of May and August, alongside the biggest decrease in MLD (40% decrease in mixed layer or 26.77m shoaling of the MLD) between the months from February and March. The PM region was the area with the greatest mixing overall for each month, with the shallowest MLD value of 15.5m in August and 39% of the water column being mixed. There are similar trends between the PM and IS zones, which experience deep MLD from October to February, with the water column being 90-100% mixed. MLD then shoaled from March to August, with the shallowest MLD in August for both sites (15.5m and 7.48m respectively). MLD then deepens from August back up to baseline winter MLD values. Overall IS had shallower thermocline than the PM region but followed the same trends. Trends for the OS region slightly differed from the other two sites, with MLD reaching its shallowest values in May and maintaining this value for the summer months. When compared to the other two sites, MLD constantly shoaled until it reached a shallowest MLD in August.

Table 6. Average monthly mixed layer depth (M) for each zone in 2022.

					Mixed layer depth (m)							
Zone	Jan	Feb	Mar	Apr	May	Jun	Jul	Aug	Sep	Oct	Nov	Dec
OS	62.55	61.21	34.44	27.89	9.71	8.96	9.86	9.07	17.64	30.68	51.42	61.94
IS	22.26	21.93	18.41	18.95	13.91	9.03	7.22	7.48	15.71	21.83	22.33	23.57
PM	39.58	39.53	36.59	36.09	28.25	20.56	17.20	15.50	26.43	38.91	39.58	39.58

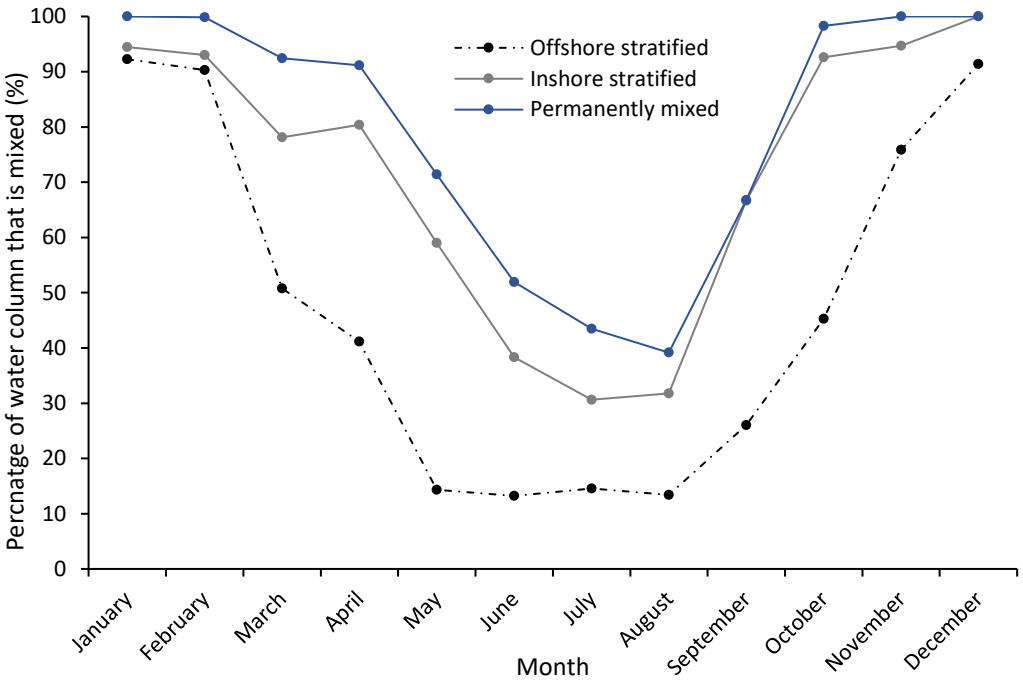

Figure 11. Monthly zone average for percentage of the water column that is mixed in 2022.

Water temperature:

Water column temperature:

In June, southern regions were warmer than northern regions, with the coolest waters (~11°C) being observed around the mid-latitude of the survey area at 54°N (Figure 12). The inshore region at a latitude of 53°N and a longitude between 0°E and 0.5°E had the highest SST recorded (ranging from 13.5°C to 16°C) for the whole study site. There was approximately a 3°C to 5°C temperature difference range between the coolest and warmest parts of the North Sea in June.

Figure 12 also presents a high level overview giving context to the subsequent Figure 13. The latitude and longitudinal lines displayed in Figure 12 (black horizontal lines) were used to analysis water column temperatures along each displayed longitudinal transect. Figure 13 presents water column temperatures along the longitudinal lines at each latitude depicted in Figure 12. Grey areas on the longitude-latitude water column temperature plots are areas of no data – due to this being areas of land mass or seabed. The pink box around the approximate location of the Dogger bank was added to Figure 12, to provide context to the shallowing of the water column observed in the plots at latitude 54.5 and 55,0N and longitudes of +1E to +2.6E (Figure 13).Sea water potential temperature (units of sea water temperature used in Figure 12 and Figure 13) is the temperature that a water parcel would have if it were raised adiabatically (no heat exchange with the surrounding) from a particular depth to the sea surface without change in its salinity.

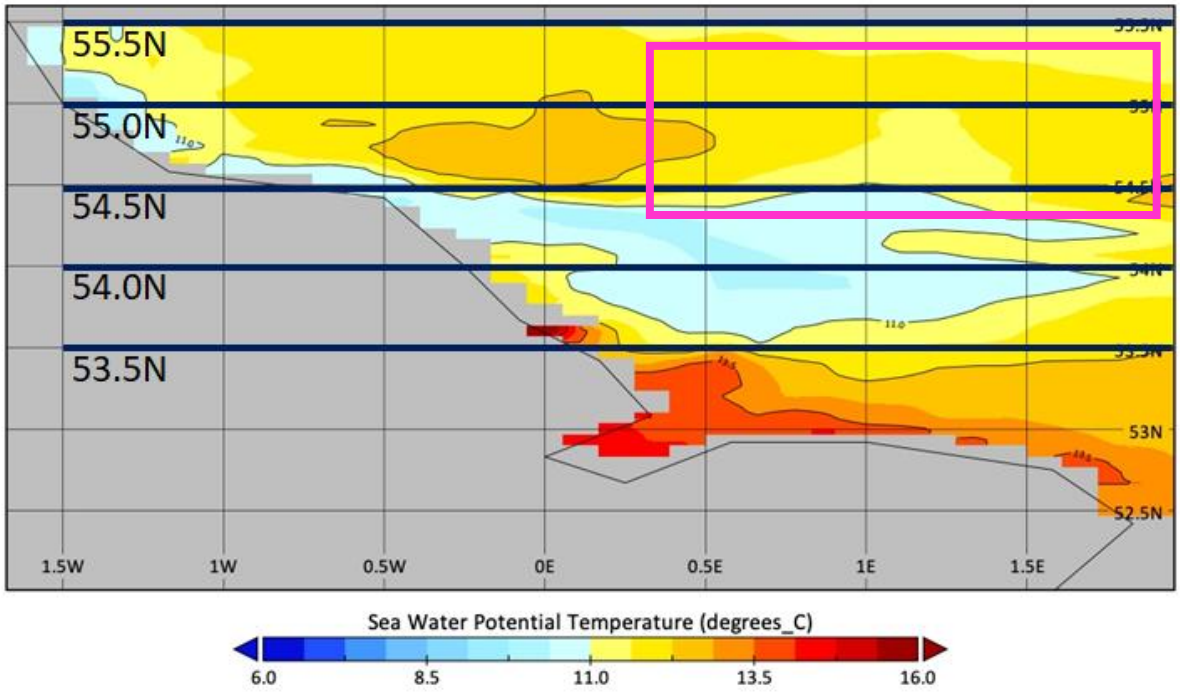

Figure 12 Sea surface temperature monthly mean for June 2022 (Table 2). Horizontal lines show longitudinal transects for five sections of the north-east coast with the pink box roughly outlining the location of the Dogger bank.

Temperature -depth plots:

The temperature depth plots showed the general trends of a north – south gradient with thermocline formation occurring first in the northernmost latitudes and moving south with time (Figure 13). The southernmost longitudinal transect at 53.5°N remained permanently mixed throughout 4-month sampling period. The water column was fully mixed for all longitudinal transects plots in March apart from the transect at 55.5°N latitude. At this northern latitude, there is evidence of the formation of thermocline at around 10m between longitudes 0.38°E to 0.8°E and 1.6°E to 2.2°E. There is approximately a 1 °C difference in temperature above and below the thermocline at this region. Progressing into April, water column stability at the northernmost latitude increased because of the formation of a thermocline over greater longitudinal distances when compared to March. The inshore regions remained completely mixed to the seabed with the beginning of thermocline forming at a longitude of 0.3°E. The thermocline deepened to approximately 25m on this longitudinal transect. Stratification starts to form on the transect at 55°N in April. The thermocline on this transect was constrained to the deeper waters, away from the coast and the shallow areas of the central North Sea where the Dogger Bank is situated (starts at 1.3°E).

Observations in May showed an increase in bottom and surface temperature for all transects. Thermocline formation began to form at 54.5 °N within the deepest locations on the transect (Figure 13). A thermocline was present for the whole longitudinal transect at 55.5°N, alongside 3 distinct water temperature layers being present within the stratified layer. At 55°N latitude, the thermocline covered greater longitudinal distances, where the stratified layer extended towards the coast, but was still constrained by shallow water situated at the Dogger Bank. The remaining transects for this month showed no evidence of thermocline formation. June saw a further increase in sea surface and bottom temperature with an increase in water column stability in the longitudinal transects at the latitudes of 55.5°N, 55°N and 54.5°N. This was due to an increase in temperature difference between surface and seabed, alongside the increase in spatial coverage of the thermocline on each transect. At 54°N there was a small thermocline in regards to spatial coverage present at the most offshore end of the transect. It was situated where the deepest waters were observed at this latitude. There was the overall trend for all months, in which stratification formed within the deepest regions at each latitude first, and then increased in spatial distribution as water temperatures increased each month.

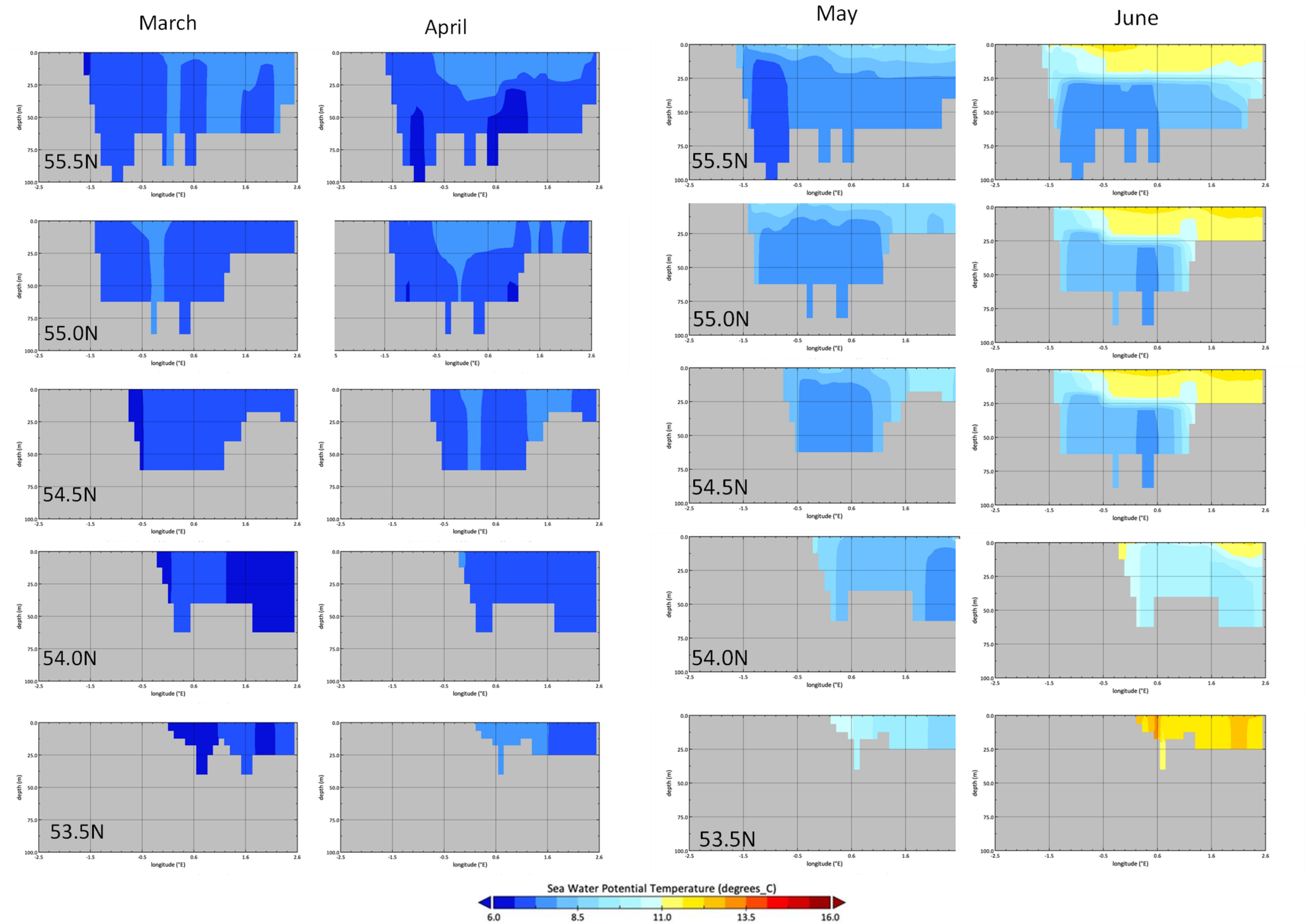

Figure 13. Longitude-latitude plots displaying water column temperature for 5 longitudinal transects (Location of transects displayed in Figure 12) for the months of March, April, May and June in 2022.The latitudes on each plot corresponds to a horizontal line in Figure 12. The grey areas on the plots are areas of no data as a result of these depths either being areas of land mass or seabed.

Sea surface temperature:

Satellite observations for sea surface temperature (SST) show a clear seasonal pattern of surface water warming each month from March to June (Figure 14). The lowest temperature from satellite observations was 6.5°C in March, rising to a maximum of 15°C in June (Figure 14). In March, the colder areas of water coincide with the regions in the North Sea that have the greatest MLD. The central North Sea in March was approximately 1°C warmer than the southern and north-eastern regions (Figure 14A). Between the months of April to June, sea surface warming was coupled with decreasing water column mixing. In May and June, the central North Sea had the highest temperatures which coincided with the region in the North Sea where greatest stratification was evident. A potentially anomalous result was identified, with April to June showing elevated water column mixing along with high temperatures in the region of the southern North Sea, south of the Dowsing SmartBuoy. However, looking at the bathymetric map (Figure 5), there could be a correlation with shallow water and higher SST alongside proximity to river outflows. This region had consistently high temperatures from May to June as well as being the shallowest area of the whole sample region. Another anomaly observed was the inshore coastal region between Whitby and Scarborough, which remained relatively cool in comparison to the surrounding areas. In particular, water temperature for the Scarborough and Whitby wave buoy site was approximately 1°C cooler than the Hornsea site and 2°C cooler than the area around the Tyne/Tees buoy. This area was characterised by a highly mixed region with relatively deep bathymetry compared to the area below Flamborough Head.

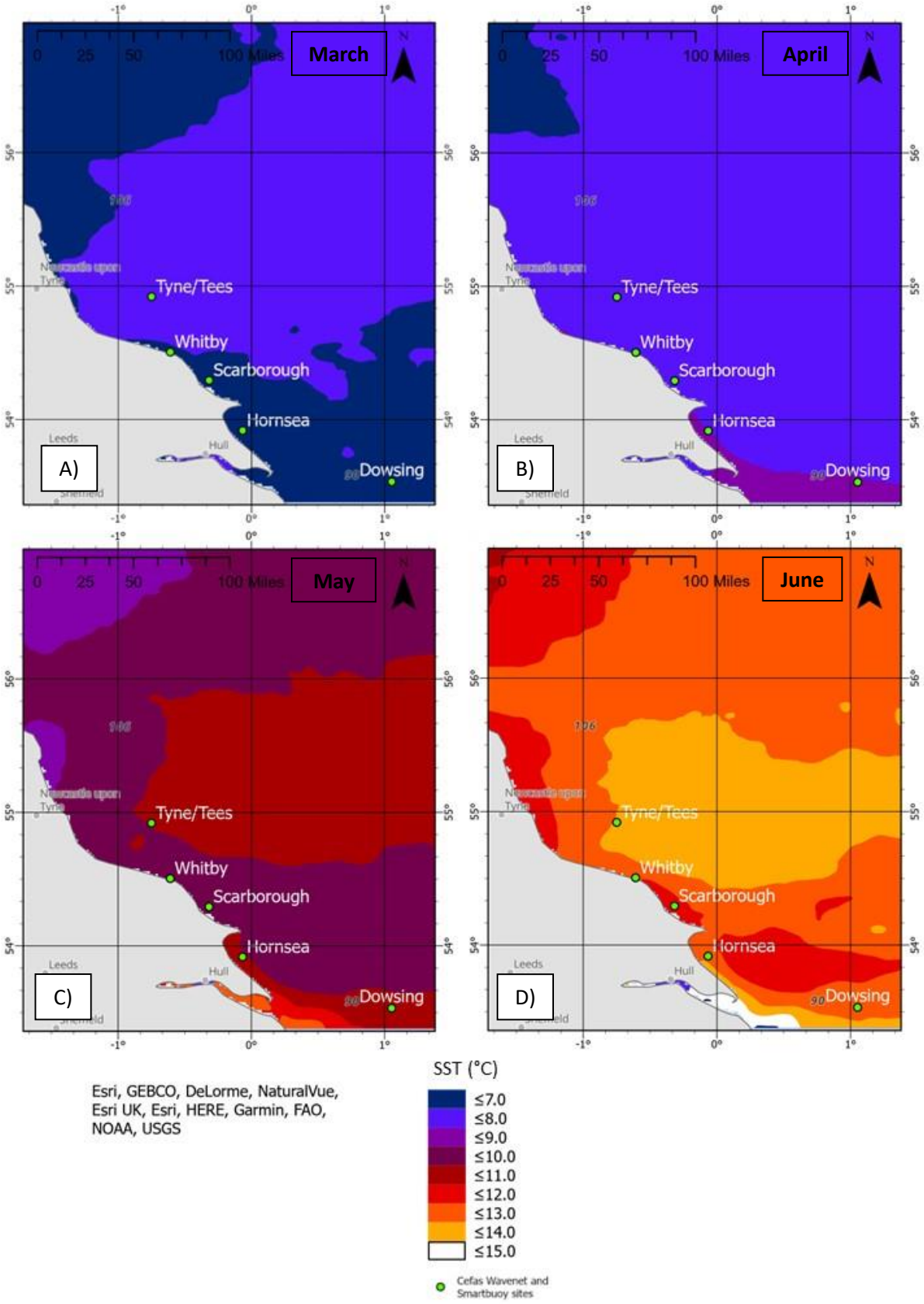

Figure 14. Monthly averaged SST for the months March (A) – June (D) 2022 with CEFAS Wavenet and SmartBuoy locations shown. Tyne/Tees, Whitby, Scarborough, Hornsea and Dowsing labels are the names of each of the CEFAS wavenet and smartbuoy used.

SST measurements for all Cefas SmartBuoy sites showed clear seasonal patterns in surface warming during the spring and summer months, with a decline in temperature in autumn and winter (Figure 15). SST was lowest for all wave buoy sites in February, with the highest SST recorded from all buoys in August. The overall highest temperature recorded was 17.1°C at the Dowsing buoy in March, with the lowest observed temperature recorded at the Hornsea site in February with a value of 6.5°C. The Dowsing and Tyne-Tees buoys had the overall highest temperature from early spring to late summer, with both sites having closely matched SST from March to July. The Dowsing site then experienced greater warming from July to June with 0.52 °C difference when compared to the Tyne-tees. This correlated closely with the observed satellite-derived SST shown in Figure 13. The SmartBuoy that recorded the overall lowest monthly SST from spring to late summer (March – August) was Scarborough, (maximum 15.5°C in August, minimum 7.2°C in March).

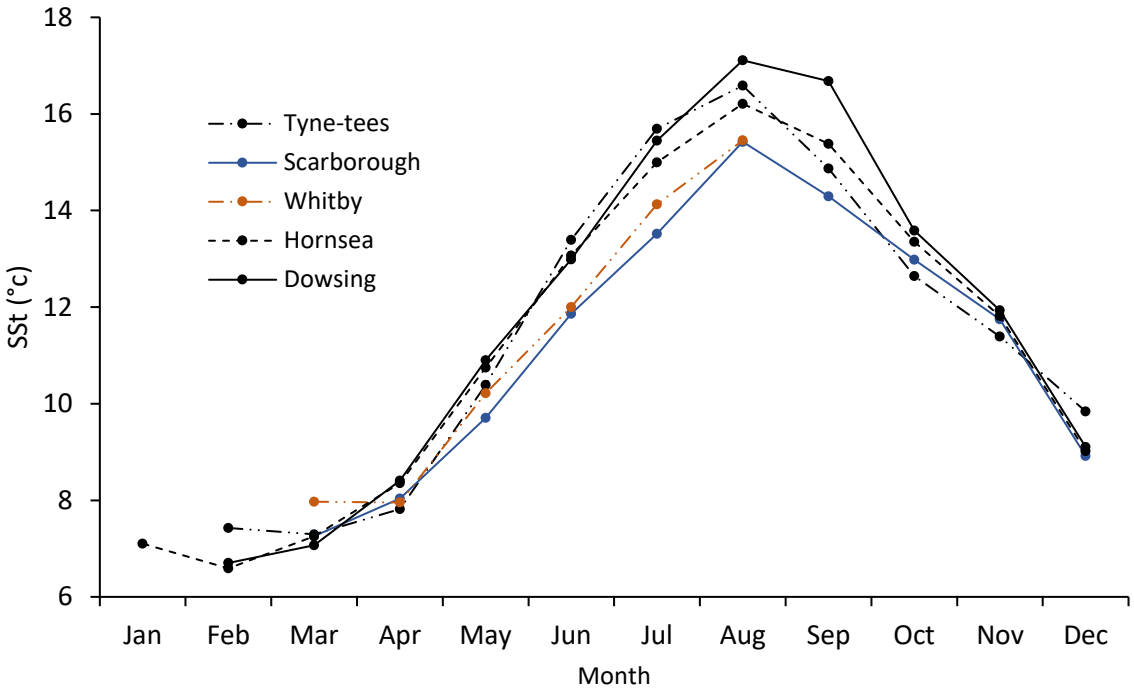

Figure 15. Average monthly Sea Surface Temperature (°C) from a range of CEFAS Wavenet and smartbuoys sites on the north-east coast of the Uk in 2022.

Three Cefas SmartBuoy sites were chosen (located at the top, middle and bottom of our sample area) to check the reliability of SmartBuoy SST against satellite observations. Measured temperature values from the buoy data matched closely with extracted values from remotely sensed data as seen in Figure 16. This helps to verify the accuracy and reliability of satellite SST data being used within the project, in particular the use in the spatial SST maps depicted in Figure 14.

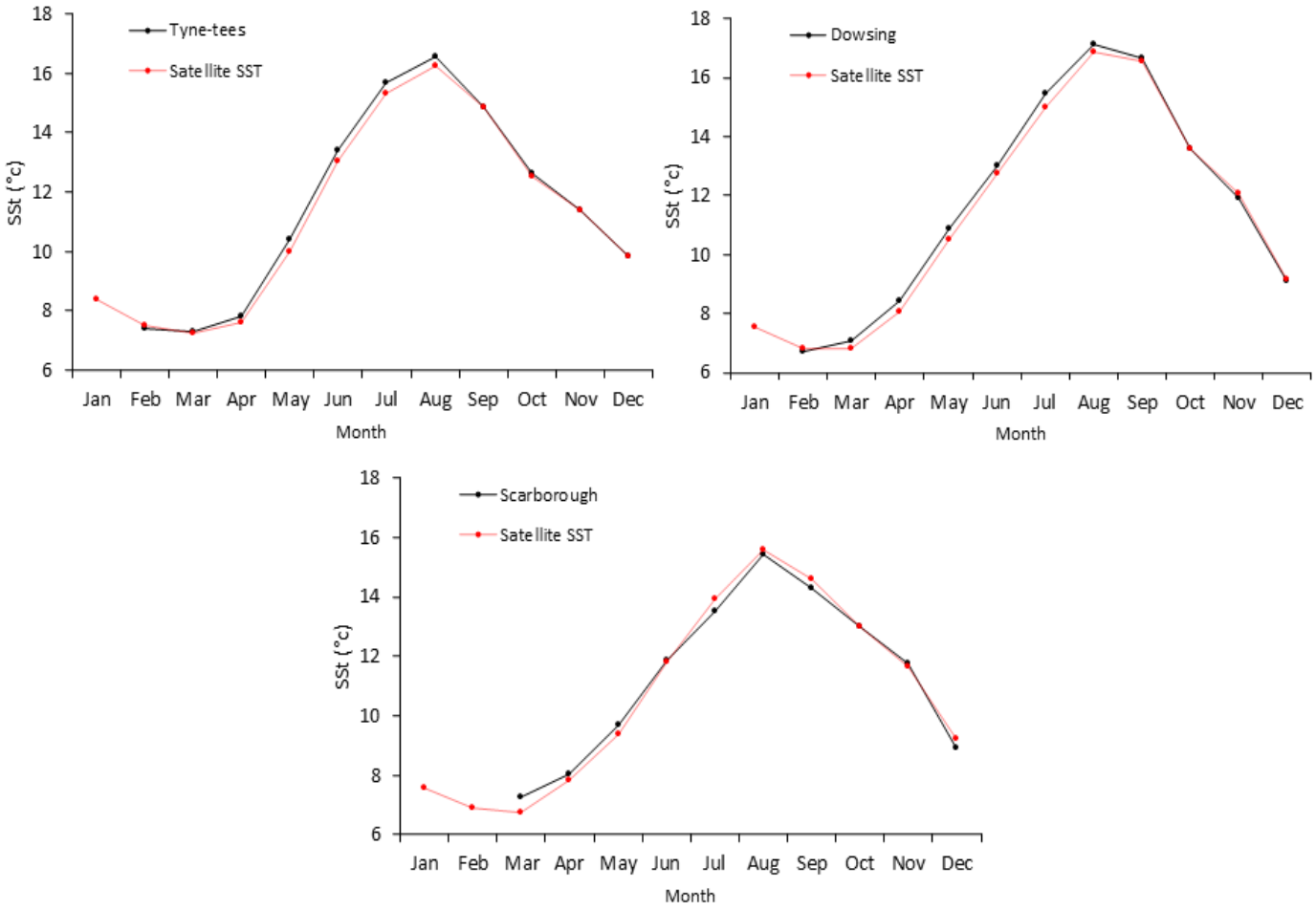

Figure 16. Average monthly CEFAS Wavenet and SmartBuoy SST recordings(black line) (°C) compared against OSTIA satellite extracted monthly average SST (Red line) (°C) for the corresponding buoy site. The SmartBuoy sites used were the Tyne-/Tees (A), Dowsing (B) and Scarborough (C).

In situ CTD casts:

Site M19 (Staithes cruise, Inshore) in the permanently mixed region showed trends of a weak thermocline due to the gradual temperature gradient within the thermocline (Figure 17). Temperature began to decline with depth at around 7m (Top of the thermocline) then reached coldest values at around 20m (Bottom of the thermocline). The temperature difference between the surface and bottom was 1.5°C. A weak subsurface chlorophyll maximum (SCM) was observable with maximum values of 9.5 RFU being measured at 10m. However, there is variability within CHL measurements within the top 13m of the water column. Dissolved oxygen (DO) is supersaturated within the depth

region around where CHL is greatest and then declines with depth, reaching its lowest values at the same depth the thermocline ends. The water profiles for salinity showed a potential fresher water layer sitting above a more saline layer. This was apparent by a rapid increase in salinity and density from 1-3m. Salinity and density then had gradually increased with depth and reached lowest values at 20m. These salinity trends were Similar to those observed at station M17 (Figure 19).

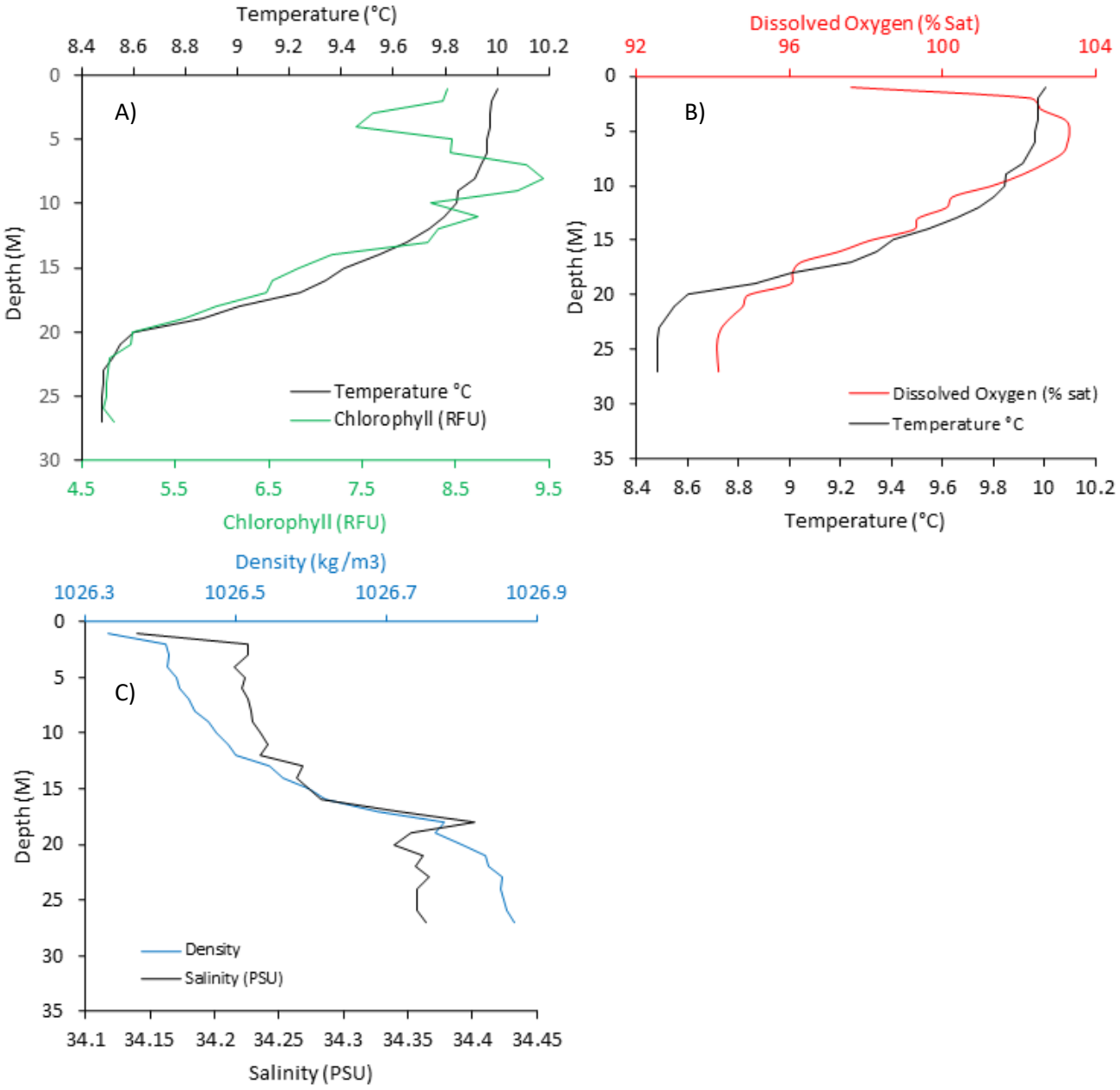

Figure 17. CTD water profiles for site M19 on the Staithes cruise on the 12th May 2022. A) Temperature (℃) and chlorophyll (RFU) water column profiles, B) Dissolved oxygen (%sat) and Temperature (℃)water column profiles, C) Density (kg/m³) and salinity (PSU) water column profiles

The CTD plot for site M16 (Staithes cruise, Offshore), situated in the offshore stratified zone, showed the area to be stratified, with evidence of strong thermocline/pycnocline (Figure 18). The thermocline/pycnocline were between 13-18m deep, with approximately a 2°C temperature difference

and 0.5 (Kg/m^3) density difference between the water above and below the thermocline/pycnocline. Salinity generally followed the same trend as temperature and density (limited variability up until 13m and then increased with depth up until 18m); however, the salinity levels of the surface water could be a potential anomalous result. In addition, there was clear evidence of a strong sub chlorophyll maximum (SCM) at approximately 11m, located just above the thermocline, due to maximum chlorophyll fluorescence (8.5 RFU) being observed below the surface. Chlorophyl fluorescence was 7 RFU greater than the maximum values recorded on the Bridlington cruise (Figure 20, 20 & 21). Sub surface DO was super saturated for the first 11m which coincided with peak Chlorophyll RFU providing further evidence of an active SCM.DO then declines by approximately 9% from 12m to 20m.

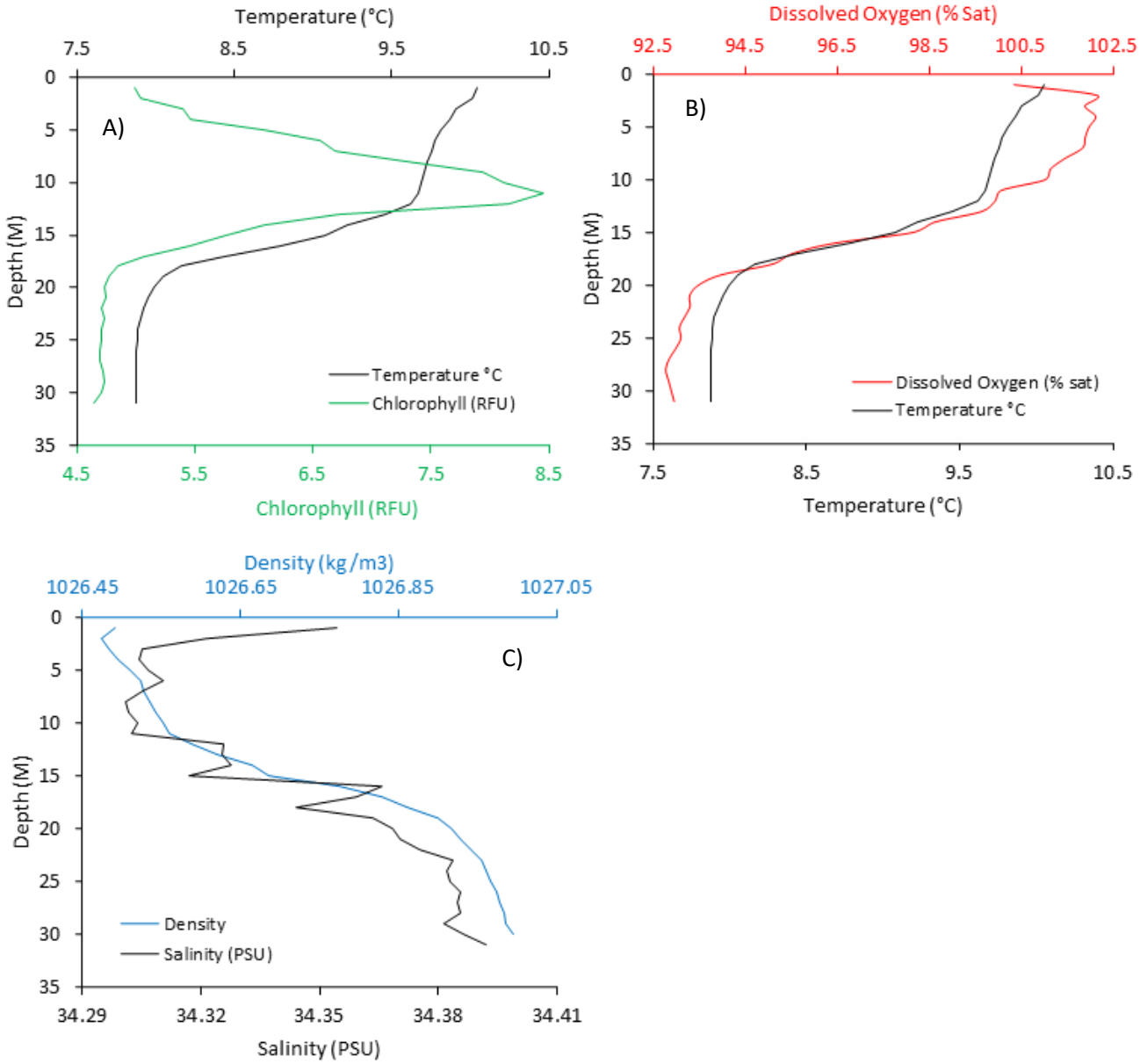

Figure 18. CTD water profiles for site M16 on the Staithes cruise on 12th May 2022. A) Temperature (℃) and chlorophyll (RFU) water column profiles, B) Dissolved oxygen (%sat) and Temperature (℃)water column profiles, C) Density (kg/m³) and salinity (PSU) water column profiles

At site M17 (Staithes cruise, Offshore), there was evidence of stratification as shown in Figure 19. The thermocline started at around 15m with a temperature difference from surface to bottom of around 2.3°C. A halocline was also present at site M17 due to the rapid increase in salinity by 0.55 PSU within the top 4m of the water column. This could suggest a fresher water layer sitting above a more dense and saline layer (halocline),. An SCM was also apparent between 10m – 15m where the concentrated chlorophyll values sit just above the thermocline. Chlorophyll values reached a maximum of approximately 9 RFU which is 0.5 RFU greater than at site M16. Super saturation of DO between 2m – 15m provides further evidence of a SCM as well as DO decreasing with chlorophyll and increasing depth.

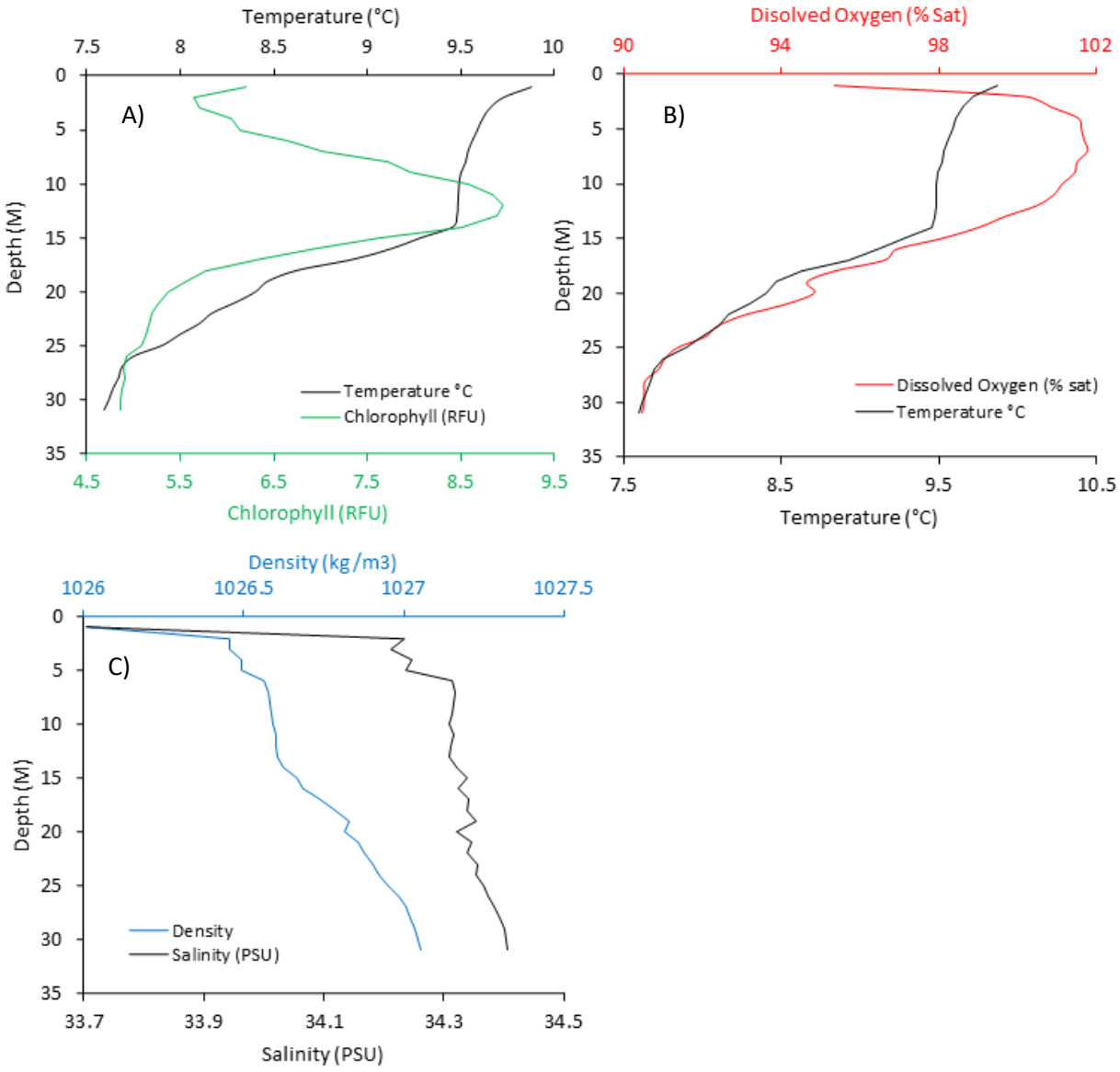

Figure 19. CTD water profiles for site M17 on the Staithes cruise on 12th May 2022. A) Temperature (℃) and chlorophyll (RFU) water column profiles, B) Dissolved oxygen (%sat) and Temperature (℃)water column profiles, C) Density (kg/m³) and salinity (PSU) water column profiles

The CTD plot for site J5, which was located in the inshore stratified zone (Bridlington cruise, inshore), showed a mixed water column (temperature difference of less than 0.7°C between the surface and bottom at 9m) (Figure 20). There was also variability in salinity to depth with PSU fluctuating by +/- 0.1 for the whole cast, suggesting the absence of halocline layer(s) at site J5. Density increased with depth, with the greatest increase in density at 3m – 4m (0.15kg/m^3). Chlorophyll was overall relatively low but had the highest RFU of all the Bridlington cruise sites. Chlorophyll increased at around 3m which coincided with the temperature decrease and density increase. DO percentage saturation decreased with depth, but overall, surface dissolved oxygen was low when comparing to every other CTD cast.

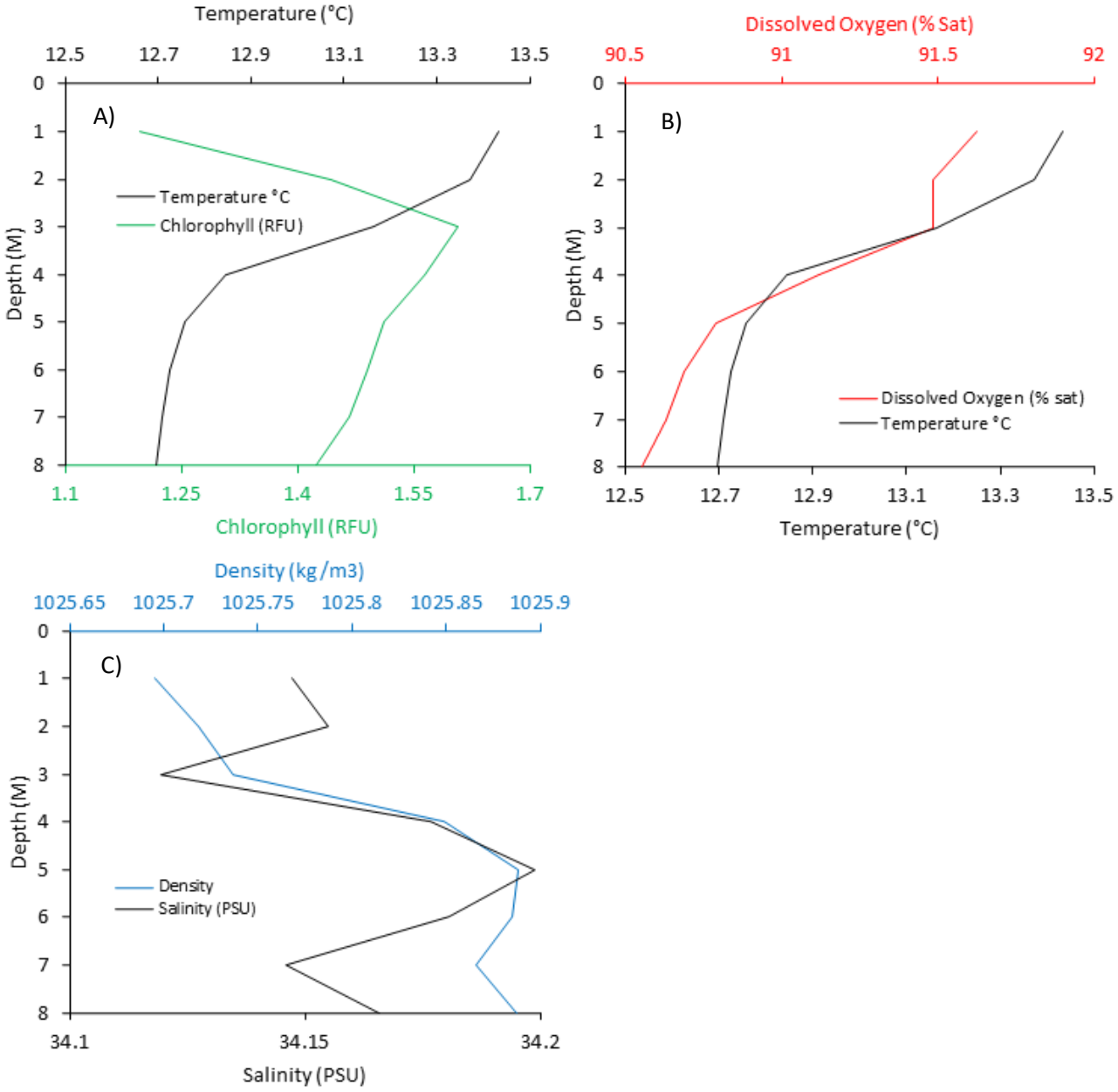

Figure 20. CTD water profiles for site J5 on the Bridlington cruise on the 9th June 2022. A) Temperature (℃) and chlorophyll (RFU) water column profiles, B) Dissolved oxygen (%sat) and Temperature (℃)water column profiles, C) Density (kg/m³) and salinity (PSU) water column profiles

J7 has the coldest surface temperature of all the Bridlington sites (Figure 21). Temperature decreased by approximately 1°C within the first 11m of the water column, with temperature remaining constant for the subsequent 32m. Density and salinity followed the same trend as temperature, with the largest rate of decrease occurring in the top 11m. This suggests there could have been a weak stratified layer at this site. Salinity trends showed a possible fresher water layer sitting on top of more saline water as shown by an increase in salinity at approximately 4m - 5m. Chlorophyll was greatest within the first 5m of the water column and fluctuated throughout the top 11m. It was then constant from 11m to the bottom. Dissolved oxygen was greatest within the top 5m of the cast, and then gradually decreased with depth for the rest of the cast.

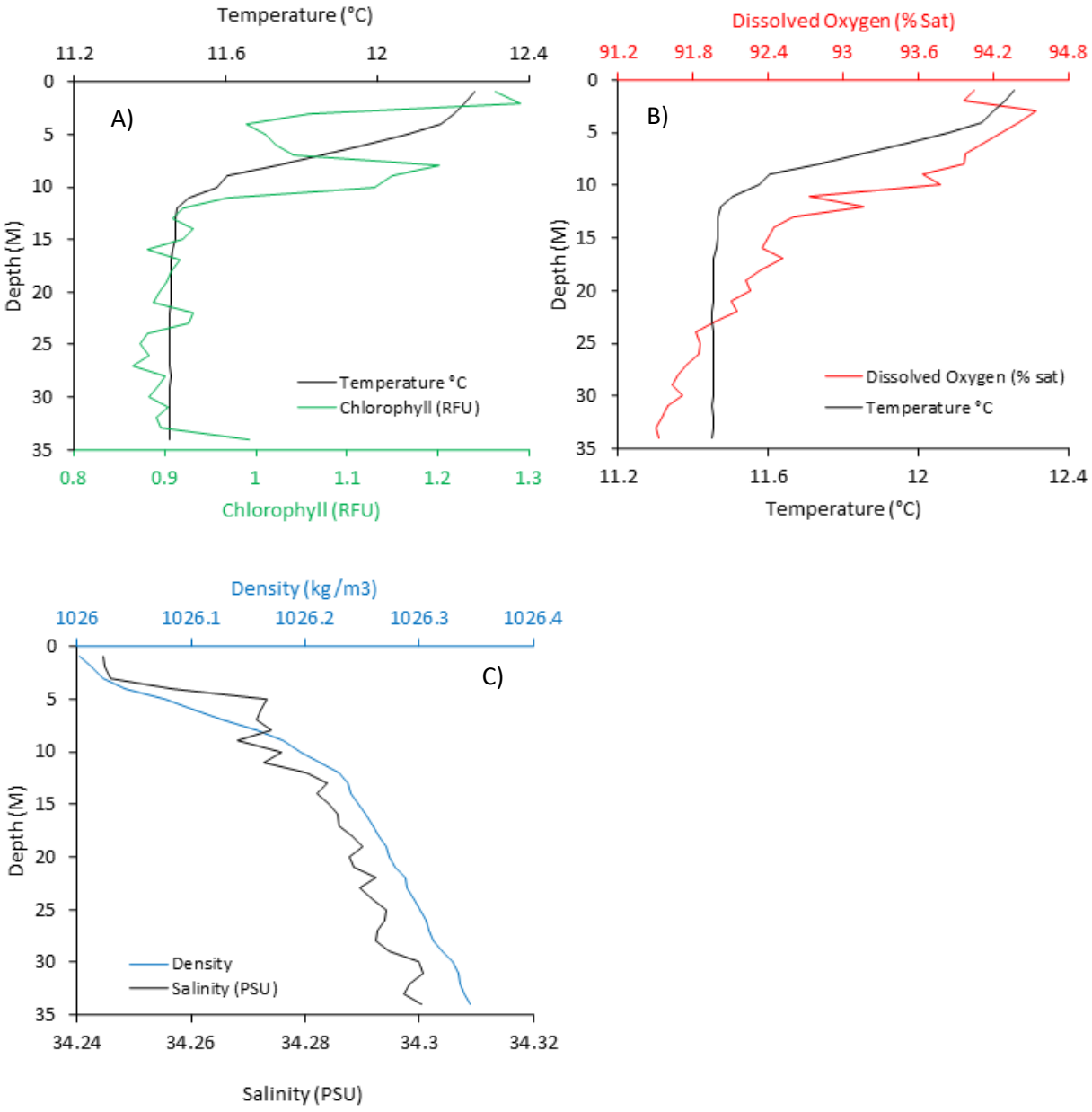

Figure 21. CTD water profiles for site J7 on the Bridlington cruise on the 9th June 2022. A) Temperature (°C) and chlorophyll (RFU) water column profiles, B) Dissolved oxygen (%sat) and Temperature (°C)water column profiles, C) Density (kg/m³) and salinity (PSU) water column profiles

At site J6 (Bridlington cruise, offshore) the casts showed the greatest temperature difference in the water column when comparing to the other Bridlington sites (Figure 22). There was a steep decrease in temperature by 1.5°C in the first 5m of the water column which coincided with an increase in density by approximately 0.3 Kg/m^3 within the same depth range. A potential anomalous result was from an observed spike in salinity by 0.7 PSU at around 3m, which was then followed by a rapid decreased of 0.6 PSU within the next 1m of the cast (Figure 22C). Chlorophyll values were almost negligible, with the highest values being recorded at 10m and 43m. Dissolved oxygen decreased with depth up until approximately 25m where it becomes constant down to 43m.

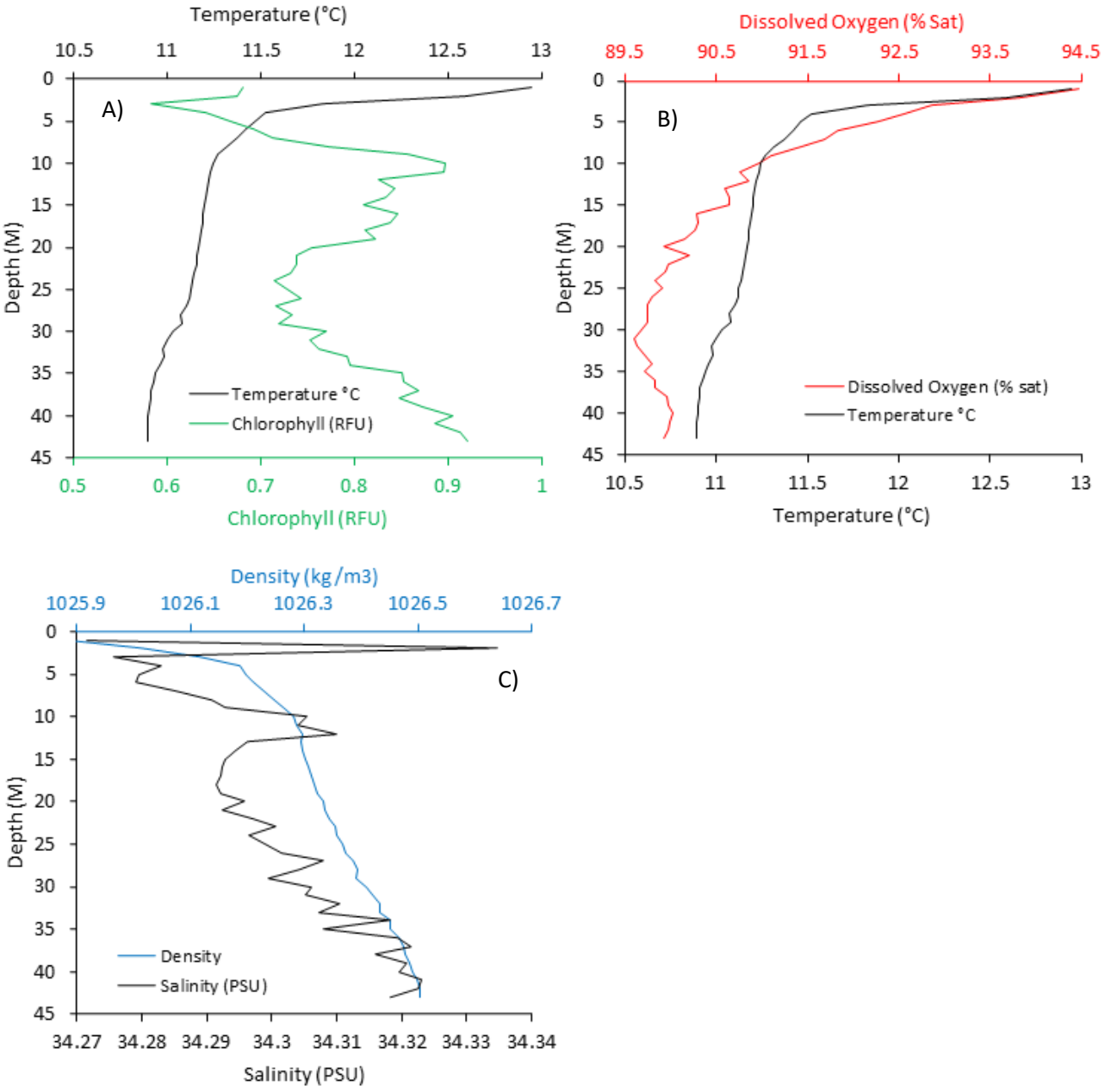

Figure 22. CTD cast profiles for site J6 on the Bridlington cruise on the 9th June 2022. A) Temperature (℃) and chlorophyll (RFU) water column profiles, B) Dissolved oxygen (%sat) and Temperature (℃)water column profiles, C) Density (kg/m³) and salinity (PSU) water column profiles

Comparing the CTD plots, Bridlington cruise sites (Stations J5, J6 and J7) had overall higher water temperatures at the surface and at depth, with lower chlorophyll values compared to the Staithes sites (Stations M16, M17, M19). Surface DO values were lower at Bridlington with a smaller DO gradient with depth. There was negligible difference in density and salinity between the Bridlington and Staithes cruise sites, with the overall lowest salinity being measured at site M17(Staithes) and lowest density at site J5 (Bridlington) . Both the Bridlington and Staithes transects showed trends of decreasing surface and bottom temperature with distance from the shore and fresher water being observed at inshore sites on both transects.

Phytoplankton:

Satellite observations:

All 10-day CHL average figures showed high CHL readings for all coastal areas between March and April (Figure 23). During May and June, lower CHL values were present in the coastal zone between the Northumberland coast and Flamborough Head (inshore stratified and permanently mixed zone). Figure 23A and Figure 23B showed no blooming in the central North Sea (map label ①) between the start and middle of March. An increase in CHL values off the coast of Northumberland (offshore stratified zone, map label ②) was observed with a maximum recorded 10-day average between 11/03/2022 to 20/03/2022 of 4 mg/m^3, showing early signs of the spring bloom forming (Figure 23B). The last 10 days in March (Figure 23C) saw a rapid increase in CHL concentration to values in excess of 10 mg/m^3 (inshore/offshore stratified zone, map label ②). This covered a large proportion of the North Sea which is depicted in the area outlined by Figure 23C (map label ①&②). The CHL in the central North Sea remained relatively low for this period (map label ③) with slightly elevated values of <6mg/m^3 around the Dogger Bank (permanently mixed zone, map label ④) and deep coastal regions from Middlesbrough to Flamborough Head (permanently mixed zone, map label ⑤).

At the start of April (Figure 23D), values of CHL remained high off the coast of Northumberland (inshore/offshore stratified zone, map label ②), meaning CHL for this region had maintained values of ≥ 10mg/m^3 on average for around 20 days. The central northern parts of the North Sea (Figure 23D, Point ①) had decreasing CHL concentrations. Satellite coverage in mid-April (Figure 23E) was limited due to clouds throughout this period. However, a decrease in CHL values was observed off the coast of Northumberland (inshore/offshore stratified zone, map label ②), decreasing to a maximum value of 6 mg/m^3. A central North Sea (Figure 23E, map label ③) bloom appeared with high values of around 10 mg/m^3. A secondary bloom in late April (Figure 23F) for the northern part of the North Sea re-appeared and extended south to more central areas (map label ①&③). CHL values in the inshore and

offshore stratified zone off the coast of Northumberland in late April (Figure 23F, map label ②) increased again to values of ≥ 10 mg/m^3, extending further North and South along the coastal region than the previous blooming event in late March.

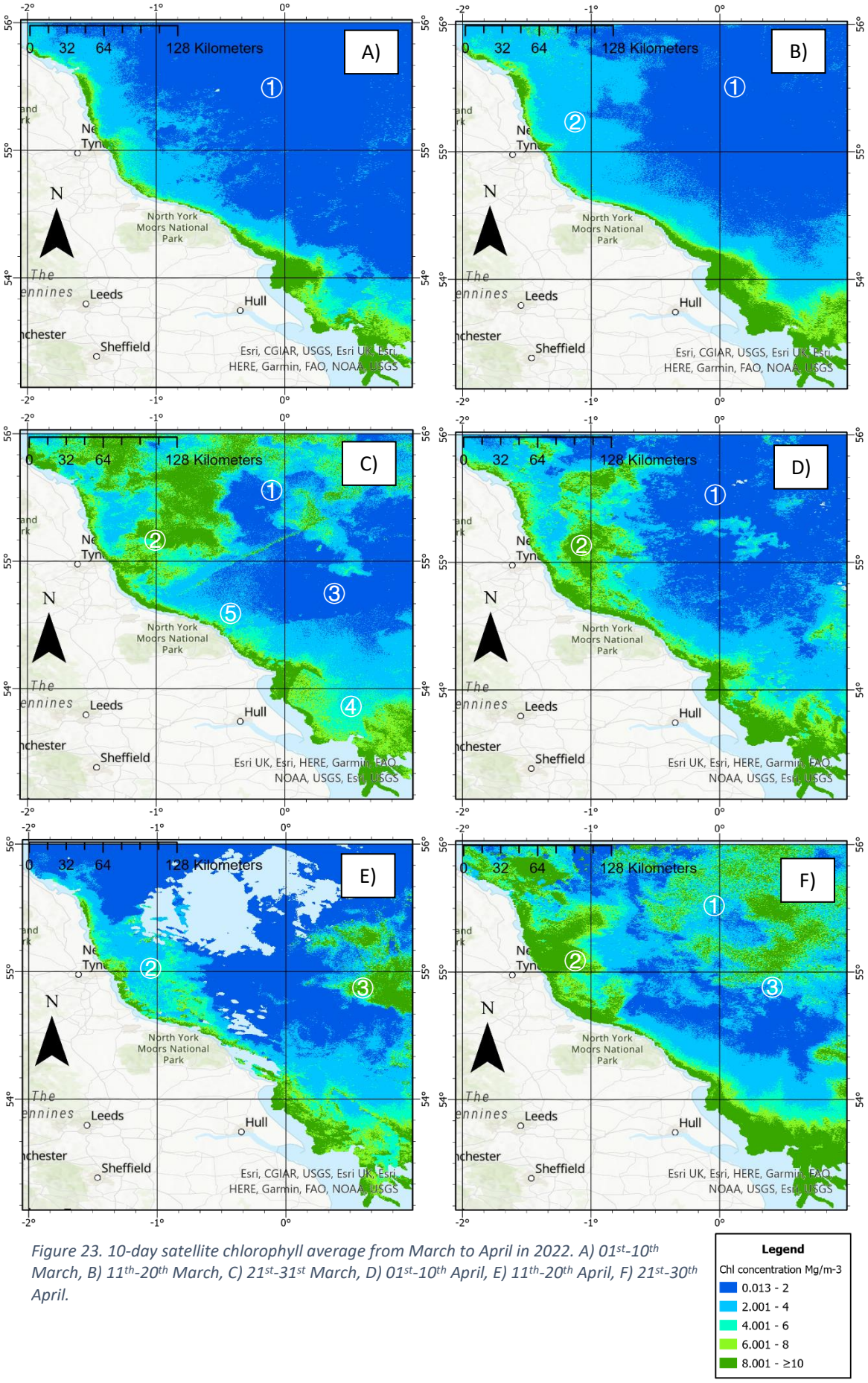

Figure 23. 10-day satellite chlorophyll average from March to April in 2022. A) 01st-10th March, B) 11th-20th March, C) 21st-31st March, D) 01st-10th April, E) 11th-20th April, F) 21st-30th April.

Figure 24A also had limited satellite coverage for the 10-day maximum CHL average, but there were key signs of the bloom reducing in the northern North Sea at the start of May (map label ①). A small area off the coast of Whitby (permanently mixed zone) had small pockets of highly concentrated areas of CHL (map label ②). In the mid-May CHL satellite observations (Figure 24B) showed a new bloom between Flamborough Head and the Dogger Bank (map label ③) with maximum CHL values of ≥ 10 mg/m^3 (permanently mixed zone). In the mid-May 10-day CHL average, the central North sea (Map label ④) had the most significant blooming across the area of interest, alongside it being this region's first blooming event of the season, with the majority of the blooming events occurring at more Northern latitudes. In Figure 24B and at map label ②, elevated CHl values of <8 mg/m^3 off the coast of Whitby were observed (inshore areas within the permanently mixed region, with more offshore blooming occurring in the offshore stratified zone). For the last 10-day average in May (Figure 24C), blooming was reduced to <6 mg/m^3 off the coast of Northumberland (map label ⑤) and was present at more northern latitudes than previously observed in that area. Blooming at map label ④ reduced in magnitude and spatial coverage in late May, with values not exceeding 6 mg/m^3. At the start of June (Figure 24E), there were no significant blooming events that exceeded 4 mg/m^3 in Latitudes above 55°N, however, there were small patches of raised CHL values between Flamborough Head and the Dogger Bank (permanently mixed zone, map label ③) where values were predominantly <4mg/ m^3. There were small patches of raised CHL values off the coast of Northumberland (Figure 24E, Figure 24F, map label ⑤) in mid to late June, alongside a small bloom with maximum values of 8 mg/m^3 off the coast of Flamborough Head (permanently mixed zone, map label ⑥). Overall trends observed between March and June, show that blooming events occurred first in more northern latitudes (offshore/inshore stratified zone) , with bloom timings in southern latitudes (permanently mixed zone) being delayed until early summer.

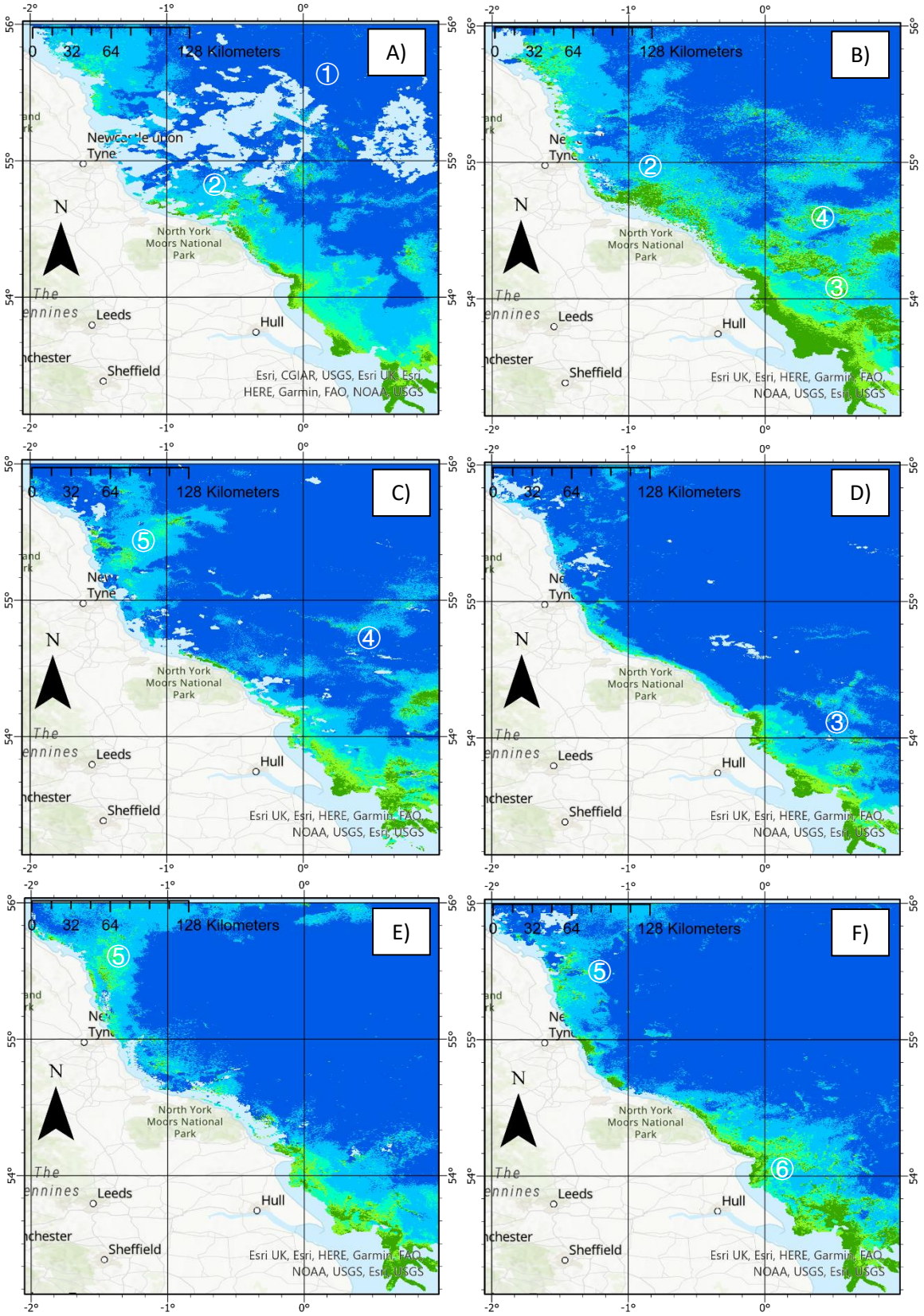

Figure 24. 10-day satellite chlorophyll average from May to June in 2022. A) 01st-10th May, B) 11th-20th May, C) 21st-31st May, D) 01st-10th June, E) 11th-20th June, F) 21st-30th June

In situ chlorophyll measurements

Maximum *In situ* chlorophyll measurements across the survey areas are displayed in Figure 25. The trends observed showed maximum chlorophyll concentrations on the 02/04/22 where CHL reached a maximum value of 7.7 mg/m^3. Thereafter, the overall trends show decreasing chlorophyll up until 01/06/22 (0.8 mg/m^3). Chlorophyll then began to increase thereafter. This coincided with blooming events represented in Figure 23 at the end of March and beginning of April. Decreasing chlorophyll concentrations from April to May and May to June are observed from both Figure 23 and Figure 24, helping to validate the reliability of remote sensing for chlorophyll data. Variability in chlorophyll concentrations was obsevred between the 05/05/22 and 12/05/2022, which may be a result of the samples within this time period being taken in more northern latitudes where chloprhyll blooming events were more pronounced.

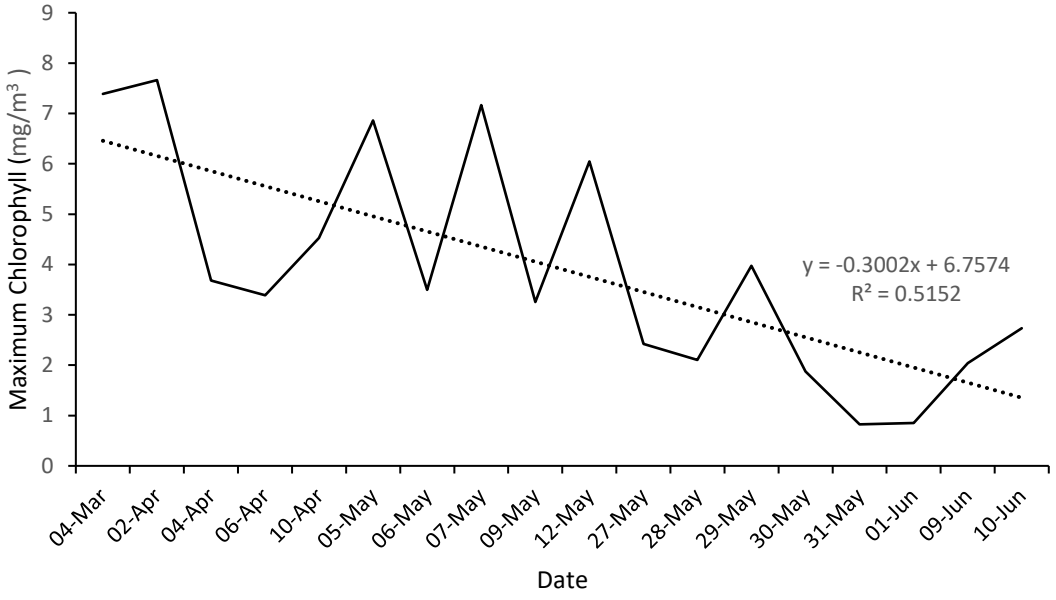

Figure 25. Maximum chlorophyll values (mg/m^3) for all in situ sites sampled in 2022 with a trendline overlayed

In situ chlorophyll a extractions were averaged monthly and graphically displayed in Figure 26. As a result of limited data from outside our sampling period of March to June, Environment Agencies monthly sampling regime sites were used to fill any outstanding monthly gaps for the year of 2022 (limited data points for the offshore stratified zone due to their sampling regime being predominantly coastal). Zonal averages were taken and trends were observed from this data, which showed the inshore stratified region to have the highest recorded monthly chlorophyll concentration (8.8 mg/m^3 in April. This was 4.9 mg/m^3 and 8.13 mg/m^3 greater than the permanently mixed and offshore stratified zone respectively. However, results should be viewed with caution due to limited data points within

the inshore stratified and offshore stratified region for these months. Peak chlorophyll values were also greatest in April for the permanently mixed region, whereas the offshore stratified zone contained the greatest chlorophyll concentration in May. The monthly averages for the permanently mixed regions, show chlorophyll concentrations to be lowest in winter months, with elevated values in spring and summer. There are two clear peaks in chlorophyll concentrations in the monthly time series which suggest a blooming event in April and July. The rapid increase in chlorophyll in April for the inshore stratified zone, coincides with elevated chlorophyll a concentrations as depicted in Figure 23. A potential anomalous result within this data is that the offshore stratified region had the lowest chlorophyll values compared to the other zones. Looking at the maps in Figure 23, the inshore stratified/offshore stratified region bloom earliest, with the largest chlorophyll concentration for the area, but the *in situ* values do not reflect this. This could possibly be a result of limited data points which skews the findings for these regions.

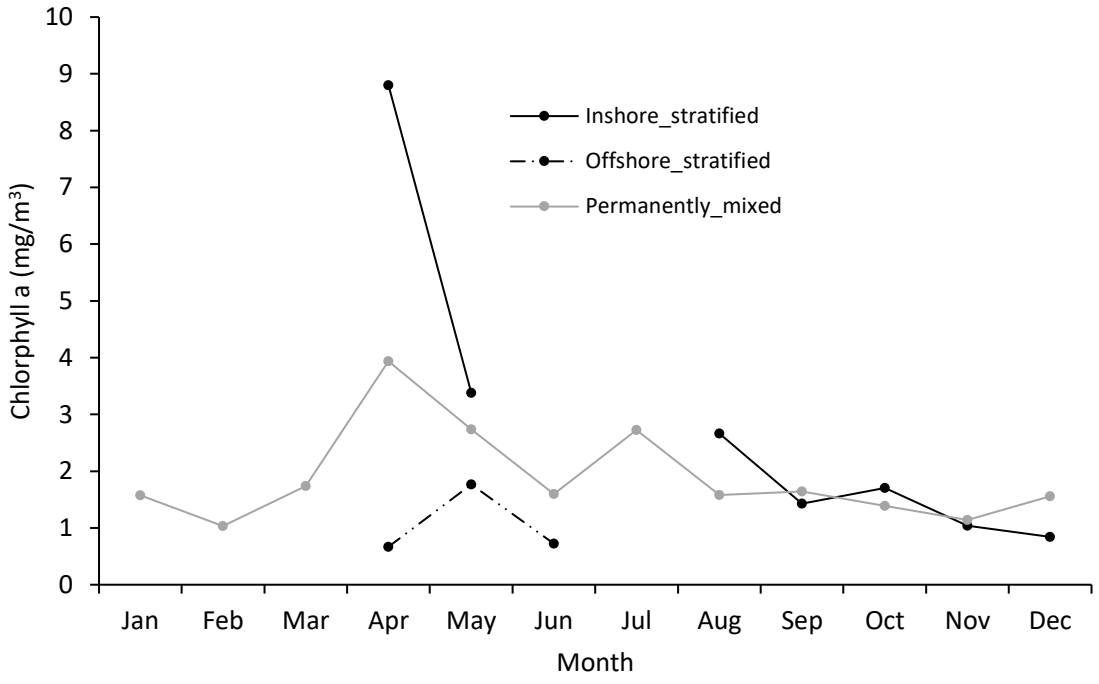

Figure 26. Monthly zonally averaged in situ extracted chlorophyll a measurements (mg/m³) from Environment agency sampling and our own sampling for 2022.

Satellite monthly averaged chlorophyll concentrations for each hydrodynamic zone (Figure 27) portrays spatial and temporal dynamics of chlorophyll to be elevated in the majority of months when compared to *in situ* values. Winter chlorophyll values are highest for all zones, specifically in regards to January and February when compared to spring and summer months. The inshore stratified region also has elevated values in October which could suggest these elevated concentrations in winter months are an artefact of turbidity. The three zones have elevated SPM and wave height during the months of

January, February and October which coincide with elevated satellite chlorophyll measurements. In addition, the decline for all three zones in chlorophyll concentrations from February to March suggests these elevated values in winter are attributed to SPM, with March being the month where MLD starts to shallow, wave height decreases and chlorophyll concentration increases which is observed from Figure 23 and Figure 24. This further verifies that turbidity skews the data. There are similar trends in chlorophyll concentrations when compared to monthly averaged SPM (Figure 27 and Figure 36). The greatest correlation was between the offshore stratified region, which had the lowest SPM and lowest chlorophyll when compared to the other two zones. There were similar patterns with regards to the peak and troughs in monthly averages between the two variables. Figure 27 shows that the offshore stratified zone has the lowest chlorophyll concentration of all 3 sites, with the inshore stratified region recording the highest chlorophyll values every month. Chlorophyll values recorded for each zone are not beyond the realms of possibility with maximum recorded chlorophyll concentrations peaking at 10.57 mg/m^3 in May within the inshore stratified region. There is clear evidence of blooming events in April and May due to highest recorded chlorophyll values being observed when compared to the remaining summer months. The inshore stratified region showed peak chlorophyll in April and May, whereas the offshore stratified region and permanently mixed region did not have the highest values in this spring period, but instead was highest in the summer period. Inshore stratified zone had a spring bloom of the greatest magnitude, with a value of 10.57 mg/m^3 in May, with the offshore region recording the smallest bloom in April with a value of 2.87 mg/m^3. The inshore stratified bloom had concentration of 7.7 mg/m^3greater than the offshore stratified region.

These blooming event timings observed from satellite chlorophyll data correlate closely with elevated chlorophyll a values in the *in situ* data alongside the satellite maps in Figure 23 and Figure 24. With regards to chlorophyll concentrations, there was a correlation between zones which had the highest concentrations and lowest concentrations, with both *in situ (*Figure 26*)* and satellite extracted data (Figure 27) deeming the inshore stratified region to have the largest bloom and the offshore stratified to have the smallest. However, values recorded between the two methods show weaker trends. The peak bloom in April for all sites showed satellite chlorophyll concentrations to be 2.04, 2.11 and 2.2 mg/m^3 greater than the *in situ* values for the inshore stratified, permanently mixed and offshore stratified regions respectively. In addition, there is a potential anomaly with satellite data showing sustained elevated chlorophyll values in May for the inshore stratified region, but the *in situ* values shows a significant decrease in concentrations from April to May. Another potential anomaly is elevated values in the *in situ* chlorophyll extractions in July, against satellite data which shows a gentle decrease in concentrations from May through to August in the permanently mixed zone.

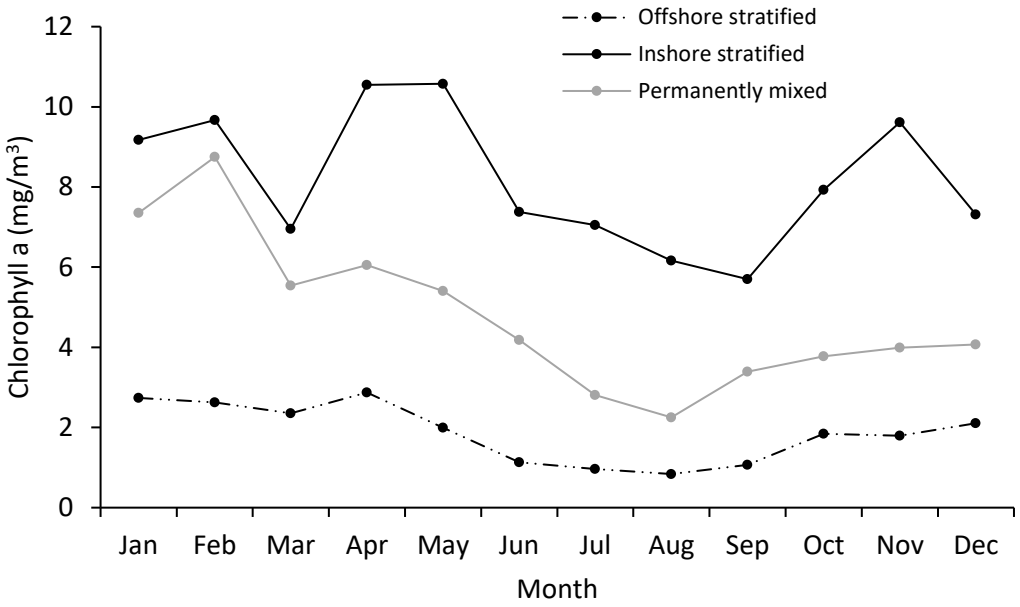

Figure 27.Monthly averaged satellite chlorophyll a concentrations for derived zones in 2022.

Underwater light and light attenuation:

In situ light attenuation vs Jerlov light attenuation:

A proposed classification by Jerlov in 1951 suggested global ocean water types can be categorized by differences in their downwelling diffuse spectral attenuation coefficient K_d (in m^{-1}). Over time, the classifications have evolved into 10 different characteristic waters, and consist of 5 coastal and 5 offshore water types. The features of each of these water types are summarized in Figure 28 (Williamson & Hollins, 2022).

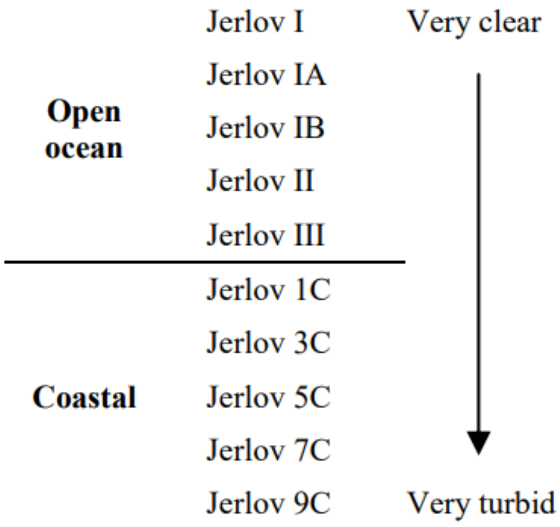

Figure 28. A summary of the Jerlov water types (Williamson & Hollins, 2022).

Figure 29 presents Jerlov's 10 different characteristic waters types (water types were derived from underwater light attenuation (K_d) measurements) and our own light attenuation (k_d) data collected from each cruise. Both sets of data are displayed so that our stations data can be assigned a water type classification based off Jerlov's defined water types (Figure 28). This provided a way of classifying water types around the North East coast. Each of our site data was assigned one of Jerlovs water classification based on which Jerloev water type it resembled closest too when comparing the differences in k_d at each specific wavelength. The location of each of our *in situ* sampling locations mentioned within the section below can be seen in Figure 2.

Light attenuation was lowest for the Staithes transect, with the lowest K_d of 0.149 m^{-1} at 555 nm at site M16 on 12th May (offshore sample in the offshore stratified zone) (Figure 29A). The highest light attenuation at Staithes was at site M19 (inshore, permanently mixed zone)with a K_d of 0.189 at wavelength 555 nm. M16 had the clearest water of the stations along the Staithes cruise transect, with spectra resembling closest to f_1c on the Jerlov plot, and M17 and M19 matching closely to g_3c. For each site, K_d was greater in the red wavelength channel bands (Figure 29A).

In Figure 29B, site J5 (9th June) on the Bridlington transect (inshore sample in the permanently mixed zone) had the highest light attenuation across the whole cast with the largest K_d value being 1.177 at 412.5nm. This site most closely resembles to Jerlov's j_9c spectra plot with a partial overlap with Jerlov's i_7c casts. Site J6 had the lowest K_d compared to all sites from the Bridlington cruise (offshore sample in the permanently mixed zone). The lowest k_d was recorded at 532.5 nm with a K_d (m^{-1}) value of 0.203. At the wavelength of 532.5 nm, site J5's K_d (m^{-1}) was 0.439 greater than that of site J6. Site J6's and J7's spectra closely follows the trends of Jerlov's g_3c with partial spectral overlap with f_1c spectra at 412.5 and 443.5nm. Sites J5 and J6 had higher spectral K_d in the blue wavelength bands of their casts compared to site J7 where the spectral K_d was greatest in the red wavelength channels.

Figure 29C compares the K_d spectra for the cruise from Grimsby to Whitby on 10th June (inshore samples in the permanently mixed zone). J16 had the highest K_d of all sites on the transect. This resembled the most turbid water on the Jerlov plot which ultimately correlated with spectra j_9c. The highest light attenuation for this cast had a $K_d(\lambda)$ value of 1.523 m^{-1} at 412.5nm. The clearest water and lowest attenuation was found at J13 with a lowest $K_d(\lambda)$ value of 0.243 at 555.1 nm. Comparing site J13 with Jerlov's spectra, it resembled closest to g_3c. A side-by-side comparison between the most turbid site at J16 and the least turbid site at J13, shows K_d at the wavelength of 555.1nm at site J16 was 2.956 times greater than at site J13. Sites J11,12 and 14 all had fairly similar spectral K_d profiles resembling parts of Jerlov's h_5c and i_7c casts respectively. K_d was highest for all sites - apart from site J12 - in the blue wavelength bands of the spectra.

The Staithes transect sites all closely resembled the least turbid coastal water sites on the Jerlov plot, whereas, at Bridlington, the inshore site resembled the highest turbidity water types, with the two more offshore sites resembling the second most least turbid water type. With regard to the Grimsby to Whitby cruise, due to the cruise sampling in inshore coastal regions, patterns were slightly different to the other cruises. The site closest to the Humber resembled the highest turbidity coastal water on Jerlov's plot, with the forthcoming sites moved towards lower turbidity coastal water types as they moved further offshore/greater distance away from the River Humber plume. The final site on the cruise then broke this trend, with increased turbidity and it was more representative of a more turbid coastal region on Jerlov's water types.

Comparing all our site's K_d spectra (Figure 29D), site M16 (offshore sample in the offshore stratified zone)had the lowest K_d, with J16 having the highest (inshore sample in the permanently mixed zone). Green wavelength bands, in particular 555.1nm, had the lowest K_d for the majority of the sites. Inshore sites tended to have higher K_ds for the blue wavelength channel's, whereas offshore site's spectra had greater K_ds in the red light wavelengths of the spectral cast. Overall, K_d decreased the greater the distance away from the shore, however the furthest offshore site sampled at Staithes did not have the lowest K_d. The mid-station site (M16) had the lowest K_d, with the furthest offshore sites having slightly higher values. In addition, for the EA Grimsby to Whitby cruise, K_d decreased with distance away from the Humber, up until the final site in Robin Hood's Bay (J14), where K_d increased again to the 4th highest K_d of all sites sampled.

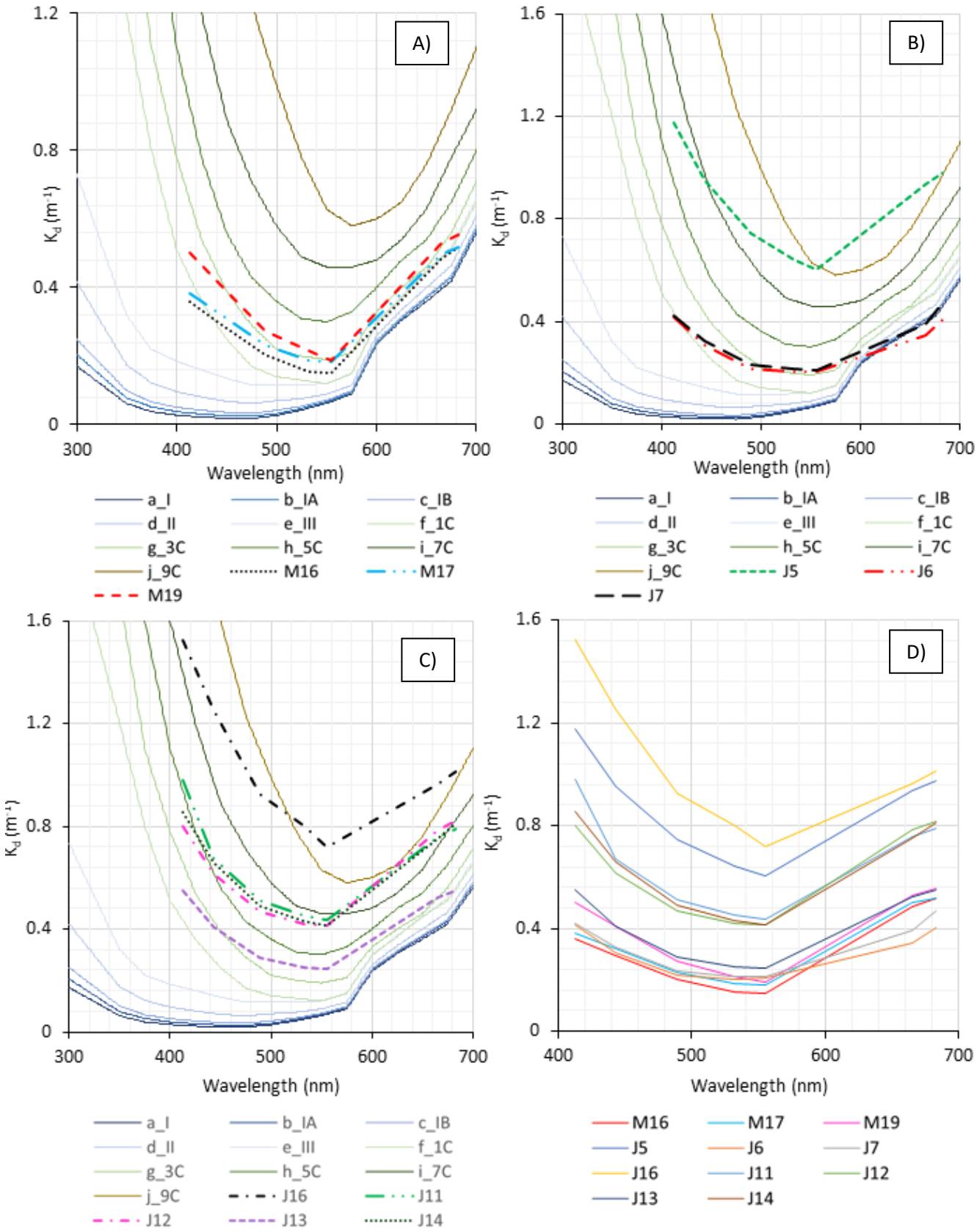

Figure 29. Jerlov's water classification types (water types were derived from underwater light attenuation (K_d) measurements) are overlayed on graphs A,B and C alongside our in situ *K_d light curves (data collected from the multispectral radiometer). A) – Staithes cruise (12th May), B) – Bridlington cruise (9th June), C) – Grimsby to Whitby cruise (10th June), D) – All in situ K_d measurements without Jerlov water classification overlayed. The Jerlov water types are displayed in plots A,B and C so a comparison can be made with our stations data. Each station can then be assigned a water type classification based off Jerlov's defined water types (Figure 28). This provided a way of classifying water types around the North East coast. Each of our site data was assigned one of Jerlovs water classification based on which Jerloev water type it resembled closest too when comparing the differences in k_d at each specific wavelength data was collected at*

Light attenuation:

Light attenuation measured *in situ*, and calculated K_d, shows a positive trend between the two methods (Figure 30). This trend helps verify the reliability of both satellite data and data collected *in situ*, providing evidence that the data collection methods were reliable and accurate. An outlier which skews the strength of the positive trend is highlighted by a red circle in Figure 30. This value was recorded at a significantly lower K_d *in situ* than observed from the satellite SPM derived K_d.

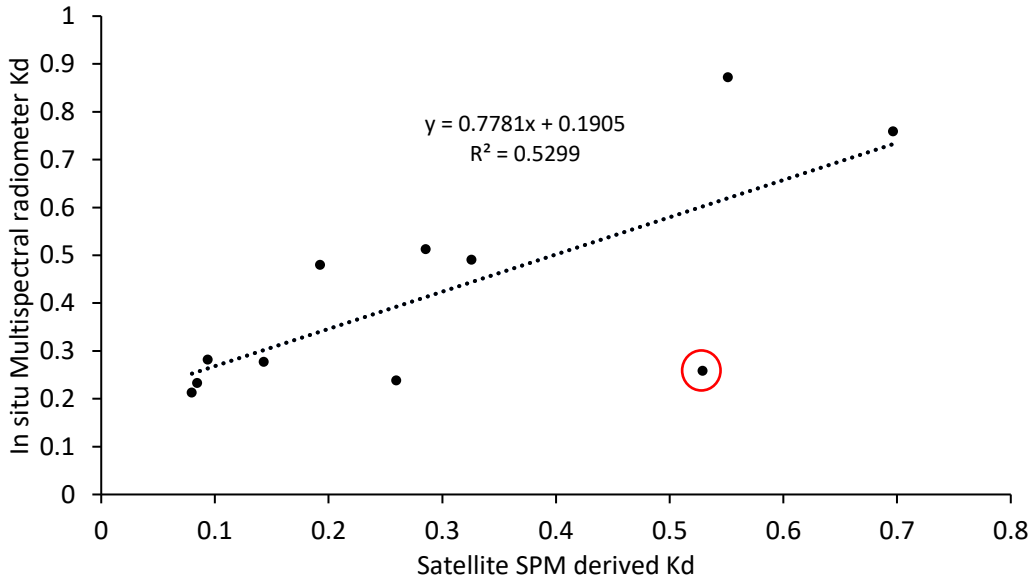

Figure 30. In situ K_d values against satellite SPM derived K_d for each in situ sample site in 2022. Red circle shows a potential anomalous result.

With satellite data being deemed as close to *in situ* K_d values, a monthly average K_d for each zone was calculated for 2022. The trends observed from Figure 31 show the permanently mixed region to have the greatest light attenuation for every month, when compared to the other zones. This correlates to Figure 11, where the region is a highly mixed zone, inferring that greater mixing increases SPM and therefore increased K_d respectively. The largest K_d observed in the PM zone was in February with a value of 0.613 m^{-1}. The offshore stratified zone had lowest light attenuation for each month, with the lowest observed being 0.073 m^{-1} in August. Each zone followed the same trend of elevated light attenuation between November and February with decreasing light attenuation from March through to August. The lowest K_d values for each zone were recorded in August. The PM zone showed the greatest decrease in light attenuation, with a difference in K_d of 0.5 m^{-1} from the maximum light attenuation recorded in February to the lowest value in August. In comparison, the OS zone had low amounts of variability in K_d between months, with only a 0.163 K_d difference between the maximum and lowest values recorded. A potential anomalous result is that all regions show an increase in K_d for September which then reduces

through into October, as well as slightly elevated values in April when compared to the previous month for the OS and IS regions. The Offshore stratified zone had the lowest and least variable diffuse attenuation coefficient out of all the zones.

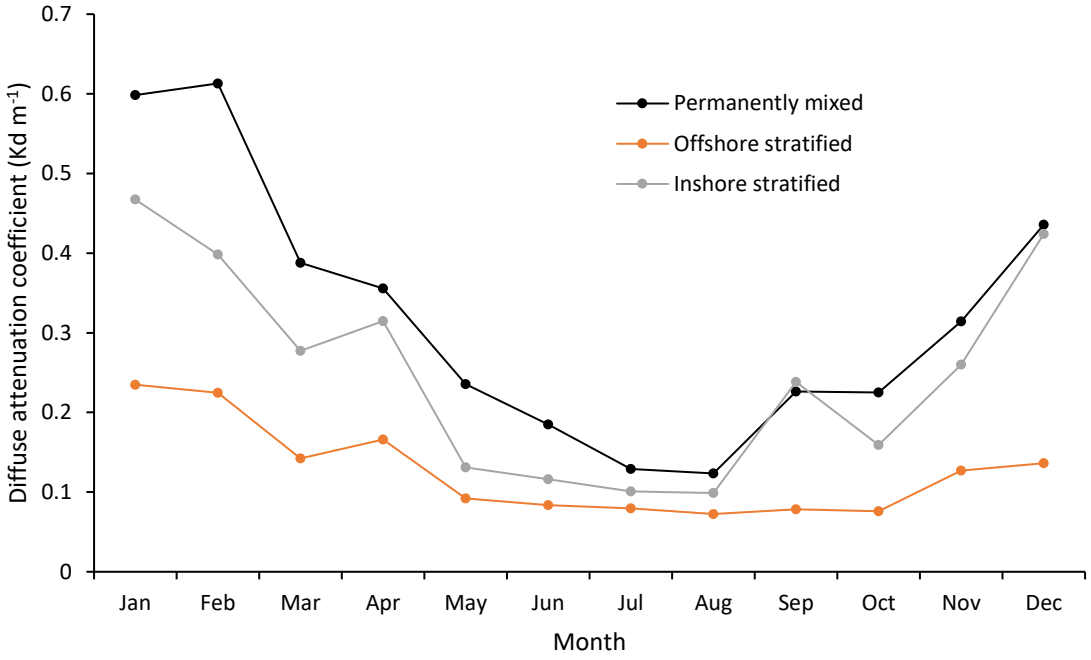

Figure 31. Average zonal monthly K_d derived from Satellite SPM for 2022.

To determine the factors that are influencing variability in light attenuation at our sites, K_d 489.2 was plotted against SPM, CHL, and CDOM (Figure 32). The trends that were observed showed SPM to be the main factor in influencing higher light attenuation. There was a positive trend between SPM and K_d 489.2 (Y=5.975, R^2=0.3592). When K_d was plotted against CHL, there a slight weak negative trend (Y=-0.8715, R^2=0.0096) and also no trend was found when K_d was plotted against CDOM. This helps validate that SPM has the greatest influence on light attenuation for the sites sampled in the months of May and June. In general, the Staithes sites (offshore stratified zone) had the lowest SPM with lower K_d. There was an anomaly where a high SPM value for one of the Bridlington sites (J6, permanently mixed region) was observed, but subsequently had the second lowest K_d value. This site also had the second lowest recorded values for CHL and CDOM. In regards to CHl and CDOM, two Bridlington sites (permanently mixed zone) had the lowest CHL values which coincided with the second lowest K_d value of all the sites. Another potential anomalous result was the highest recorded CHL value of 6 mg/m3 and also the highest CDOM value of 306 AU at a Staithes site (M19, permanently mixed zone), but which subsequently had the fifth lowest K_d of all 10 sites. The EA Grimsby to Whitby cruise sites (permanently mixed region) generally followed the trends of increasing SPM,CHL and CDOM

correlating most closely with K_d and with no significant outliers observed. The offshore stratified zone had the lowest and least variable light attenuation coefficient out of all the zones.

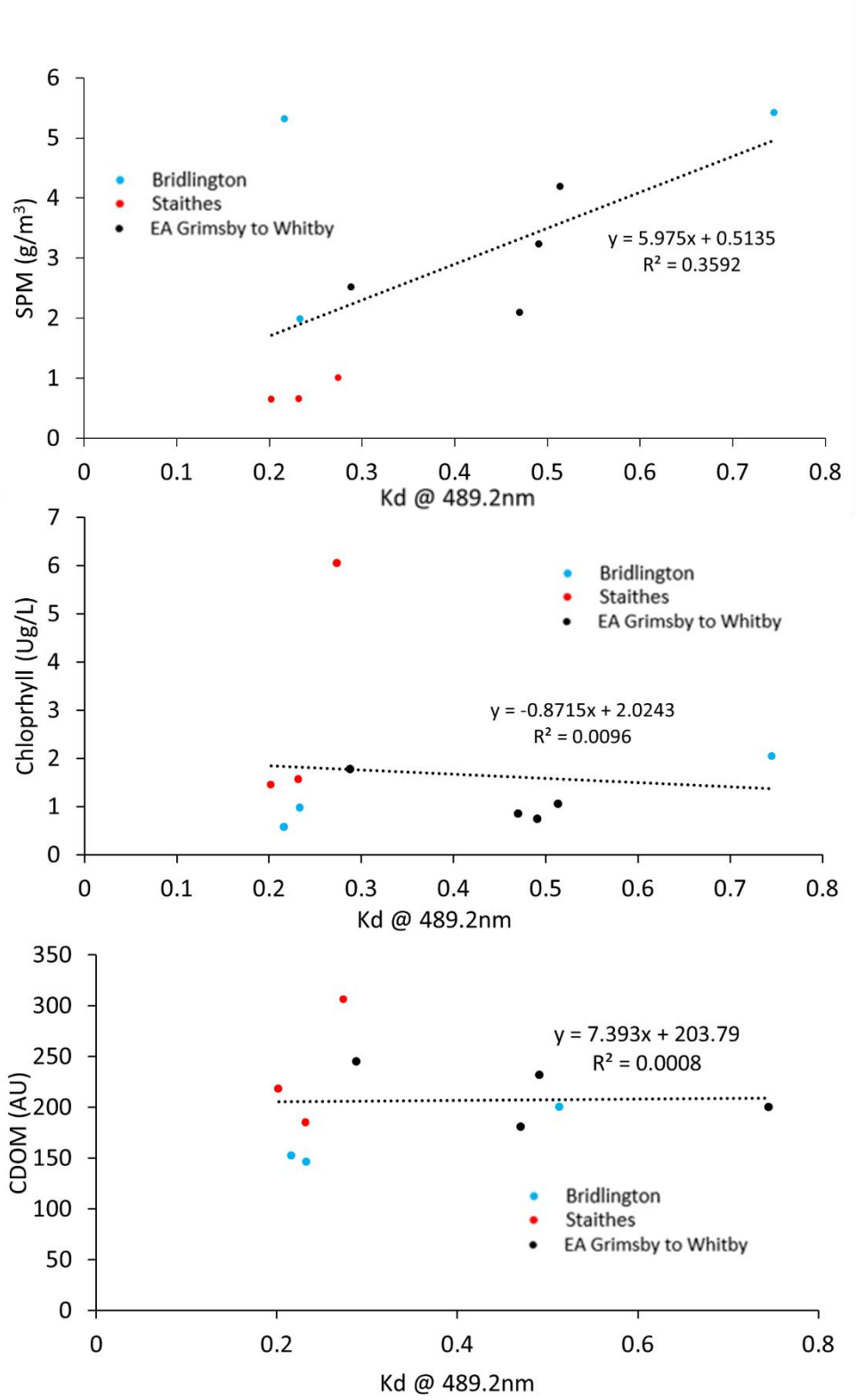

Figure 32. K_d 489.2nm plotted against SPM (A), CHL (B) and CDOM (C).

Euphotic depths:

The euphotic depth varies between each site, but a clear trend between all sites is that green wavelengths of light penetrate deepest for all spectral casts (Figure 33). The site in which light penetrates deepest is M16 (offshore sample in the offshore stratified zone), with 1% of light at 555.1 nm reaching 32.4 m. At this location, the depth was 53.6m, meaning approximately 60% of the water column has access to green wavelengths of light. Site M16 also had the deepest 1% euphotic depth for the violet and blue wavelength channels. Violet wavelengths at 412.5 nm penetrate to 12.8m while the blue wavelengths at 443.5 nm and 489.4 nm penetrate to 15.7m and 23.1m respectively. This site had the deepest 1% euphotic depth of all sites for the same wavelength. For the red wavelength bands, the euphotic depth was not the deepest out of all the sites sampled. There were two other sites that penetrated deeper (J6 and J7). Site J6 (offshore sample in the permanently mixed zone) had the deepest 1% depth for the red wavelength bands, penetrating to 13.4m and 11.4m at wavelengths 664.8 nm and 682.4 nm respectively. The site that had the shallowest 1% depth for the whole cast was J12 (inshore sample in the permanently mixed zone). The deepest penetrating wavelength for this site was 555.1 nm, reaching a depth of 6.8m. This site also had the shallowest euphotic depths for the violet and blue wavelengths with 1% light reaching 3m and 3.7m. The red wavelengths shared the shallowest 1% depth with site J5 (inshore sample in the permanently mixed zone) where the 1% light reached 5m and 4.7m.

Overall, the Staithes cruise light penetrated deepest for all three sites in the green wavelength when compared to the other sites. The spectral 1% depth cast profile varies according to the site. At Staithes, we see the largest difference between 1% depth from the varying spectral wavelengths. The difference between the 1% depth from the blue wavelength (489.4nm) to the green light (555.1nm) at site M16 was 9.3m. Using the same blue and green wavelengths used to calculate the 1% depth difference at site M16, site M17 and M18 had a difference of 5.5m and 8.1m respectively. The average difference in 1% depth between the wavelengths of 489.4 and 555.1nm at Staithes was 7.6m. The trend for the sites at Staithes shows a significantly larger difference in 1% depth between the blue and green wavelengths of light in comparison with the Bridlington cruise and the EA Grimsby – Whitby cruise.

At Bridlington, the difference in 1% depth from 489.4nm to 555.1nm for sites J5, J6, and J7 was 1.5m, 1.2m and 2m respectively with an average difference of 1.9m. With the difference in euphotic depth between the blue and green wavelengths from each site being calculated, Staithes had a 5.7m greater euphotic depth difference between the wavelengths that of the Bridlington site. The inshore Grimsby to Whitby cruise showed similar results to Bridlington, in the fact that there was minimal difference in

euphotic depth between wavelengths. There was only a 2m difference in depth between the blue and green wavelength bands.

A general trend is that inshore sites have shallower euphotic depths than the offshore sites. However, one anomaly is that, despite M17 being the furthest of the offshore site sampled, it did not have the greatest euphotic depth. Instead, M16 (which was our mid-station site at Staithes in between our inshore and offshore sites) had the deepest euphotic depths of all the stations sampled. Euphotic depth also followed the same trends as K_d, in that euphotic depth increased with distance away from the Humber estuary up to site J14, where the euphotic depth shallowed.

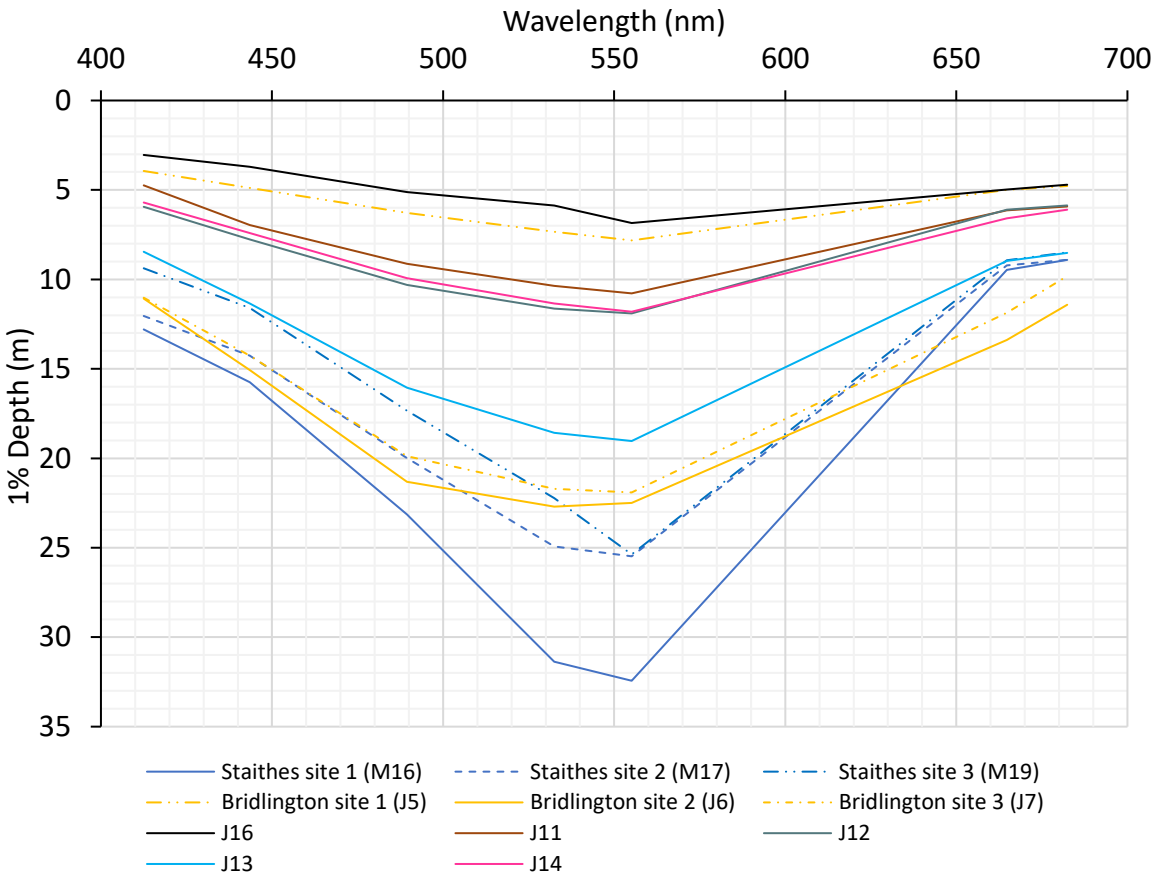

Figure 33. 1% Euphotic depth (m) for each wavelength of light for the in situ site measurements in 2022.

Reflectance ratio :

Reflectance trends for each corresponding wavelength showed for every site, except M19, that reflectance increased from the wavelength 412.5nm to 555.1nm (Figure 34). Wavelength values were greatest at 555.1 nm with the highest reflectance recorded measuring 0.157 at site J16. Site M17 had the overall lowest reflectance at 555.1nm with a value of 0.016. M19 was an anomaly because of the

elevated reflectance observed at wavelength 532.5nm. There was a spike in reflectance to 0.3 at this wavelength, which was the highest reflectance value recorded of all wavelengths and sites. This differs greatly from all the other sites where the highest reflectance was measured at wavelength 555.1nm. In addition, there was reduced variability in reflectance between measured values at different wavelengths in comparison to site M19. Reflectance reduces as wavelength increases from 555.1nm to 682.4nm, with exceptions at sites M16, M17, M19 and J14 where reflectance values increase. This may be an anomaly. The sites that do not see an increase in reflectance at 682.4nm show a decrease in reflectance at this wavelength. The reflectance follows trends closely with the euphotic depth and spectral K_d plots, with inshore sites demonstrating higher reflectance than offshore sites, alongside reflectance being greater at sites closer to the Humber estuary. This suggests SPM plays a pivotal role in dictating reflectance values on differing spatial scales.

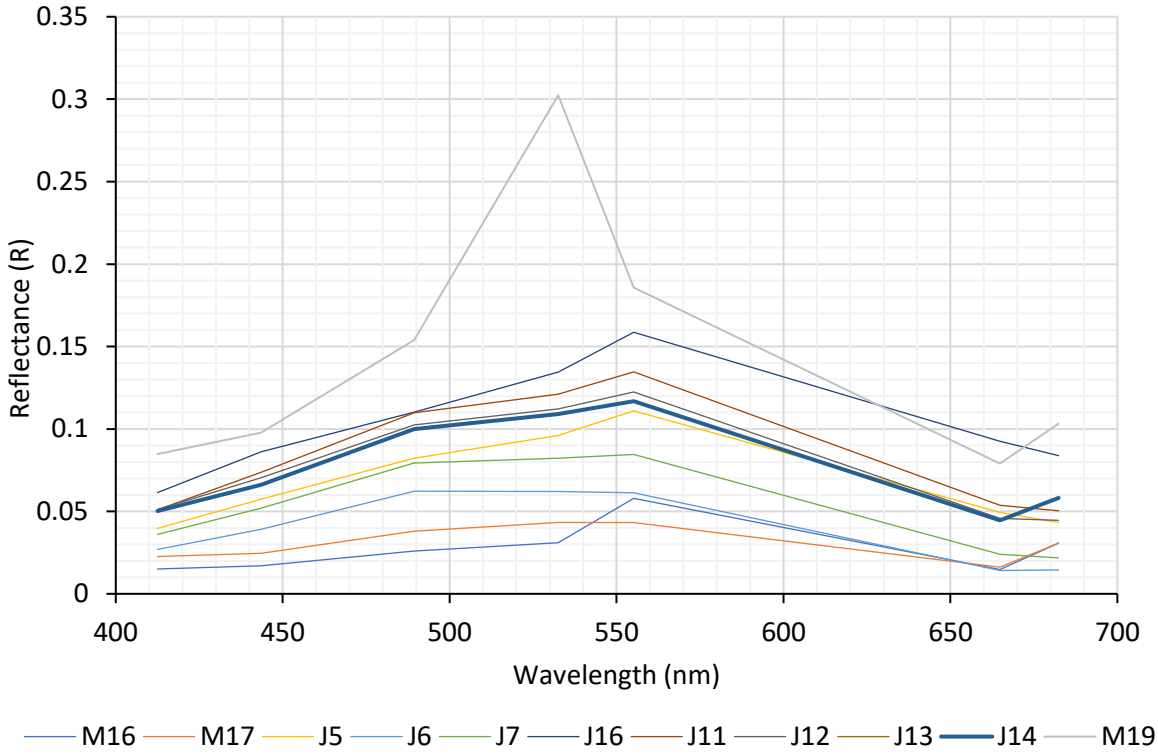

Figure 34.Reflectance measured for 7 wavelength channels from in situ multispectral radiometer sites for 2022.

Surface photosynthetically active radiation (PAR):

Monthly averaged surface PAR measurements obtained show the trend of decreased surface PAR during the winter months, followed by increasing PAR throughout spring and peak PAR values during the summer (Figure 35). The lowest PAR values recorded were in December (3.76 Einstein m^{-2} day^{-1}) with highest values being obtained in June at a monthly average PAR measurement of 48.93 Einstein

m^{-2} day^{-1}. The general trend showed increasing PAR from January to April, with PAR maintaining the same value in May as the previous observations in April. PAR then peaks in June and drops in July to the same values observed in April and May. A value of around 40 Einstein m^{-2} day^{-1} is maintained into August (similar values for April, May and July), where subsequently the average monthly PAR decreases each month, until the lowest recorded value in December. The rapid increase in surface PAR coincides with the onset of the spring bloom at the end of march in Figure 23 and Figure 24. This infers that increasing PAR intensity is a factor that affects spring bloom timing.

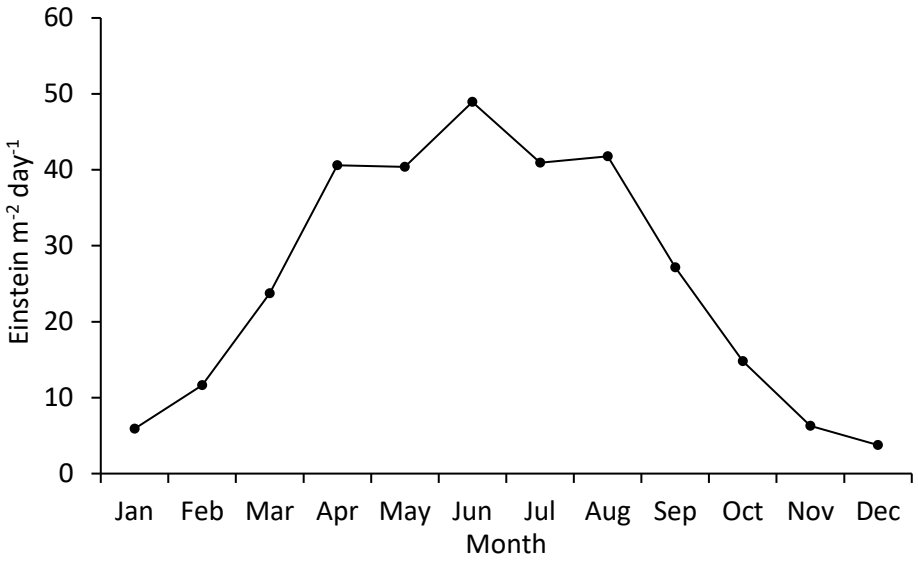

Figure 35. Average monthly surface PAR measurement in 2022 taken from a defined zone with the coordinates -0.020828,53.9375,0.270839,54.1875.

Suspended particulate matter (SPM):

SPM varied temporally and spatially over the year of 2022 (Figure 36). The trends discovered showed elevated values in winter months, with the inshore stratified (IS) and offshore stratified (OS) zones recording highest values in January. The highest SPM recorded of all zones was in February in the permanently mixed zone (PM), which had a peak monthly average value of 8.57 g m^{-3}. SPM decreased from February down to the lowest recorded SPM for each site in August. The OS zone had the lowest recorded SPM in August with 0.5 g m^{-3} of sediment found within the water column. Thereafter, SPM increased monthly up until December. The three defined zones (OS, IS and PM) can clearly be identified using the SPM data. The SPM data correlates closely with trends and patterns in wave height shown in Figure 7. There is minimal overlap in SPM data between each region, apart from the IS and PM zone in September. This result aids in verifying that three distinctly different water body types were chosen. Based on the zonal data, there is clear evidence that the PM region has the highest turbidity of

all the other zones. This result is coupled by shallow bathymetric depth and a deep annual MLD for this zone. Monthly averaged K_d (Figure 31) also followed similar trends and patterns, further supporting the influence of SPM on light attenuation. The OS zone had the overall lowest SPM for each month, with peak SPM values being recorded in January (2.92 g m^{-3}). This value was significantly lower than the other two zones, with the OS zone having much less variation in SPM throughout the year. The range for the OS zone was around 2.5 g m^{-3} in comparison to ranges of 6.75 g m^{-3} and 5.5 g m^{-3} for the PM and IS respectively. The low SPM in this region could be associated with shallow MLD and deep bathymetric depth. This region also has slightly different trends to the other two regions, with extended periods of low SPM and minimal variability between May and October. Alternatively the IS and PM zones have elevated SPM in September and October when compared to summer months, whereas the OS zone maintains summer low values for these corresponding months. Each zonal SPM time series closely matches the corresponding K_d time series shown in Figure 31.

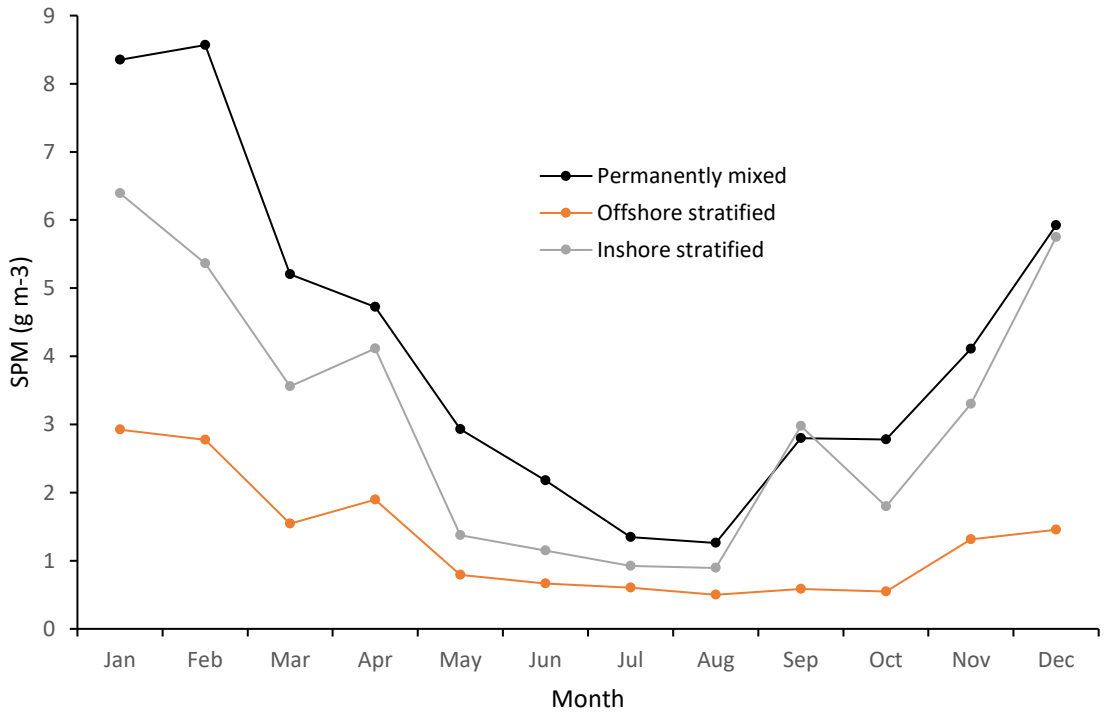

Figure 36. Monthly averaged satellite SPM (g m^{-3}) was derived for each of our outlined zones for the year 2022.

To verify the SPM data being used for a yearly time series, *in situ* turbidity measurements were collected during the sample regime to help determine the reliability of satellite SPM. There was a positive trend (Y=0.4913x + 1.9488, R^2= 0.7044) between FNU measured using a turbidity meter and satellite SPM (Figure 37). The trend observed shows increasing FNU turbidity corresponded with increased satellite SPM.

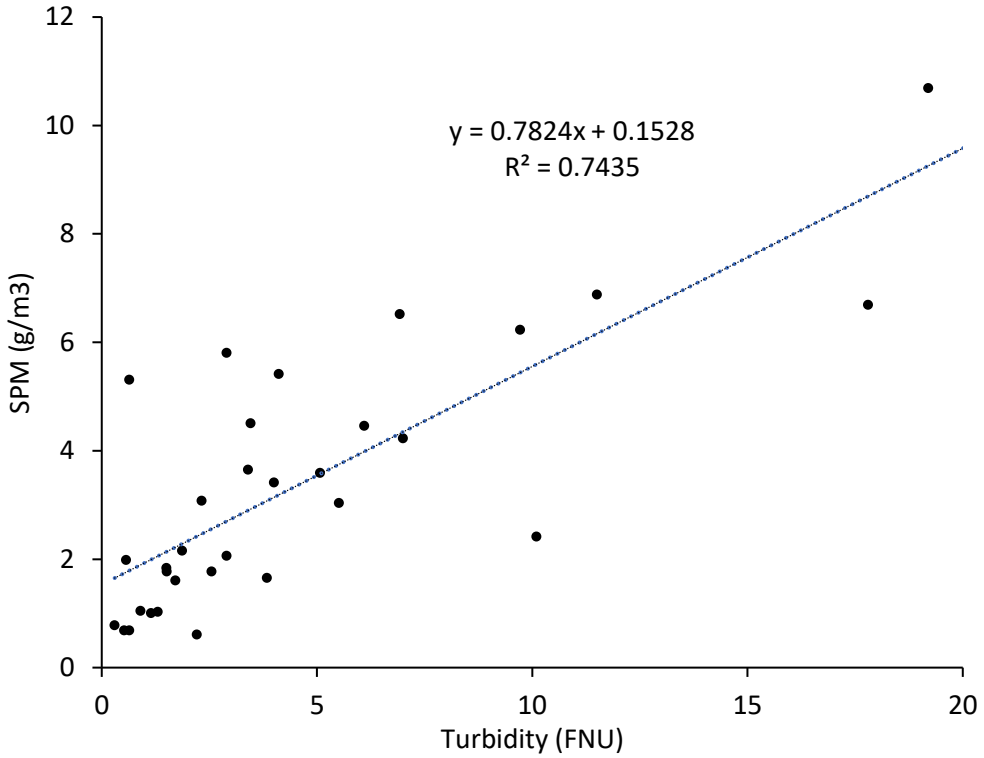

Figure 37. In situ turbidity (FNU) against satellite SPM (g m-3).Outlier have been removed to prevent skewing of the data

Nutrient Availability:

Figure 38 shows the greatest nitrate concentrations to be observed in January and December in the inshore stratified region and permanently mixed region respectively. Overall trends showed nitrate concentrations to be greatest in the winter months, with increasing values from October through to January. Nitrate values decrease in February from their winter highs and then rise back to values above 0.25 mg/L in March. Within both zones, there was a rapid biological drawdown of nitrates from March into April which coincided with blooming events within the respected months. The permanently mixed region showed a decline in nitrate concentration of 0.217 mg/L from March to April, with the inshore stratified regions nitrates declining less significantly with a 0.171 mg/L reduction in concentration. Summer values for each zone remained low in comparison to winter concentrations. However, the inshore stratified region had more variability in nitrate concentrations within summer months, with the most significant observation being a large increase in nitrate by 0.098 mg/L from May to June. In the permanently mixed region, the lowest nitrate concentration was recorded in July with a value of

0.0065 mg/L. Values within this zone from May to November remained below 0.055 mg/L, potentially suggesting that nitrates could be limiting in this region. The inshore stratified region had the lowest concentration of nitrates in August with a value of 0.0696 mg/L, which was 0.0630 mg/L greater than the lowest concentrations recorded in the permanently mixed zone. When comparing the temporal trends in nitrate concentrations between the two zones, the inshore stratified region had greater concentrations in 9 of the months' observed. Concentrations within the peak spring bloom period in April were very similar alongside closely matched values in January.

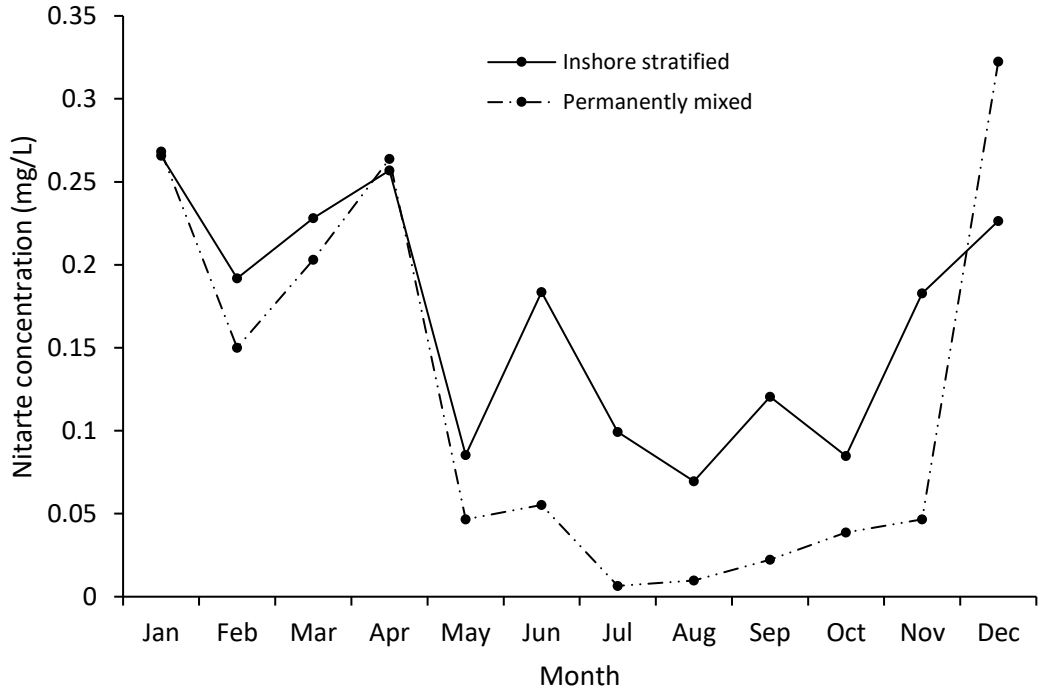

Figure 38. Monthly averaged nitrate measurements from combined data from the Environment agency (EA) and our in situ measurements for two of the zones in 2022.The offshore stratified zone was not displayed due to the lack of nutrient data available for this zone.

Results shown in Figure 39 show elevated nutrient concentrations in early spring with the exception of ammonium. Nitrate and nitrite concentrations were greatest in April with values of 0.35 mg/L and 0.006 mg/L respectively. In contrast, silica and phosphate concentrations were greatest in March (0.247 mg/L and 0.091 mg/L respectively) with ammonium concentrations being greatest May (0.224 mg/L). All nutrients except ammonium showed the greatest decrease in concentration from April to May. Lowest recorded values for all nutrients were observed in May, with the exception of nitrite where the lowest concentrations were recorded in June. Ammonium concentrations were lowest in April, with a rapid increase in concentration in May. These trends may be inversely correlated with nitrate concentrations. Overall nutrient concentrations patterns for each month appear to be correlated with increased chlorophyll concentrations present in spring, suggesting spring bloom events

within the study site may result in increased biological drawdown of nutrients from April to May. Increased chlorophyll concentrations in April may also be a possible reason for increased ammonium values observed in May. In general, when analysing the various nutrients, it was observed that nitrate was present in higher concentrations compared with all other nutrients examined, while nitrite was found to have the lowest concentration among the analysed substances.

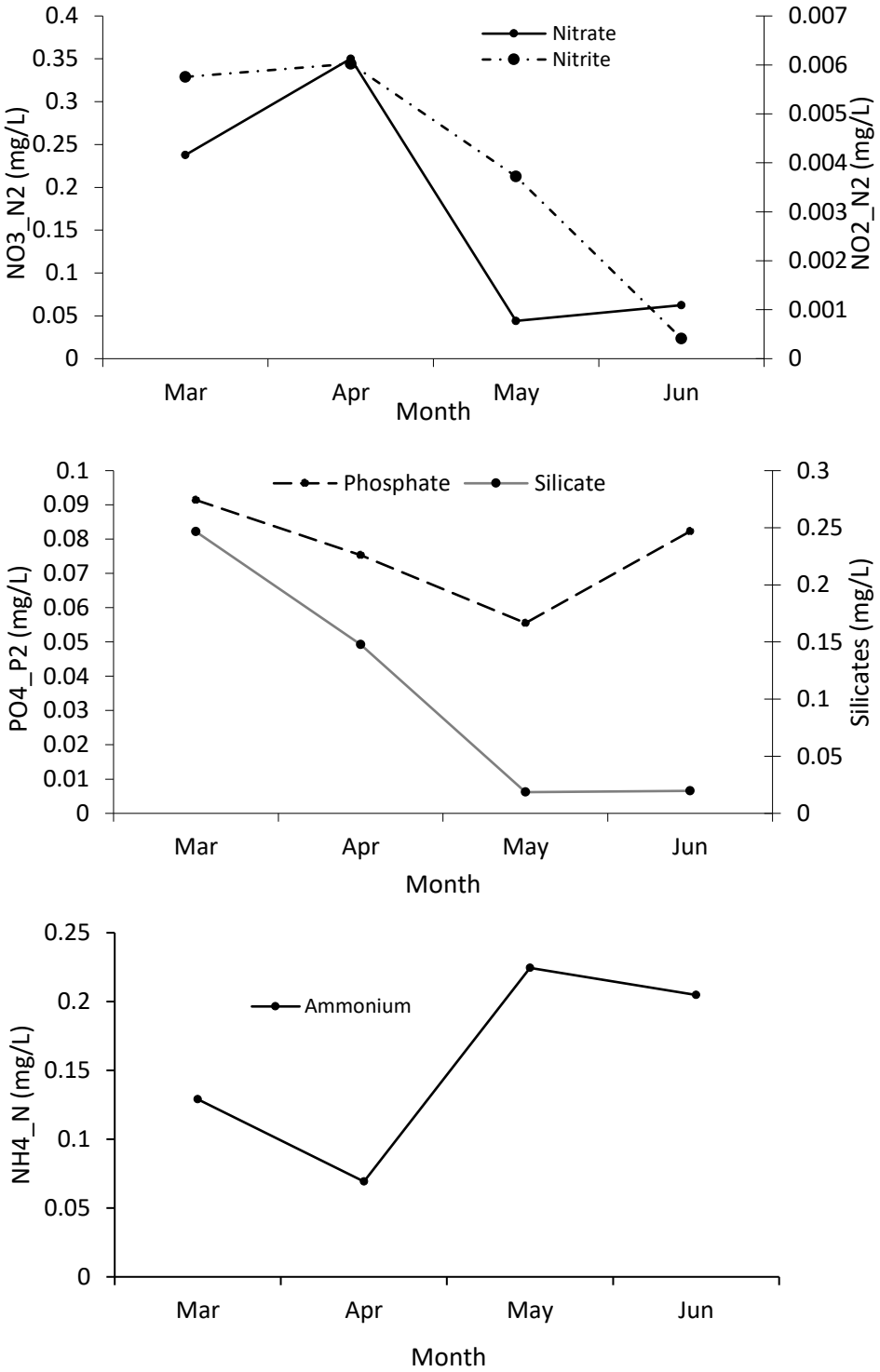

Figure 39. Monthly averaged nutrient concentration for all in situ sites in 2022.

Modelling:

S2P3 Model runs in different water types:

Station J6 (permanently mixed water type):

The model output for sea surface temperature in the water type PM (represented by station J6, Figure 10) was first compared against the OSTIA satellite sea surface temperature product to check the reliability of the model output results (Figure 40). There was a close relationship between the model output and observed satellite temperatures for the first 193 days, but thereafter, the model output showed warmer sea surface temperatures for the remaining days of the year. The largest difference in temperature began at day 243, where the temperature was on average 2 °C warmer than observed satellite-measured SST. The difference lasted from days 243-305. After day 305, the model output had SST recordings of approximately 1-1.5 °C warmer than satellite observations. However, during the period from days 243-365, both the model output and satellite SST recorded very similar trends in SST cooling rates throughout this period. There was a close resemblance between the satellite and model, where patterns of peaks and troughs in temperature throughout the year were aligned. When surface temperature spiked in the satellite SST, this was predominantly replicated with the model data, even though the latter was warmer. The model over-estimated the SST warming properties in late summer, with reduced cooling of SST in late summer/early autumn also being observed. The maximum temperature predicted from the model was 19.5 °C at day 227 with the warmest recorded temperature from satellite being 16.6 °C at day 239. This was 12 days later than the warmest SST predicted from the model outputs and was approximately 2.9 °C cooler than the predicted maximum SST temperature estimated from the model.

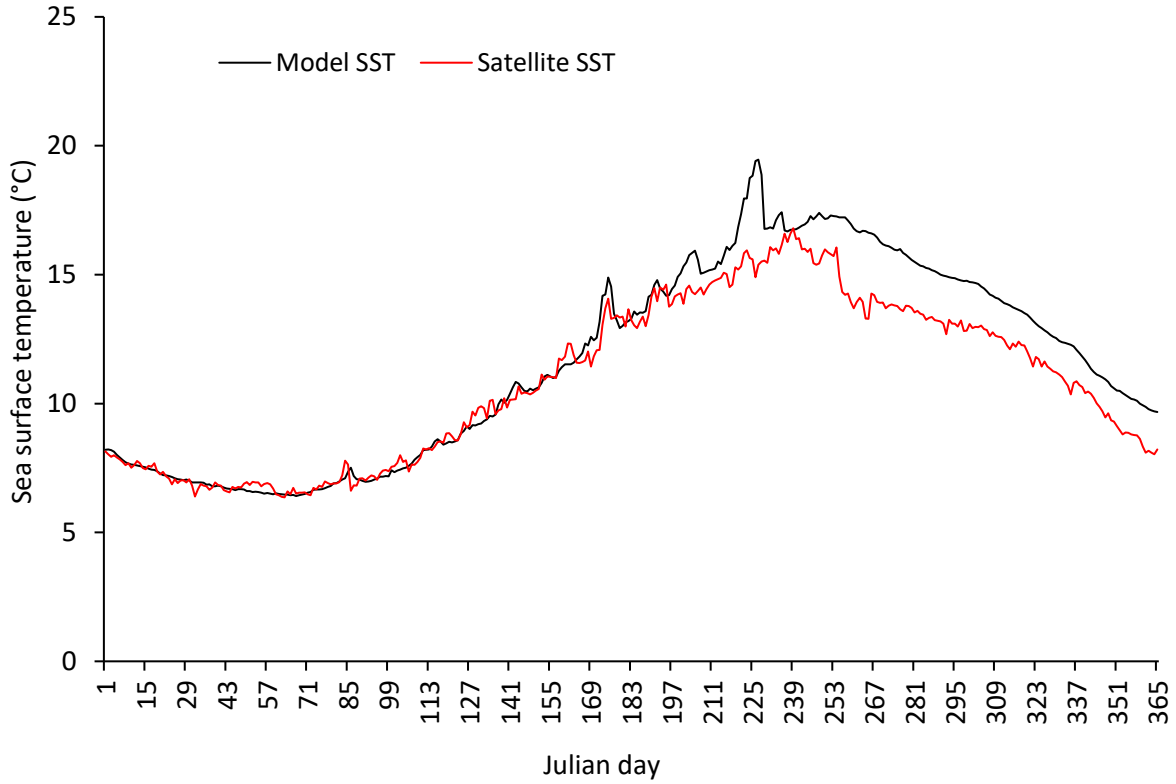

Figure 40. SST comparison between model output and OSTIA satellite observations for site J6 (Permanently mixed zone).

Temperature-depth plot:

Depth related temperature from the model output shown in Figure 40, showed the water column to be highly mixed throughout the whole year. At approximately day 228, there is evidence of potential stratification within the first 5m of the water column. The stratified water was estimated to be just below 20 °C with the remaining water column being approximately 16° C. This was the clearest period of stratification but there were other days with reduced temperature differences between surface and bottom water that were not as clear.

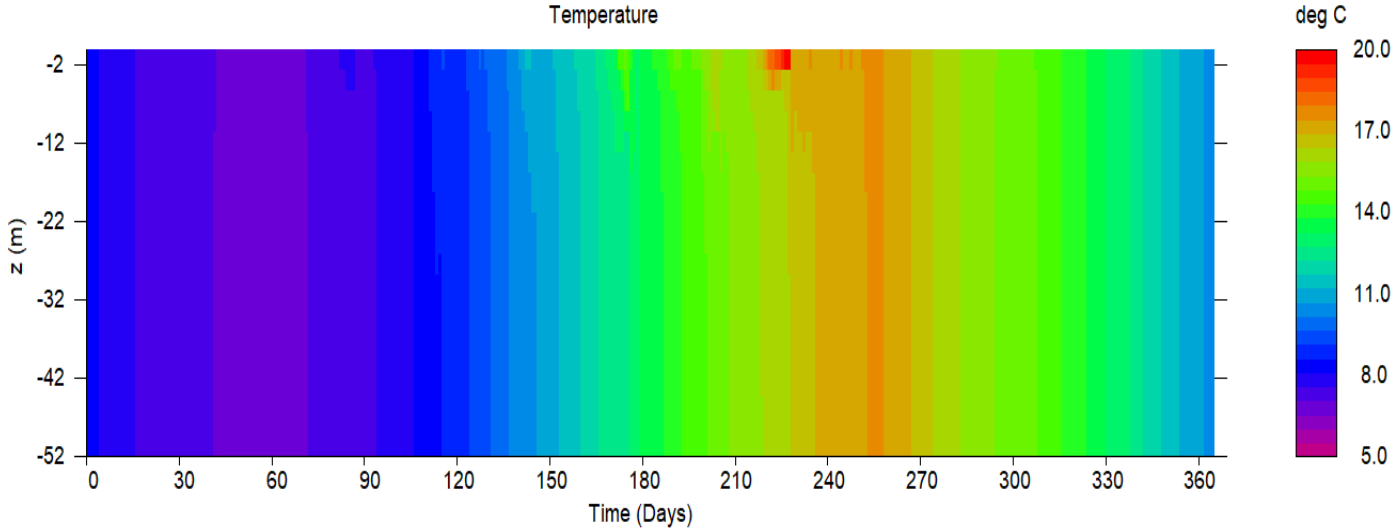

Figure 41. Temperature-depth plot from outputted results from the S2P3 model at station J6 (permanently mixed zone).

Station J6 model run:

The S2P3 model run for the station J6 (permanently mixed zone) is shown in Figure 41. Chlorophyll concentrations were close to zero throughout the first 113 days of the year, and then increased sharply at day 172, with elevated chlorophyll values above 1 mg m^{-3} lasting for 75 days between the Julian days of 175 and 250. There were 6 clear significant blooming events within this period of elevated chlorophyll, with each individual bloom lasting 12.6 days on average. There was an average of 15.4 days between each peak of the 6 major blooming events which could potentially coincide with fortnightly tidal cycles. Each bloom increased in magnitude up until day 221, with the highest concentrations of chlorophyll being observed (10.16 mg m^{-3}) on this day. The bloom dissipated quickly in the model, to a lower peak at day 249 of 2.78 mg m^{-3}. Chlorophyll concentrations then declined from day 249 and returned to baseline winter values at day 295 for the remainder for the year. Sea surface and bottom temperatures were the same and followed the same trends from days 1-70 where temperature decreased from 8.1 °C to 6.9 °C. Temperature then increased from days 71 to 259 with some variability between bottom and surface temperature between these days. There were several occasions where temperature difference between the surface and bottom exceeded 2 °C resulting in short periods of thermal stratification at this site. The greatest period of stratification lasted 23 days between day 215 to 238 where there was a maximum temperature difference between surface and bottom of 4 °C. Sea surface and bottom temperature then declined at the same rate from day 260 to 365. There was a positive trend between thermal stratification and increased chlorophyll concentration, with the result that periods of greatest stratification resulted in greater magnitude blooming events. There was an annual net primary production value of 35 g C m^{-2} $year^{-1}$ with an annual gross primary production value of 67 g C m^{-2} $year^{-1}$ for site J6.

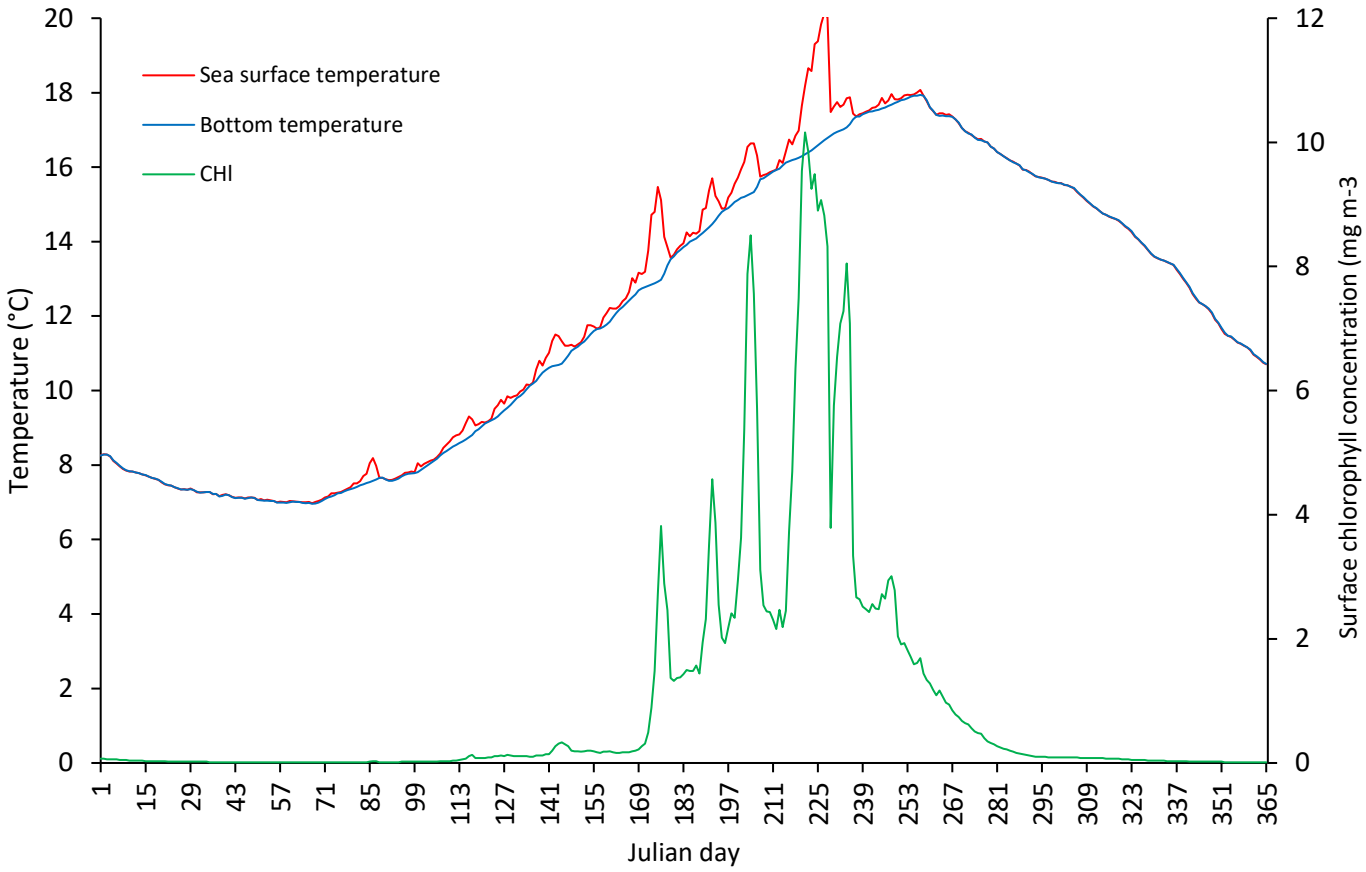

Figure 42. S2P3 model run for station J6 (permanently mixed region). The graph shows the correlation between surface (red) and bottom (blue) temperature with chlorophyll concentration (green) in the year of 2022.

Station 13 (stratified water type):

The model output for sea surface temperature in the water class OS (represented by station 13, Figure 10) was first compared against the OSTIA satellite sea surface temperature product to check the reliability of the model output results (Figure 42). There was a close annual resemblance between both measurements. Both SST measurements follow similar trends in SST variability, with the peaks and troughs of SST temperature observed from satellite data being closely replicated in the model output. Model output deviated slightly from observed SST satellite values from days 228-260, with model SST maintaining temperature while satellite observations showed signs of cooling. There were differences of approximately 1°C in SST between satellite and model observations during this time period. This suggests that SST cooling parameters in late summer and early autumn may be underestimated in the model. Initial and day 365 SSTs match closely with <0.1 °C difference between the modelled outputted SST and satellite observations. The close match between the initial and end temperatures alongside similar annual patterns, suggest meteorological data and modelled parameters were accurate and mostly reliable, helping to verify the reliability of chlorophyll, gross primary production and net primary production values generated by the model. SST trends follow the same patterns observed at

site J6 in regard to SST cooling from days 0-70, followed by a steady increase in SST from days 71-227 and subsequent cooling from late summer high values back to temperatures below 10 °C at day 365.

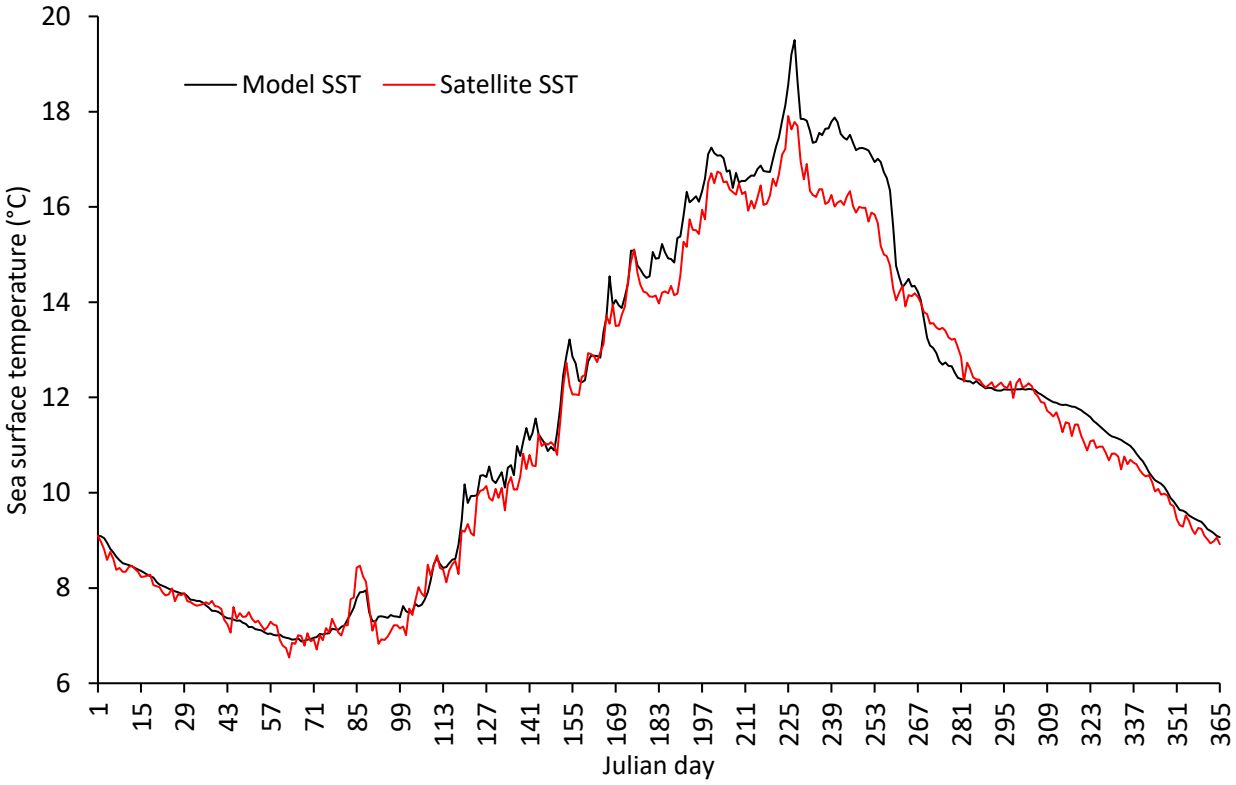

Figure 43. SST comparison between model output and OSTIA satellite observations for station 13 (offshore stratified zone).

Temperature-depth plot:

Temperature with depth varied at station 13 (Figure 44) when compared to site J6, with the most noticeable difference being that station 13 is a stratified water body within the summer months. In Figure 43, the water column was fully mixed until day 120 with clear evidence of thermal stratification forming at day 120, with stratification remaining unbroken for a period of 150 days. The thermocline extended to approximately 20 m for the period where stratification is evident. Station 13 was cooler to sea bed depth than site J6 within the summer months by approximately 3 °C when comparing temperature at depths below the thermocline.

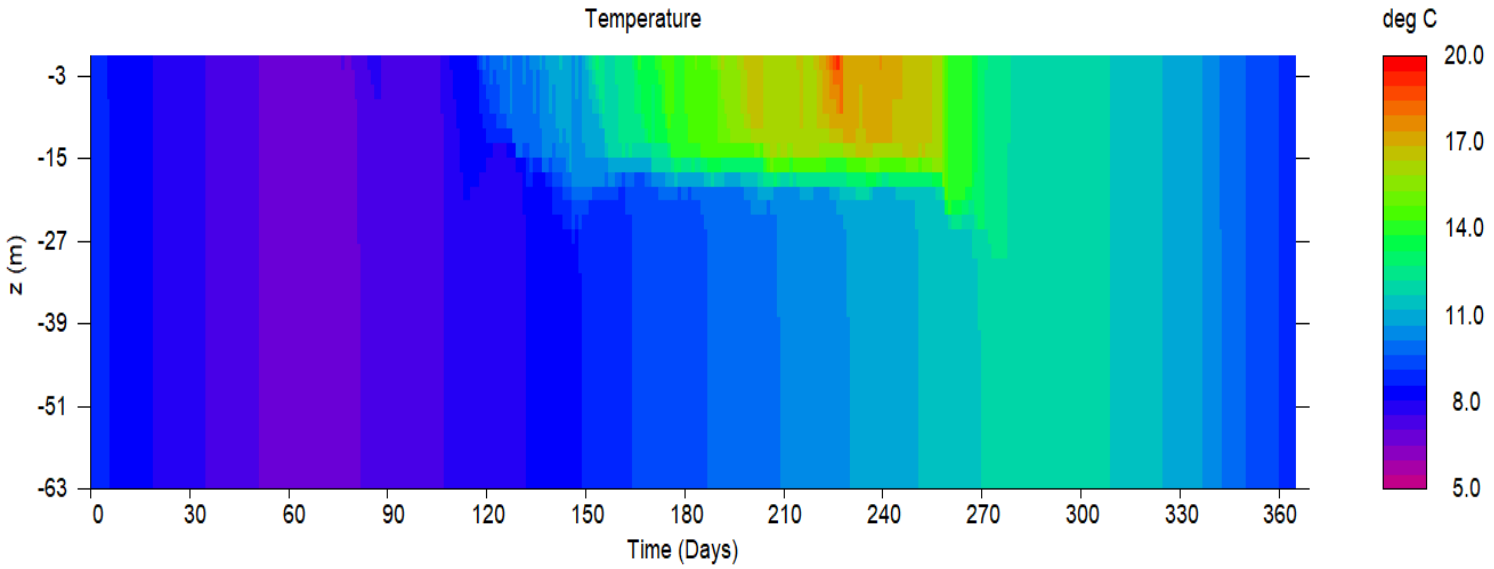

Figure 44.Temperature-depth plot from outputted results from the S2P3 model at station 13 (offshore stratified zone).

Station 13 model run:

The S2P3 model run for ICES station 13 shown in Figure 45, depicts 2 significant chlorophyll blooming events in 2022. At day 108, there was a rapid increase in daily chlorophyll to a peak concentration of 5.88 mg m^{-3} at day 123. This bloom was the most significant for this modelling site in 2022. Chlorophyll concentrations then declined gradually from day 123 to 244, but remained above 1mg m^{-3} for a period of 96 days between these dates. A secondary autumn bloom was also observed, which began at day 244 and peaked at 2.2 mg m^{-3} at day 276 with values above 1mg m^{-3} during this 25 day period. Chlorophyll concentrations then decrease to winter baseline values from day 318. In total, chlorophyll values exceeded 1mg m^{-3} for a period of 121 days: 32 days longer than the values observed at site J6. Water temperature varied in comparison to site J6, with bottom water temperatures being significantly colder. Station 13 model outputs show significant stratification for this site between days 108 to 277 (water was stratified for a period of 169 days) with maximum SST of 19.5 °C at day 227 with bottom temperature at 10.8 °C. This was an 8.7 °C temperature difference between surface and bottom temperature. Station 13 also followed similar trends in SST and bottom temperature from days 1-68 where temperatures cooled. Station 13 recorded a higher starting temperature at day 1 in comparison to site J6, but both cooled to values within 0.1 °C at day 68. Station 13 exhibited reduced heating effect at greater depths, which can be seen by a shallower gradient in temperature rise (Spring into summer) in bottom temperature when compared to a steeper gradient in temperature increase for site J6 at seabed depth. SST for site 13 followed very similar trends to station J6, with the heating of the surface waters experiencing similar gradients in temperature increase. At station 13 there was evidence of a positive trend between blooming events and periods of stratification. The first significant bloom began during the days where the water column first became stratified, with the autumn bloom occurring in

the final stages of water stratification for this site in 2022. The water column then became fully mixed from day 282 onwards. There was annual net primary production of 43 g C m^{-2} $year^{-1}$ with an annual gross primary production value of 82 g C m^{-2} $year^{-1}$ for station 13.

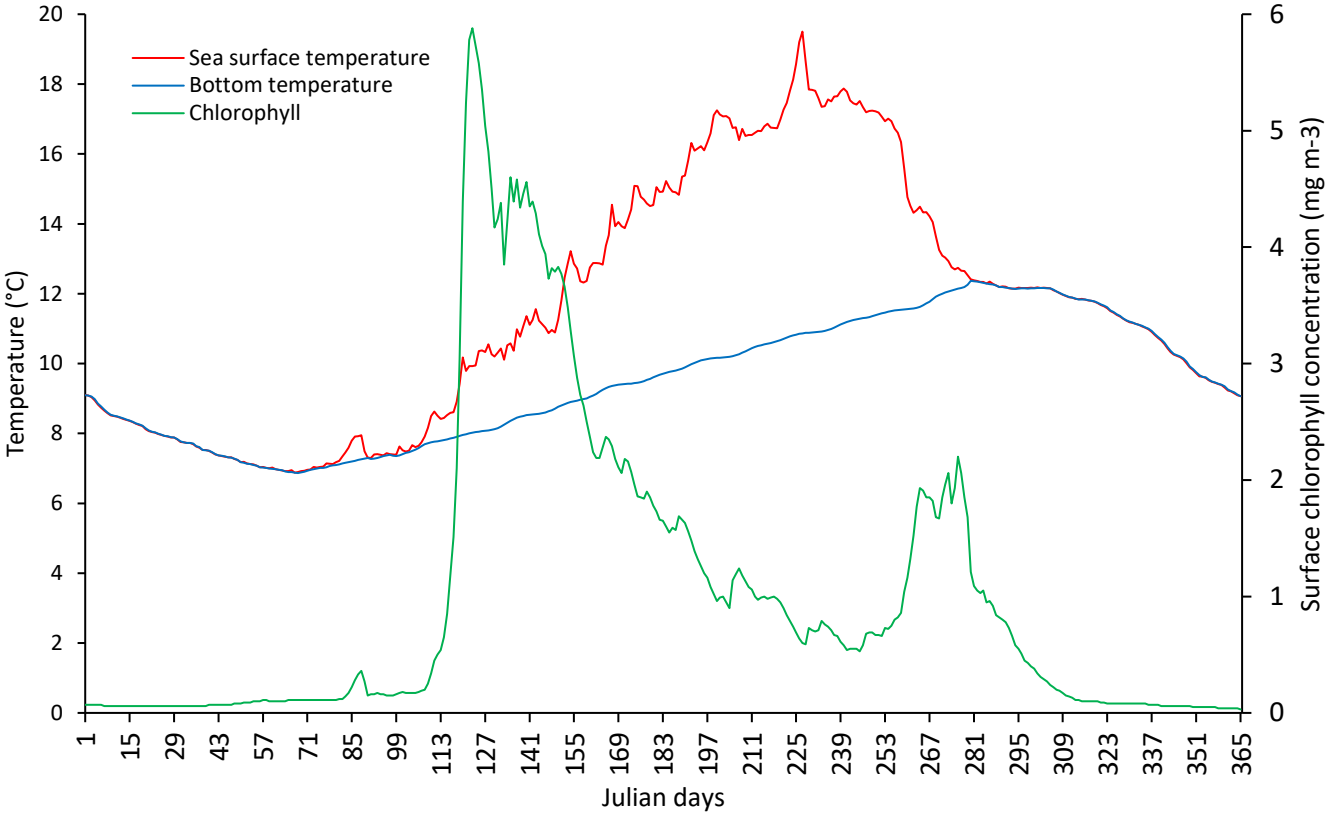

Figure 45. S2P3 model run for station 13 (offshore stratified region). The graph shows the correlation between surface (red) and bottom (blue) temperature with chlorophyll concentration (green) in the year of 2022.

Simple depth-irradiance PP model:

Net and gross primary production (NPP & GPP) outputs from the simple depth-irradiance model at station J6 (Figure 46), showed negative NPP from days 0 to 89 with an average of -600 mg C m^{-2} d^{-1}. GPP for the same period was positive, with values averaging 400 mg C m^{-2} d^{-1}. This suggests that respiration was greater than photosynthesis in this period with strong negative NPP values indicating low productivity. Primary production increases, with NPP values becoming positive, from day 90. From day 90 to 142, NPP and GPP become positive and values increases throughput this period. However, there was still consistent gap between NPP and GPP, with early spring displaying indications that respiration significantly outweighs productivity, reducing overall NPP. Productivity then begins to outweigh respiration going into early summer allowing greater primary production as evidenced by a reduction in the difference between GPP and NPP (NPP increases) values alongside increasing NPP from 700 mg C m^{-2} d^{-1} to 3400 mg C m^{-2} d^{-1} at day 150. Between days 150 and 300, there is a close

trend between GPP and NPP suggesting that respiration throughout this period is no longer a key driver, as a result of which primary productivity increases. Elevated primary productivity values remain between 1000 and 5000 mg c m^{-2} d^{-1} for 58 days from day 167. These elevated NPP levels from the Excel model suggests phytoplankton blooming occurs in summer. The SP23 output provided further evidence of elevated chlorophyll values for the same period (Figure 42), suggesting the initiation of phytoplankton blooming events occurred in summer for the PM zone. GPP and NPP peak at day 179 with an NPP output of 7081 mg c m^{-2} d^{-1}. GPP and NPP then decrease from day 225 and reach baseline winter values at day 309 where the difference increases between GPP and NPP indicating that respiration may have exceeded primary production. There were anomalous results at day 179 and 308 where a rapid increase in GPP and NPP were observed to be significantly higher than values either side of these days, which suggests a potential error in parameters on these days.

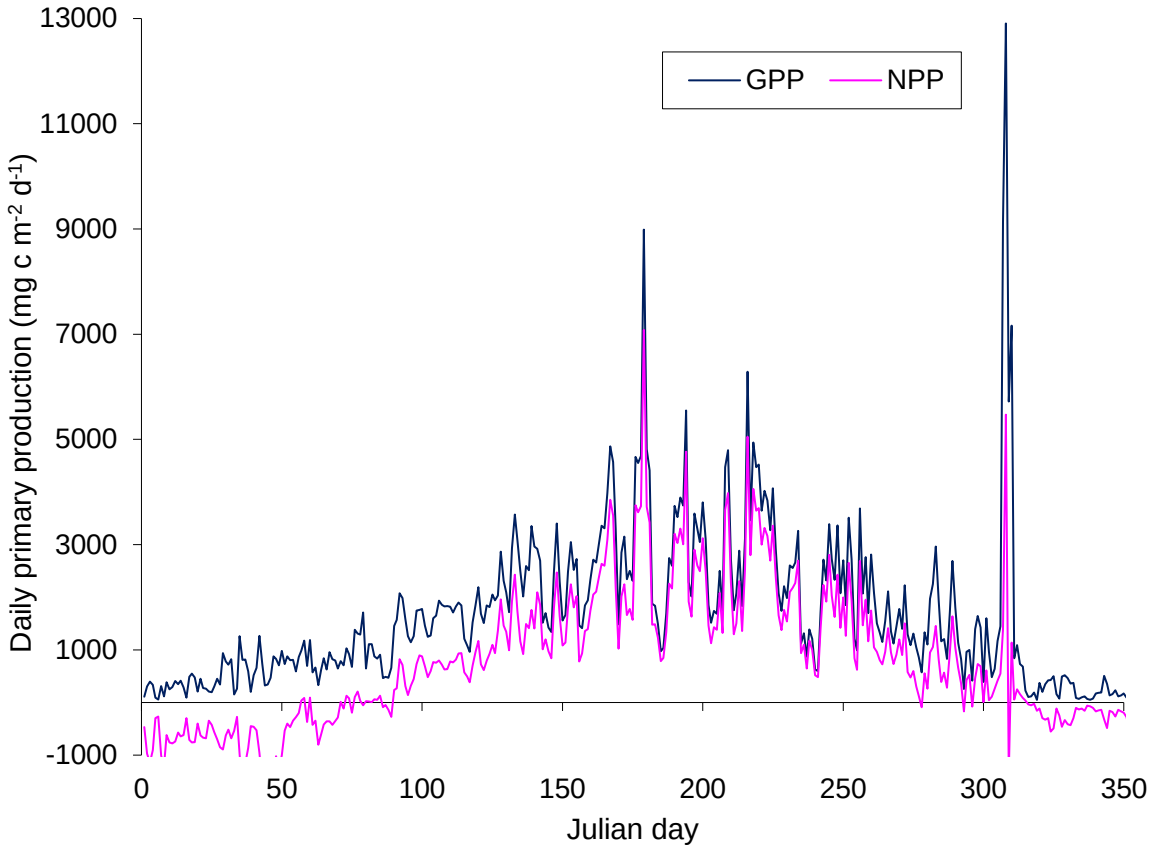

Figure 46.NPP and GPP simple depth-irradiance PP model output comparison for site J6 (permanently mixed region) in 2022.

The Excel model run for station 13 (Figure 47) suggests GPP and NPP align in spring with higher elevated NPP in spring when compared to station J6. GPP and NPP remain elevated above 1000 mg C m^{-2} d^{-1} for a longer period of time when compared to site J6, with overall larger maximum NPP displayed for a single day. From days 0-72, there is evidence that respiration outweighs productivity because of GPP and NPP not aligning, with NPP values recording approximately 300 mg C m^{-2} d^{-1} below GPP. The GPP values predominantly remain below 1000 mg C m^{-2} $d^{-1,}$ with NPP ranging from 400 to -600 mg C m^{-2} d^{-1}. Day 72 is when GPP and NPP begin to align and become broadly comparable. There is evidence of an low magnitude early spring blooms a result of elevated NPP of 3350 mg C m^{-2} d^{-1} at day 85. Productivity then drops back down to below 1000 mg C m^{-2} d^{-1} at day 111. Between days 116 and 285, NPP values generally remain above 1000 mg C m^{-2} d^{-1}. These elevated productivity estimates at station 13 last 111 days longer than observed estimates at station J6, making this site a more productive area of the North Sea. A secondary late spring bloom is evident between the days 119 and 149 where the highest NPP and GPP values are recorded. The highest NPP value recorded was at day 139 with a value of 24,355 mg C m^{-2} d^{-1}. The fact that this result is 12,461 mg c m^{-2} d^{-1} higher than the second largest NPP recorded indicates that it may be a potentially anomalous result. This suggests there is an over estimation due to potential anomalous result in chlorophyll or K_d data inputted into the model. Day 320 is when NPP becomes negative and there is a difference between GPP and NPP values (not as significant as at the beginning of the year), suggesting respiration outweighs productivity again. The overall main difference observed between sites J6 and 13, was increased productivity at station 13, with peak values being recorded in spring compared to highest productivity values being recorded in late summer for station J6.

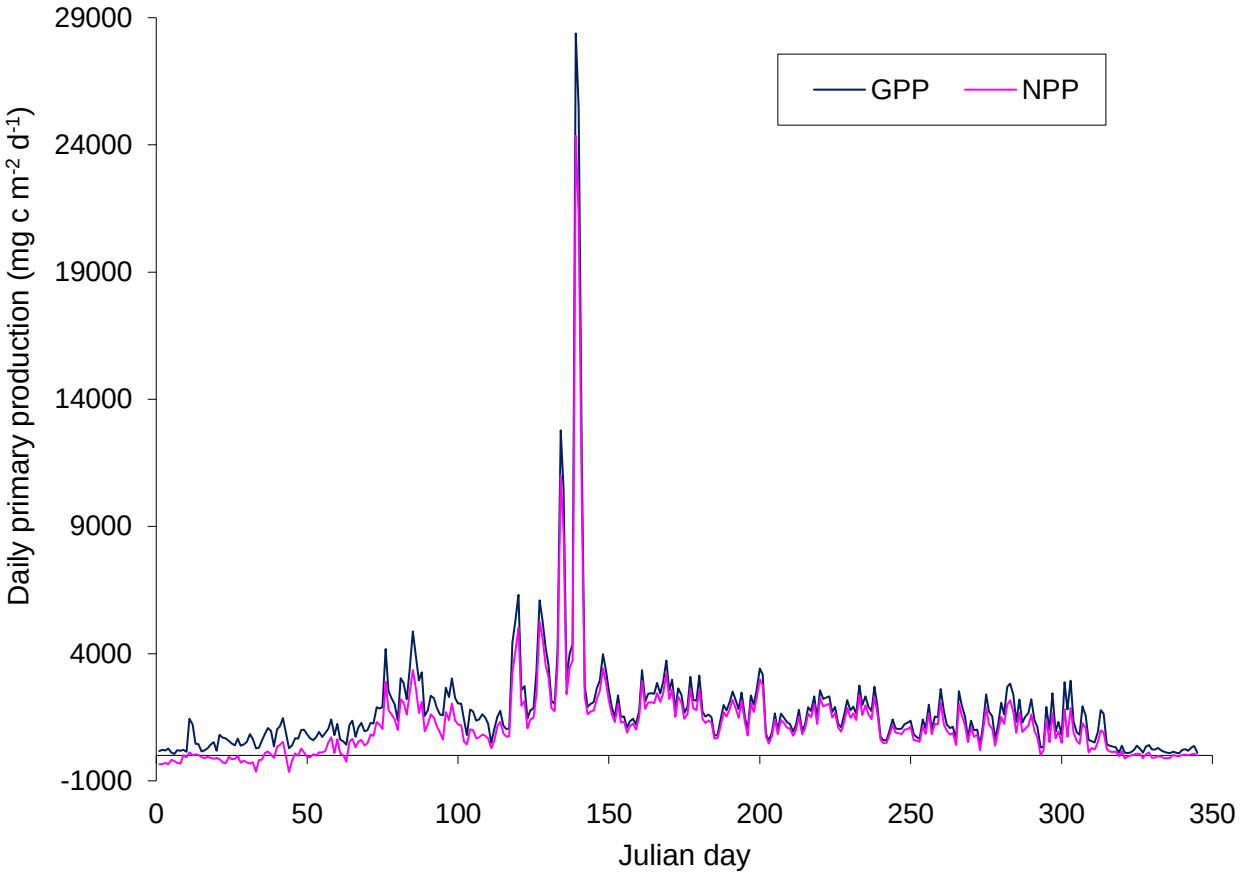

Figure 47. NPP and GPP simple depth-irradiance PP model output comparison for station 13 (offshore stratified region) in 2022.

When comparing NPP between the S2P3 and excel model outputs for station 13 (Figure 48), there is a close resemblance between trends in elevated productivity between the two models. However, although trends between both models were aligned closely, the key difference between them is the productivity values outputted. The Excel model's estimation is significantly higher than that observed from the S2P3 output. The highest NPP value generated from the S2P3 model was 780 mg C m^{-2} d^{-1} while, in the excel model, values were in excess of 1000 mg C m^{-2} d^{-1} for a large proportion of the year. The early spring bloom observed in the excel model is not replicated in the S2P3 NPP output. The Excel model predicts the first blooming event in early spring (day 75), while the S2P3 predicts the first blooming event in mid spring (day 120). There are only two clear blooms observed from the S2P3 model, with these being replicated in the Excel model just to a greater magnitude. Overall, the excel model predicted significantly higher yearly NPP yields when compared to S2P3. The S2P3 model estimated 43 g C m^{-2} $year^{-1}$ while the excel model predicted a productivity of 435 g C m^{-2} $year^{-1}$.

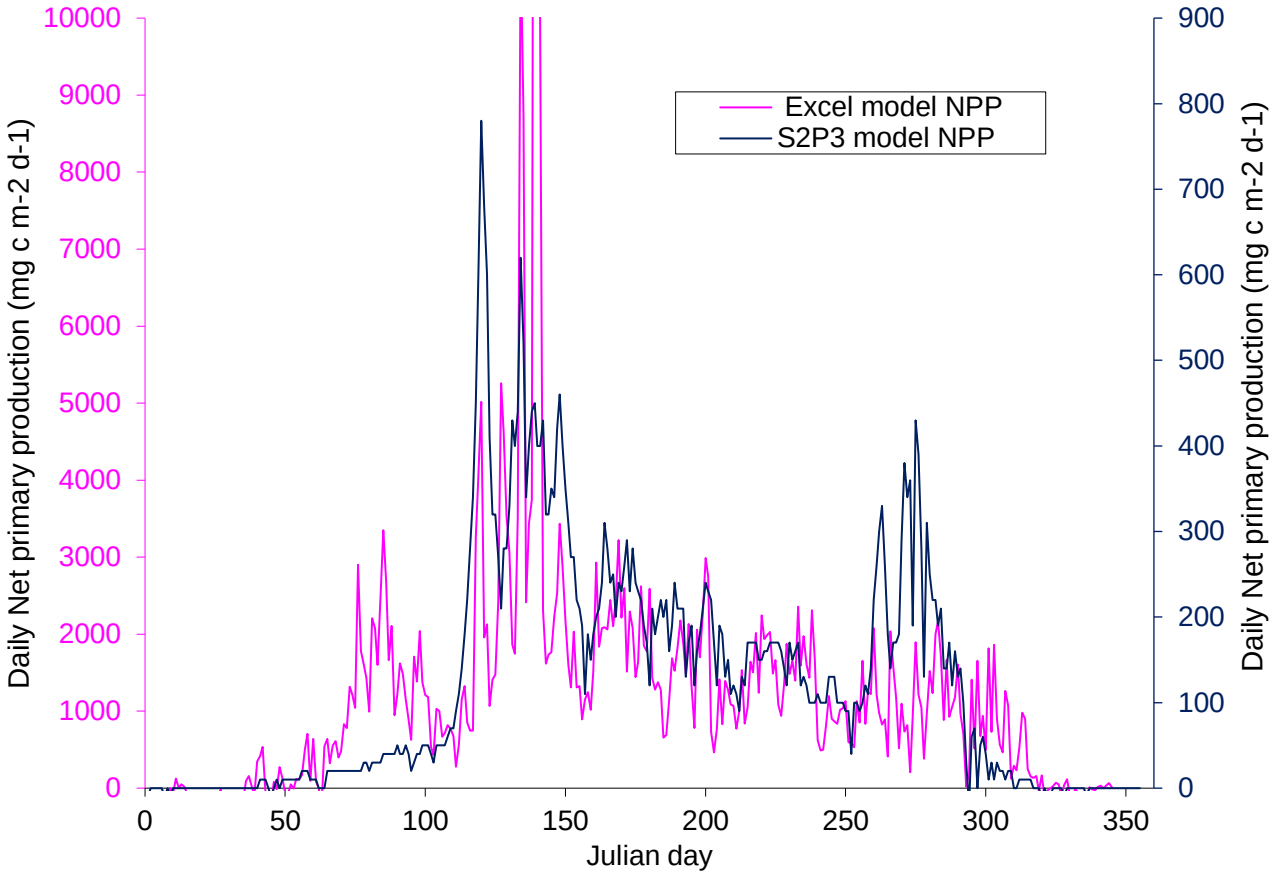

Figure 48. NPP comparison between the S2P3 and the Simple depth-irradiance PP model outputs for station 13 (Offshore stratified zone) in 2022.

There is a close resemblance observed between trends in NPP from both models at station J6 between days 170 and 275 (Figure 49). Overall, the main period of elevated NPP for the S2P3 model is replicated in the excel model, with the highest NPP values recorded in S2P3 corresponding to the same time period as the excel model output. NPP estimates in early spring (days 73-173) from the excel model are observed to be significantly higher than the S2P3 model outputs.. S2P3 estimated a maximum of 50 mg C m^{-2} d^{-1} while the excel model predicted a value of 3853 mg C m^{-2} d^{-1} between the same dates. Phytoplankton bloom initiation for the Excel model suggests phytoplankton biomass increased early spring, while the S2P3 model predicted blooming to initiate in summer. As with station 13, when comparing NPP yields between both models, they were significantly different all year round, with the Excel model predicting NPP at considerably higher rates. Annually NPP was predicted at 35 g C m^{-2} $year^{-1}$ for the S2P3 model, whilst the excel model estimated 284 g C m^{-2} $year^{-1}$. The anomalous result at day 308 on the Excel model is not shown from the NPP output from the S2P3 model, providing further evidence that the estimated NPP at day 308 was an anomaly.

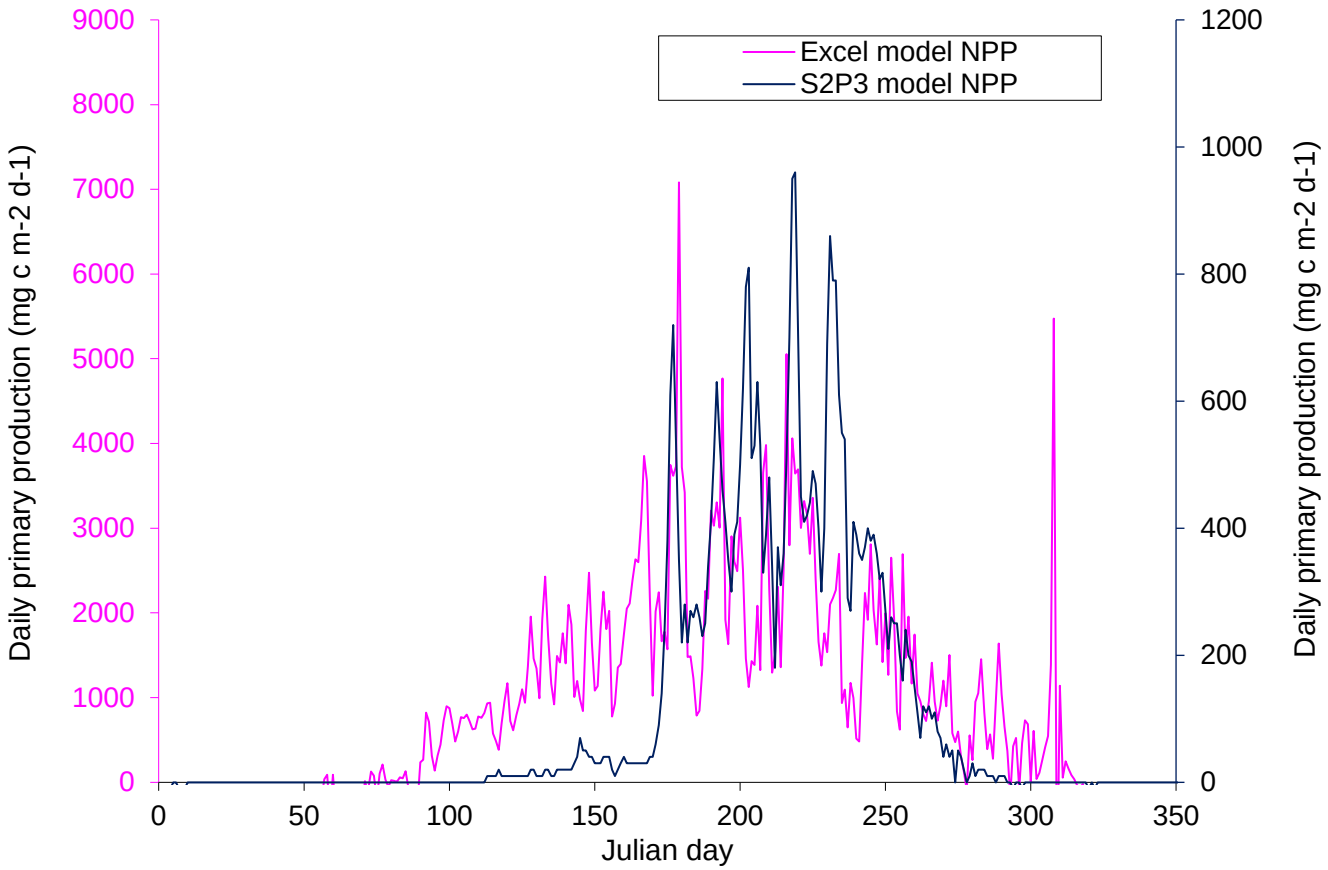

Figure 49. NPP comparison between the S2P3 and the simple depth-irradiance PP model outputs for station J6 (permanently mixed zone) in 2022.

S2P3 current speed:

S2P3 model outputs for daily and depth averaged current speed based on tidal constituents shows station J6 within the permanently mixed region to have greater daily current speed than station 13 (Figure 50). For both stations, there were trends of reduced maximum and minimum current speeds every 14 days which coincides with spring-neap tidal cycles. On average maximum current speeds at station J6 were 0.28 m s^{-1} greater than speeds observed at station 13.

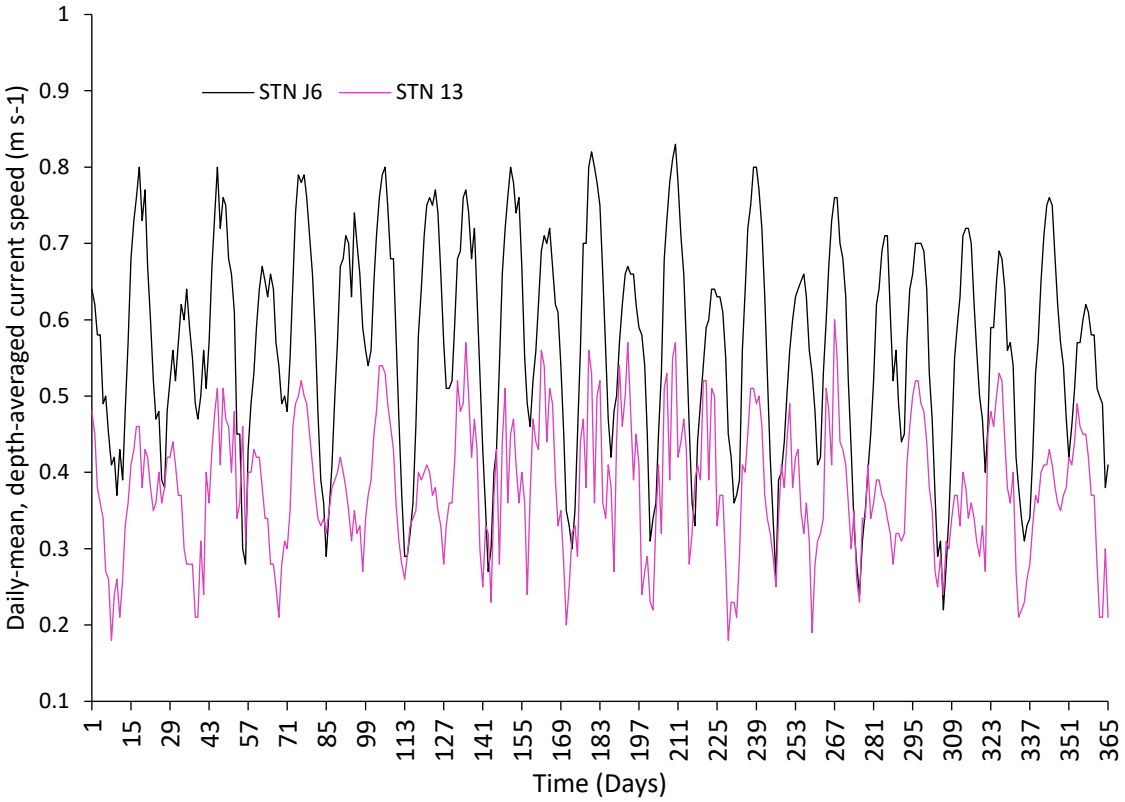

Figure 50. Current speed (m s^{-1}) comparison between station J6 and 13.

Section 4- Discussion

Phytoplankton primary production in the North Sea forms the base of marine food webs whereby variation in productivity can directly or indirectly affect the higher trophic levels species (Capuzzo et al., 2017). Productivity drives zooplankton and ichthyoplankton dynamics; influencing the high biodiversity of marine wildlife such as planktivorous fish, seabirds, seal and cetaceans present in the sea off the north-east coast of the UK. Changes in phytoplankton productivity can influence commercial fish stock populations (Chassot et al., 2010), which would cause drastic socio-economic impacts on the north-east coast. The port of Hull in 2022 had 8.6 kilotons (Kt) of demersal and pelagic landings and this figure excludes the important shellfish fisheries located in the ports of Whitby , Scarborough and Bridlington (Reade et al., 2022). The Current value of landings on North East coast (Hull and Bridlington only) equate to approximately £37.6 million (Reade et al., 2022), meaning a decline in fish stocks would heavily and negatively impact an important fishing industry sector for this region of the UK. Phytoplankton abundance and composition can also serve as indicators of the North Sea's ecological health (Tett et al., 2008). Changes in phytoplankton communities may reflect shifts in nutrient availability, pollution levels or other environmental factors. This is particularly relevant with the ongoing investigation on the mass crustacean die off events that occurred in 2021 off the north-east coast of the UK (*Sealife mortality off the North East Coast - Committees - UK parliament,* 2022; DEFRA, 2023).

To our knowledge, this was the first study that observed the spatial and temporal distribution of phytoplankton blooming events in this study region, alongside the investigation of the causes of phytoplankton blooms. This study was based on a blended approach using remote sensing, model outputs and *in situ* measurements. The results showed clear evidence of spring blooms being present for this region, with distinct differences in magnitude and timing of blooms between different hydrodynamic regions. Correlations with water column mixing and light attenuation alongside timings of stratification are key drivers of phytoplankton bloom growth for this region.

Temporal and spatial distribution of blooming events off the north-east coast:

The timing, onset, duration and bloom peak has high latitude and longitudinal variability within the study site due to differing oceanographic factors creating variability within environmental conditions along the north-east coast. The specific controls affecting phytoplankton blooming are discussed in detail within subsequent sections of the discussion. The initialisation of the spring bloom began between the 21st–31st March (Julian days 80-90) with the most noticeable increase in chlorophyll occurring off the coast of Teesside and Northumberland during this time period (Figure 23). A

secondary bloom arose eastwards from the first, occupying more central areas of the North Sea. This was approximately a month later (21-30th April, Julian days 111-120) than when the original bloom started. A final third distinguishable bloom (11th-20th May, Julian days 131-140) was observed south of the secondary more central bloom, which covered the offshore regions around Flamborough Head. Figure 25 showed trends of elevated chlorophyll concentrations between 4th-11th April 2022 (Julian days 94-111). Recording of increased chlorophyll levels further supports the evidence for phytoplankton spring blooms off the North-East coast for 2022. Understanding the timings of phytoplankton blooming events is an important concept to aid in understanding ecosystem dynamics and carbon cycling , alongside in aiding with fishery management planning. Phytoplankton blooms serve as primary producers at the base of marine food webs, providing energy and nutrients to higher trophic levels(Capuzzo et al., 2017). The timing of blooms influences the availability of food resources for zooplankton, fish, and other organisms, impacting ecosystem structure and dynamics (Chassot et al., 2010). Many commercially important fish species depend on phytoplankton blooms as a food source during critical life stages. Understanding the timing of blooms helps fisheries managers predict the availability of prey for fish larvae and optimise fishing strategies to sustainably harvest marine resources (Dai et al., 2023). Phytoplankton also play a significant role in carbon sequestration and the global carbon cycle by photosynthesising and removing carbon dioxide from the atmosphere. The timing of blooms affects the seasonal patterns of carbon fixation and export to deeper ocean layers, influencing carbon storage and climate regulation (Dai et al., 2023).

Blooms appeared to advance down the coast in a southerly direction with increasing time (Shaw & Purdie, 2001), following similar trends in current direction observed in Figure 4. Peak phytoplankton biomass was observed in the inshore stratified zone where bloom amplitude peaked at chlorophyll concentrations of ≥ 10 mg/m^3 from satellite remotely sensed chlorophyll in April. This peak phytoplankton biomass had a duration of approximately 40 days, which started between 21st and 31st March, and terminated between 21st and 30th April. This was the most significant and noticeable bloom with the study area. *In situ* measurements recorded slightly lower peak chlorophyll concentrations of 8.8 mg/m^3 for the same zone and month. In comparison, a study by Desmit et al., (2019), estimated chlorophyll concentrations in the Belgian coastal waters and more offshore locations, observed bloom amplitude peaking at concentrations of 15 mg/m^3 and 9 mg/m^3 respectively in 2010. The concentrations observed within this study, are relatively well matched with concentrations observed at the more offshore location (closer to the central North Sea) off Belgian coast. Additionally, Alvera-Azcárate et al., 2021used remotely sensed data to estimate chlorophyll concentrations during May 2018 off the north-east coast of the UK and reported concentrations of 4.25 mg/m^3. This corresponded closely to values observed within the inshore and offshore stratified

region in the current study (peak bloom values of < 6 mg/m^3). However, these values were underestimated in comparison to chlorophyll concentration estimates from remotely sensed data for the permanently mixed region. Within this zone, bloom amplitude reached a maximum of < 8 mg/m^3 for the furthest offshore areas of this zone.

The inshore stratified region:

The inshore stratified region was observed to have largest magnitude in blooming which was seen by prolonged periods of high chlorophyll concentrations (20th March - 20th May) from remote sensing. *In situ* values also showed the greatest concentrations in April (8.8 mg/m^3) compared to the other two zones. The data outputs in regards to phytoplankton blooms need to be used with caution, as there is limited *in situ* data for this region to verify anomalies or provide accurate averages for this zone. This region's close proximity to land could also result in unreliable remotely sensed chlorophyll concentrations because of high levels of turbidity, further supporting the need for *in situ* measurements. As a result of insufficient *in situ* data for model parameters and for comparison against model outputs, no model runs were completed for this region. This subsequently meant no NPP values were derived for this zone.

The offshore stratified region:

The offshore stratified zone was the most productive region of the two stations that were used to model productivity. Remotely sensed chlorophyll images showed evidence of significant blooming within this zone between 21st March and 30th April (Julian day 80-120). The amplitude of the bloom peaked at ≥ 10 mg/m^3. Zonally averaged *in situ* and remotely sensed chlorophyll extracted data estimated chlorophyll concentrations to be 0.68 and 2.87 mg/m^3 in April. However, as only one *in situ* sample was collected in this zone during April, the in situ values are unreliable for this month. Model outputs for this region predicted increases of phytoplankton biomass to be aligned closely with observed bloom timings of remotely sensed data, thus helping to verify the timing of the spring bloom event for the offshore stratified region in 2022. The model estimated chlorophyll values to be above 1 mg/m^3 for 121 days, but because of the resolution of remotely sensed chlorophyll concentration products and the colour stretch and value range used to outline significant blooming events, chlorophyll values above 1 mg/m^3 were not observed from the remotely sensed data outlined in Figure 22 and Figure 23. A secondary autumn / late summer bloom was also observed from model outputs, however data was only gathered for the spring period, therefore the secondary bloom cannot be verified. Overall, the offshore stratified zone had a net primary production value from the S2P3 model of 43 g C m^{-2} $year^{-1}$, with a secondary simple P -I model estimating 435 g C m-2 year-1. The large

difference between these values and the reasons for the differences will be discussed within the 'Models' section below.

The permanently mixed region:

The permanently mixed region showed minimal blooming within the spring period. When compared to the offshore and inshore stratified region for the first blooming period of the year, there were no apparent areas of increased chlorophyll in satellite observations for the permanently mixed region. This zone was the last region to bloom, with remotely sensed chlorophyll concentrations indicating that blooming commenced between 11th and 20th May (Figure 22 and figure 23). Bloom timings observed from model outputs, estimated the start of the blooming period from day 172 (21st June) in 2022. However, although blooming began in more offshore locations of the permanently mixed region one month prior to this date as illustrated in Figure 23B, satellite observations showed blooming at the model station J6 (inshore location, permanently mixed zone) to have initiated between the 21st and 30th June. This therefore shows good resemblance between bloom initiation from satellite observations and model outputs. As data collection only occurred between March and June, no *in situ* data was gathered to verify the longevity of the bloom estimated from the model. There was a close resemblance in primary production output trends and patterns from the S2P3 model and the simple P-I model, helping to corroborate the timings of phytoplankton blooms from two different models. However, the total yearly NPP values were significantly different from the models with the simple P-I model estimating 385 g C m^{-2} year^{-1}, while the S2P3 predicted 35 g C m^{-2} year^{-1}. In regards to monthly averaged *in situ* and extracted remotely sensed chlorophyll concentration measurements, the permanently mixed region exhibited the second highest chlorophyll concentration out of all three zones. The causes for bloom timings and magnitude for each specific zone will be discussed below.

Stratification:

Stratification in the inshore/offshore stratified zones would constrain the phytoplankton within the surface layers of the water column and exposing the phytoplankton to sufficient PAR (Dominguez et al., 2022). The predominant wavelengths required by chlorophyll a to photosynthesise are 430-450nm and 640-680nm (Kirk, 2000; Roy et al., 2011). Underwater irradiance measurements taken in the offshore stratified region on 12th May 2022 showed a 1% penetration depths of 17m – 23m at 489nm and 8m – 9m at 664nm. This was correlated with a shoaling of MLD to <10.5m resulting in all phytoplankton that were constrained above the thermocline being exposed to sufficient irradiance at 489nm with 76% of the stratified surface water being within the photic depth at 689 nm. The MLD depth was also an average, meaning some regions within the offshore and inshore stratified zone would have sufficient PAR that exceeded the MLD. The rapid increase in phytoplankton biomass observed at this trophic

level indicates that there was sufficient light for phytoplankton to photosynthesise (Sigman and Hain, 2012). In comparison, the permanently mixed region had poorer light penetration. A 1% euphotic depth for 489 nm of 6m was measured at our inshore coastal site and 19-21m for our two offshore sites. At 664 nm, the inshore site had 5m 1% euphotic depth with a 12m – 13m at 689nm with both measurements being taken on 9th June. MLD in June for the permanently mixed region averaged 28m which exceeded the 1% euphotic depth for all available PAR. These factors could have contributed to the dilution and dispersion of phytoplankton away from available PAR (Opdal et al., 2019), which may be an explanation for the decrease in primary production observed in the permanently mixed region. However, some studies have suggested that photoinhibition could be reduced by mixing of the surface layer, subsequently increasing phytoplankton production (Pan et al., 2016).This was not observed to be the case, due to the permanently mixed region being least productive site, and the evidence provided that the mixed layer depth exceeded the 1% photic depth in this zone.

Key drivers:

The temporal and spatial distribution of blooming events off the north-east coast were found to be dictated by the onset of stratification. The inshore and offshore stratified regions had early shoaling of the MLD in March, with an MLD of approximately 19m - 40m. This correlated closely with a rapid increase in phytoplankton biomass for both these regions at the end of March. *In situ* measurements recorded 8.8 mg/m^3 and 3.9 mg/m^3 in April for the inshore and offshore stratified regions respectively. The permanently mixed region was highly mixed for the whole spring period, with slight shoaling to approximately 28m in June. This correlated with elevated chlorophyll values from the S2P3 model, which estimated blooming to begin at day 171 (20th June).

Tidal forcing and mixing of the water column:

Tidal forcing plays crucial role in influencing primary production due to the co-variability in hydrodynamic tidal parameters and biogeochemical data (Blauw et al., 2012; McCandliss et al., 2002). Tides amplify the vertical mixing of phytoplankton biomass and the resuspension of settled sediment and nutrients (Zhao et al., 2019). Increased mixing results in the deterioration of light conditions, but causes the injection of nutrients into nutrient depleted surface waters, thereby fuelling primary production (Allen et al., 2004). Neap and spring tidal cycles were seen to influence stratification and phytoplankton blooming within the permanently mixed region of our study site. The model outputs showed trends in cyclical blooming events approximately every 14 days. This suggested that the blooming was impacted by the onset of neap tidal cycles on a fortnightly periodic time scale. NPP and chlorophyll a concentration peaks aligned with the end of the neap tidal phase. Neap tidal phases have the characteristics of a reduced vertical water column mixing caused reduced current speeds (Sharples

et al., 2006; Sharples, 2007; Zhao et al., 2019). From the model outputs shown in Figure 50, a fortnightly cyclical trend of reduced current speeds was observed within both the permanently mixed and offshore stratified region. The low vertical mixing affiliated with neap tidal phases is associated with transient stratification events, which constrains the phytoplankton in the photic zone, and also helps reduce sediment resuspension (Zhao et al., 2019). This therefore increases phytoplankton cellular exposure to PAR, providing a stable water column for a blooming event to occur (Sigman and Hain, 2012). As the neap tidal phase concludes, spring tidal phases bring greater current speeds which cause the erosion of stratification which deepens the MLD. Increased current speeds provide a more turbid environment which causes a deterioration in light conditions and reduces the photic depth (Sharples, 2007; Zhao et al., 2019). This, coupled with increased dispersion and dilution of phytoplankton away from the illuminated surface water (Cloern, 1991), was consequently the cause of the breaking down of earlier blooming events found within the permanently mixed region in 2022. The effect of spring-neap tidal cycles was negligible for the offshore stratified region due to the overall lower daily current speeds and also because this region experienced prolonged periods of stratification that were unhindered throughout the spring and summer months. These tidal cycles in combination with a high K_d could be potential reasons for a reduced NPP yield within the permanently mixed region when compared to the offshore stratified zone.

Stormy weather conditions can facilitate the breakdown of stratification through the increased vertical mixing of the water column (Nicholson et al., 2016). The vertical mixing within storm events is predominantly attributed to wind induced surface stresses (Gronholz et al., 2017). Peak mixing is enhanced when storm events are in conjunction with spring tidal phases which provides greater potential for the breakdown of stratification (Gronholz et al., 2017). Passing storms can also result in turbulent mixing extending below the surface. Inertial mixing is the key driver to interior mixing which can last for days, or even weeks after a storm has passed (Nicholson et al., 2016). These events could have notable implications on the development and formation of phytoplankton bloom events, in particular the formation of autumnal blooms, by which storm events supply fresh nutrients into the once depleted stratified surface layer, thereby facilitating a new phytoplankton bloom (Nicholson et al., 2016; Gronholz et al., 2017).

Frontal systems can result in upwellings in stratified waters along coastal stretches which re-supply nutrients back into oligotrophic surface waters, thereby fuelling further productivity (Moore et al., 2003). There is an affiliation between tidal fronts and spring thermocline formation which is demonstrated by the Flamborough frontal system which separates cooler and deeper stratified norther North Sea waters from the highly mixed warmer southern North Sea waters off the north-east coast (Ducrotoy et al., 2000). The temperature differences observed either side of the frontal system can be

seen from Figure 14, alongside the CTD casts taken from Staithes (north of the Flamborough Front) and Bridlington (south of the Flamborough front). Bridlington observed to have greater water column temperature in comparison to staithes. These temperature differences can play a key role in the magnitude of blooming events alongside the timings as a result of the effects on stratification formation as well as increasing phytoplankton growth and photosynthetic carbon assimilation (Trombetta et al., 2019). However, increased SST in the permanently mixed zone was not correlated with increased phytoplankton productivity or growth rates. It is also believed that phytoplankton growth rates are greater than herbivorous grazers at lower temperatures, which could provide a possible explanation to increased productivity in the cooler offshore stratified zone. Lower water temperatures could be more favourable to phytoplankton than their grazers (Trombetta et al., 2019), resulting in a greater accumulation of phytoplankton biomass in the cooler of the study site. The Flamborough front provides an effective barrier that isolates the northern and southern water masses, where little exchange between the two hydrodynamic regions occurs (Holligan, 1981; Eaton et al., 2003). This could result in distinct plankton communities found within our offshore stratified and permanently mixed zones,, resulting in potential implications on phytoplankton productivity because of variations in growth rates of different phytoplankton species. Future research to decipher phytoplankton community composition within each hydrodynamic zone would be the next step to furthering this study. It would help understand the impact of different species on phytoplankton productivity, alongside investigating potential toxic species that could cause significant harm to the environment. Methodology to achieve this would include microscopic sampling, flow cytometry and size analysis. Size analysis could aid in understanding zooplankton composition within each region, due to differing phytoplankton cell sizes impacting zooplankton species composition (Finkel et al., 2009).

Suspended particulate matter and light attenuation:

Increased sediment loads and turbulent mixing were the main contributors to decreased water clarity of the study area. When assessing the trends between different water properties for all light measurements in the study site, SPM had a strong positive trend with increasing light attenuation and therefore could have been a significant contributory factor impacting phytoplankton blooming within each zone**.** There was no correlation between chlorophyll and CDOM with increasing K_d. The north-east coast is a highly erosive coastline with additional large inputs of sediment contributing to overall SPM from the Rivers Humber, Tyne and Tees. The resuspension of sediments from strong tidal mixing, waves and storm events causes less favourable underwater light conditions through elevated K_d values (Cloern, 1987; Uncles et al., 2005; Quinn et al., 2009; Porter et al., 2010). The permanently mixed region had highest SPM and K_d of all three zones, with SPM in April at around 4.7 g m-3 and with a K_d of 0.31. This could provide evidence to why there was no spring bloom present, and to why a delayed

bloom was observed from the model output. Blooming could not have occurred until the photic depth exceeded the MLD (Devlin et al., 2008). This process is known as Sverdrup's critical depth hypothesis, which states that phytoplankton growth is determined by the relationship between phytoplankton's light requirements and the depth to which enough light can penetrate for photosynthesis to exceed respiratory losses (Sathyendranath et al., 2015). The critical depth is defined as the depth in the water column at which the available light energy becomes insufficient to support net photosynthesis. When phytoplankton are mixed deeper than the critical depth, their growth is limited because they do not receive enough light (Sathyendranath et al., 2015). Conversely, when they are above the critical depth, there is an excess of light, and growth is not light-limited. The critical depth hypothesis suggests that if the depth of the euphotic is deeper than the critical depth, phytoplankton growth will be light-limited, and primary production will be reduced (Sathyendranath et al., 2015).

The offshore stratified region had the lowest SPM and thereby lowest K_d when compared to the other hydrodynamic regions, suggesting a potential reason for increased NPP and chlorophyll concentration measured in comparison to the permanently mixed zone. Significant blooming occurred In April with SPM concentrations being measured at 2.83 g m^{-3} less than the concentrations observed in the permanently mixed region. This suggests that (lack of) SPM was a key driver in bloom timing. The permanently mixed region began to bloom in June with SPM values recorded for this time at 2.1 g m^{-3}. This was 0.3 g m^{-3} greater than SPM observed in the offshore stratified zone in April. This indicated that approximately 2 g m^{-3} of SPM could be the critical threshold in which light attenuation was sufficiently low enough to facilitate blooming events, on the assumption that chlorophyll and CDOM did not significantly contribute to light attenuation. SPM is relatively easy to measure from satellite remote sensing, as the widely accessible calibrated images available from the Copernicus Marine Service increase the reliability of SPM data used.

The inshore stratified region had the second lowest SPM, which corresponded to similar temporal patterns of blooming events as the offshore stratified zone. However, *in situ* measurements showed greater magnitudes of chlorophyll a concentration in April when compared against the other zones, although the fact that limited samples were taken in this region may have impacted the monthly average and anomalies may not have been detected or averaged out.

The self-shading of phytoplankton which occurs when phytoplankton production rate exceeds zooplankton grazing (Kirk, 2000; Zhao et al., 2019) can increase K_d estimation. The shelf-shading effect was not measured in this study , despite the fact that it could play a pivotal role in productivity within our zones. The permanently mixed region could be susceptible to elevated SPM due to increased re suspension of sediments that could cause greater light attenuation. This factor could have contributed

to smaller magnitude blooming events found within the permanently mixed region by shallowing the photic depth. The self-shading effect of the large phytoplankton blooms observed in the inshore / offshore stratified region could explain the reduction in bloom longevity/period as observed by the termination of the spring bloom for stations 13 model run. Bloom intensities peaked at ≥ 10 mg/m^3, so therefore within these regions, it can be estimated that a K_d of approximately 0.2 m^{-1} would be a result of these 10 mg/m^3 blooming events. This is based off the assumption that chlorophyll-specific K_d is about 0.02 m^2 (mg chl a)$^{-1}$ (Krause-Jensen & Sand-Jensen, 1998).

The North-east waters were found to be very variable with respect to optical properties. Almost the entire range of Jerlovs' water types can be found within a short distance resulting in increased variability in productivity over short distances. The variation in productivity output resulting from differing optical properties within each zone creates issues when calculating zonal averages for the outlined hydrodynamic zones. The optical properties varied temporally and spatially, which justifies the reasoning for regular optical sampling for this region to help improve accuracy in results and identify potential trends in the study area. There was evidence that SPM was the key driver in spectral change between sites (Figure 31). Chlorophyll and CDOM were observed to have negligible impacts on light attenuation. CDOM in particular needs to be further investigated due to elevated recordings of CDOM being observed within the River Humber plume which subsequently could contribute significantly to increased light attenuation in this region.

Nutrients:

The monthly averaged nutrient data supported the presence of spring blooms off the north-east coast: a rapid biological drawdown of nitrate, nitrite, phosphate and silicates in April was followed by an increase in ammonium from April to May, which suggests there as elevated decomposition of organic matter after the initial spring blooming events in late March/early April. Areas where nutrients are < 3 µM ≈ 0.186 mg/L are referred to as 'nutrient poor regions' (Hayashida et al., 2020), which suggests the study site monthly averages for nutrients in May and June for nitrates (concentrations 0.04 mg/L and 0.06 mg/L respectively) are relatively close to values which could potentially limit phytoplankton growth

Zonally averaged nitrate concentrations showed the inshore stratified region to have sufficient nitrogen concentrations in 9 months of the year to facilitate significant blooming. However the lowest nitrate concentrations, observed in May, August and October (Figure 37) were <0.1 mg/L, which may only be sufficient enough to facilitate limited phytoplankton growth (Hayashida et al., 2020). This would provide species that can withstand lower nitrogen concentrations, such as dinoflagellates (Fouilland et al., 2007; Pozzobon et al., 2021) with their biological strategy of mixotrophy (Litchman, 2007), an opportunity to thrive, with a consequent alteration to the phytoplankton species

composition. This potentially provides evidence to why the inshore stratified region experienced prolonged periods of blooming observed from remote sensing, due to reduced silica concentrations post spring bloom (Figure 39) and lower vertical water column mixing and water clarity. This could also be the case for the offshore stratified zone, but because of limited nutrient concentration measurements for this region, it unknown whether nitrates are limiting. The permanently mixed region conditions suit diatom growth more favourably as result of increased vertical water column mixing and low irradiance (Pan et al., 2016). Diatoms rapid growth rates and inability to control their buoyancy, results in them n being circulated by currents and mixing into the high irradiance surface waters, allowing these species to thrive in turbulent conditions (Pan et al., 2016). However, although May, August and October in the inshore stratified region are supposedly nutrient poor, they are still above the half-saturation constant (0.7 micromolar (µM) ≈ 0.0434 mg/L) used for the majority of model runs in the study by Hayashida et al., (2020). This suggests that photosynthesis can still occur, but just at reduced rate, decreasing productivity and phytoplankton growth within these months.

The permanently mixed region had noticeably lower nitrate concentrations from June to November when compared with the inshore stratified region. The concentrations recorded for these months were all below 0.055 mg/L in the permanently mixed zone, which is considered to be within the nutrient poor range (Hayashida et al., 2020). Values from July to October were below the half-saturation constant of (0.7 µM ≈ 0.0434 mg/L.) estimated by Hayashida et al., (2020), possibly suggesting reduced/inhibited phytoplankton growth. The bloom timing observed for this region began in June and lasted until late summer from model outputs, which suggests that phytoplankton species composition could be different at the inshore site, as these levels of nitrate concentration would not support the majority of phytoplankton blooming events in the permanently mixed region. In addition, this region had high currents speeds and greater water column mixing , with limited stratification, meaning greater replenishment of nutrients to surface water would be expected for this region (Nicholson et al., 2016). Alongside the highly mixed zone, it is in close proximity to the Humber estuary, so nutrient replenishment should be a regular occurrence. However lower salinity levels in close proximity to the Humber estuary (fresh water input from the River Humber) were also observed, whereby fresher water was observed at the surface with more saline water close to near-seafloor depths. Salinity variations influence phytoplankton growth and distribution by altering water density and stratification (Horii et al., 2020), which in turn affect nutrient availability and mixing dynamics. The salinity gradients observed may have served as physical barriers for the transport of nutrients (Horii et al., 2020) to surface waters – limiting the amount of available nutrients for phytoplankton which in turn may have halted blooming events. These results suggest that a spring bloom may have occurred (Malone et al., 2016), but that the predictions for this zone miscalculated the bloom timing.

Alternatively, the phytoplankton in this region are highly adapted to thrive under low nitrogen conditions or use another form of nitrogen such nitrite or ammonium (Salmaso & Tolotti, 2020). Ammonium was observed in high concentrations in May, which could have potentially have fuelled the blooming for the permanently mixed region in late summer. Nutrients may not have solely been depleted by phytoplankton, and consideration needs to be given to nutrient uptake from other biological organisms such as seaweeds or seagrass which may have contributed to nutrient limitation. There are known large kelp beds along the North-east coast, alongside Zostera noltii seagrass beds within the Humber estuary

For the study site as a whole, silicate concentration decreased to negligible amounts in May, which could result in a shift in phytoplankton species composition for the north-east coast (Arteaga & Rousseaux, 2023). The decrease in silicates from March through to May suggests spring bloom events may have comprised of a large biomass of diatoms because of their requirements of silica to form opal hard parts (Oehler et al., 2015). Then, as silicate concentration becomes limiting during May, a shift in phytoplankton species from diatoms to dinoflagellates may have occurred in blooming events from May onwards. Large blooms of dinoflagellates, particularly those containing dinoflagellate species that produce harmful toxins (Karlson et al., 2021; Arteaga & Rousseaux, 2023), could potentially have negative impact on environmental health and cause devastation to the crab and lobster fisheries located off the north-east coast of the UK. Blooms during the late summer and autumn have the potential to be HABs, but further research is needed to understand the phytoplankton species composition of north-east coast of the UK.

Nutrient concentration estimations were based on surface water sampling, therefore nutrient limitation may only be occurring within the surface layer. Future research would include vertical nutrient gradient analysis, to enable the estimation of nutrient levels below the thermocline . This would provide a more complete picture as to whether nutrients are limiting within the whole water column rather than just the surface water. Observations of a potential sub-surface chlorophyll maximum from our CTD casts (Figure 17 & 18) at several locations within the offshore stratified region suggest that nutrients may not be limiting at depth. This evidence provides justification for further investigation

Sea surface temperature:

SST was highest in the permanently mixed region, possibly due to warm water outflow from the River Humber (Wang et al., 2021). From the SST remotely-sensed data, water was warmest around the Humber estuary in early summer, helping to verify the theory of warmer water from riverine outflow increasing SST. The inshore stratified region experienced the coldest waters which contradicts bloom

timing observed from the results, as it is thought that increasing SST boosts phytoplankton productivity by impacting the photosynthetic carbon assimilation under light saturated conditions (Lewandowska et al., 2012). It has been observed that, in low light saturation conditions, increased SST facilitates nutrient uptake (Trombetta et al., 2019), although, as photosynthesis cannot occur in the absence of light, SST cannot be described as a key driver on its own. This therefore suggests that the offshore stratified site may have been more productive as a result of warmer waters when compared to the inshore site. The permanently mixed region was the warmest zone, but the higher water temperatures could not assist in the increase in productivity because of the extent of light attenuation in the region. High SST in the permanently mixed region, coupled with elevated light attenuation, provides plausible evidence as to why nutrient levels were the lowest in comparison to the inshore sites (Cross et al., 2014). Increased nutrient uptake by phytoplankton in warm water, low light saturation conditions may have depleted nitrate conditions in summer when SST was greatest.

Predator prey interactions:

Predator-prey interactions may adversely affect / reduce bloom magnitude in all three zones, with phytoplankton biomass decreasing, and the reduction of phytoplankton concentrations as a result of grazing by zooplankton and other predators (Franks, 2001). Predator-prey interaction could be elevated through advection and vertical water column mixing, as a result of increased transportation of zooplankton into the area (Vernet et al., 2019; Zhao et al., 2019). In addition, elevated advection and vertical water column mixing could also increase filtration capacity for filter-feeding species such as bivalves and sponges, resulting in overgrazing of phytoplankton (Smaal et al., 2013). This could mean that increased water column mixing makes the permanently mixed region susceptible to greater phytoplankton grazing, which subsequently could be a potential reason to why NPP was lower in this zone compared to the others. There was evidence of stratification within station 13, which could have restricted transportation of zooplankton between layers, resulting in reduced grazing and an increase in phytoplankton growth and primary production In contrast, the increased vertical mixing observed in the permanently mixed zone, could also increase dispersion and dilution, which could ultimately lead to reduced predator-prey interactions (Behrenfeld, 2010). Both of these predator-prey interaction theories are described under the Dilution-Recoupling Hypothesis, in which optimum growth conditions favour the growth in numbers of both phytoplankton and predators, resulting in greater predator-prey interactions (Behrenfeld, 2010; Boss & Behrenfeld, 2010). During winter months, when MLD is greatest and stratification minimal, dispersion of predators results in reduced predator-prey interactions. Shoaling of the MLD in spring and summer, alongside increased zooplankton biomass, results in increased predator-prey interaction (Behrenfeld, 2010; Boss & Behrenfeld, 2010), thereby reducing phytoplankton growth – and ultimately primary production – through overgrazing.

Wind Farms:

The recent offshore wind farm installations in the North Sea alters hydrodynamical conditions as a result of the wind wake effect from clusters of turbines. There is evidence of shallowing of the MLD by approximately 1m – 2m due to increased wind farm wake and because of the upwelling and downwelling dipoles (Daewel et al., 2022; Floeter et al., 2022). Additionally, increased turbulence and mixing is likely to result in the resuspension of sediment in the wake of turbines (Forster, 2018) that could be a contributing factor in the deterioration of light conditions in the area. This can cause decreases in productivity in regions with the study area that are within close proximity to the wind farms. The north-east coast is a hotspot for wind farm construction, with many farms already erected and more within the planning phase. The permanently mixed region could particularly be susceptible to the effects of wind farms due to the large Hornsea 2 wind farm that was constructed just off the coast. This could therefore result in the reduction of primary production with the permanently mixed region, providing another possible explanation to lower productivity observed with this region in comparison to the other zones. The majority of studies estimate these issues to be localised, however the growing number of wind farms in the North Sea could result in the cumulative impact on stratification and increase sediment load (Daewel et al., 2022; Dorrell et al., 2022).

Remote sensing:

Reliability of remote sensing data:

Stratification and MLD:

The use of MLD data from remote sensing and models was partially verified by our *in situ* CTD casts, where stratification was observed in the offshore stratified region. Both the remotely sensed model products and *in situ* CTD casts showed stratification in May. However further *in situ* data is required to support this line of evidence, with multiple CTD casts, long-term glider transects and ferry box data required throughout the year to use as a comparison to verify the modelled MLD data from the Atlantic- European North West Shelf- Ocean Physics Reanalysis model (Copernicus Marne Service found at: https://doi.org/10.48670/moi-00059). SPM data showed a positive trend between remotely sensed extracted data and *in situ* measurements, helping to verify that the SPM data used for K_d estimates was reliable and that SPM used from satellite can be an accurate measure of *in situ* values for our study area. Finally, *in situ* SST measurements from Cefas Wavenet and SmartBuoy data showed a close resemblance with satellite-extracted SST from multiple locations spanning our sample area. This too helps verify the reliability of SST data used from remote sensing products.

Chlorophyll estimations:

Some chlorophyll values used in this study were extracted from remote sensing, but must be used with caution as high sediment loads around estuaries and coastal areas can result in chlorophyll concentrations being over estimated in some months (Yamaguchi et al., 2013). There were similar trends in remotely sensed SPM and chlorophyll a whereby variations observed in SPM during winter months were mimicked in chlorophyll a values. This could provide potential overestimation in annual productivity outputs and is particularly problematic in early spring and autumn when vertical mixing is high, but phytoplankton bloom conditions begin to align, and potential blooming events could be under/overestimated as a result of high sediment loads.

Subsurface chlorophyll maximums (SCM):

Optimal light conditions and nutrients can support the formation of SCM at the thermocline (Sharples & Tett, 1994). The sinking rate of phytoplankton is attributed to the determination of the formation of SCMs and research in the North Sea has found formations of SCMs to have varying spatial and temporal distributions within stratified waters of the northern North Sea (Sharples, 1999; Richardson, 2000). Research into sub-surface abundance of dinoflagellates found at the Dogger Bank confirmed the presence of sub-surface phytoplankton communities, and that mobile phytoplankton communities were not confined to surface waters or dictated by currents (Nielsen et al., 1993). The formation of SCMs occurs near the presence of nutriclines, where nutrient rich water below the thermocline can fuel phytoplankton growth at depths where light conditions allow (Cullen, 2015). However, nutrients at depth for our zones cannot be confirmed, due to all nutrient analysis being undertaken at the surface. Additionally, in the presence of stratification, there can be elevated surface concentrations of zooplankton which decrease with depth in line with a reduction in light and available chlorophyll (Gamble, 1978; Moeller et al., 2019). This could be a potential explanation for the presence of an SCM (observed super saturation in oxygen and increased fluorescence at depth) on the Staithes transect (sites M16, M17 and M19 in figure 16, 17 & 18) in the offshore stratified region during May. After significant blooming events that occurred in April, increased zooplankton grazing at the surface could be an underlying factor which drove SCM formation within this region. The presence of SCMs observed, could also potentially hinder overall productivity values for the offshore stratified zone, as a result of remote sensing only taking into consideration surface chlorophyll a concentrations. In addition, the model runs used may not have simulated SCMs correctly. Due to the lack of *in situ* data to prime the model, grazing and sinking parameters were set to default. This may have resulted in an underestimation of NPP for the offshore stratified region. The *in situ* CTD casts taken in the permanently mixed region provided no evidence of the presence of SCMs unlike in the offshore stratified zone, where evidence of the existence of SCMs were found. This suggests NPP estimations

were more accurate in the permanently mixed zone than the offshore stratified zone, because no subsurface blooming contributed to overall NPP.

Primary production models:

There were significant differences in primary production estimates between the two models used. Meteorological data inputs were proven to be reliable by reason of a close match-up between the comparison of model output SST and remotely sensed SST. This helps to increase the reliability of NPP outputs from the models due to the model being driven by meteorological inputs.

S2P3 O_2:

GPP and NPP estimations from the model outputs could be skewed as a result of the model's calculation being based on a single vertical plane, overlooking the crucial consideration of lateral movements such as lateral advection in the North Sea proposed by Van Haren et al., (1998). Since factors affecting primary production vary across different spatial scales, the model's output may not provide a comprehensive representation of the study area. Furthermore, the model assumes a single background K_d value for the entire year, disregarding the daily fluctuation of sediment loads and CDOM which would vary light attenuation and therefore phytoplankton production rates. Early spring storms could alter the K_d average estimates used for the model, which might distort the outputs of the model and reduce/increase primary production estimates. Additionally, the model only considers maximum seabed dissolved inorganic nitrate values, neglecting nutrients from freshwater inputs. Notably, the North-east region, where stations 13 and J6 are located, receives significant nutrient loads from agricultural land draining into the Humber and Tyne/Tees estuaries, but these inputs are not incorporated into the model (Burson et al., 2016). This limitation could hinder the accuracy of the model's primary production output. It should however be noted that increased nutrient loads do not necessarily have a positive impact on primary production. In fact, the influx of nutrients, together with run-off of other dissolved materials, can lead to 'coastal darkening', reducing primary production in coastal regions due to reduced light availability, as demonstrated in studies by Mustaffa et al. (2020).

Biological parameters used for model runs were left as default (lack of *in situ* data) which could have significantly impacted on overall productivity estimates. Phytoplankton growth rates, grazing, and detritus parameters were set to Celtic Sea default settings used by Sharples (2012), however these parameters could vary based on phytoplankton assemblages and adaptive responses to changes in varying cell exposure to PAR (Shaw & Purdie, 2001). Grazing parameters could pose particular issues in respect of the formation of SCMs, whereby both factors could significantly reduce daily productivity estimates for the region. Additionally, model outputs had depth intervals of 2.5m. This low resolution may underestimate water column activity by failing to take into consideration processes that occur at

greater resolution within the column. The blooming events predicted in this model were heavily dependent on the onset of stratification, which for this study area aligned correctly with the key driver for productivity for this region. However, the magnitude of blooms observed from the model could not be fully verified due to insufficient *in situ* data being available, therefore making this a key area for further research. Future research should also consider the use of 3-dimensionial modelling in higher resolution to estimate productivity with higher degree of accuracy for the three zones in outlined in this study. Potential models that could be used are a 3d version of S2P3 (Halloran et al., 2021) or ERSEM model (Butenschön et al., 2016).

The S2P3 model offers several advantages when investigating the physical and biological controls on phytoplankton blooming events in the North Sea. The model employs a process-based approach, incorporating high amounts of parametrisation for physical and biological processes such as nutrient cycling, light availability, current speed, metrological conditions and grazing interactions, which provides a comprehensive understanding of bloom mechanisms. The parameters can be adjusted to consider local hydrodynamics , which was beneficial for this study when three separate hydrodynamic zones were present within the survey area (PM, IS and OS zones). The model operates at high spatial and temporal scales on a vertical plane, enabling detailed simulations of phytoplankton blooms throughout the water column. Additionally, the model allows for scenario testing to investigate the impacts of various physical and biological factors on phytoplankton blooms, facilitating hypothesis testing for ecosystem management in the North Sea. The overall model outputs were validated against *in situ* measurements and satellite observations and were proven to be closely aligned, enhancing confidence in the models accuracy and reliability.

Simple P-I Model:

Remotely sensed gap free chlorophyll concentrations were used within this model. As previously discussed in the chlorophyll estimation section within this discussion, it is thought the elevated chlorophyll values in winter are an artefact of turbidity. This could have disrupted model outputs for the simple model due to high chlorophyll values being recorded within winter, which is not the case. We can see chlorophyll values based on *in situ* measurements and satellite images in early March that phytoplankton biomass did not peak within winter. This could increase the estimation of NPP from this model when compared to S2P3.

The model parameters $P_{b(max)}$ and Alpha (α) could have been overestimated as a result of the extremely high productivity estimates from the model. Overestimation of these parameters would impact overall productivity output. The $P_{b(max)}$ and (a) used were North Sea phytoplankton averages based on the research from Shaw & Purdie, 2001 and Napoléon et al., 2014. However, these values are out dated

and are not solely taken from the north-east coast, therefore providing a possible reason to why estimates were greater than the S2P3 model. Future research would require *in situ* photosynthesis-irradiance parameters to be gathered for greater accuracy in model run outputs, with particular focus on greater nutrient data collection, because of the correlation between nutrient limitation and reduced $P_{b(max)}$.

The simple P-I primary production model had high temporal resolution. This allows for a detailed understanding of phytoplankton growth dynamics, capturing short-term fluctuations and diurnal patterns in primary production rates, leading to more realistic estimations of primary production rates. Additionally, the simplicity of the model whereby only surface PAR, light attenuation, chlorophyll concentration and photosynthetic efficiency parameter were required, allows for quick and efficient primary production estimates when limited data is available.

Comparison to other studies:

Productivity estimations:

Productivity estimations for the North Sea in areas influenced by freshwater inputs had a GPP of 382 g C m^{-2} $year^{-1}$, with the least productive regions of the North Sea, which remains permanently mixed having an average GPP of 82 g C m^{-2} $year^{-1}$. (Capuzzo et al., 2017). In comparison with our GPP results, the S2P3 model estimated 82 g C m^{-2} $year^{-1}$ for station 13 (offshore stratified) and 76 g C m-2 year-1 for station J6 which is situated in the permanently mixed region. Excel model predicted 604 g C m^{-2} $year^{-1}$ for site 13 with 594 g C m^{-2} $year^{-1}$ at site J6. The S2P3 model outputs for both the offshore stratified and permanently mixed zone resembled most closely to the least productive regions of the North Sea as estimated by Capuzzo et al., (2017). Conversely, outputs from the Excel model for the same sampling sites greatly exceeded the most productive regions estimated by Capuzzo et al., (2017). This suggests the outputs from Excel model could be more unreliable than the S2P3 results due to the extreme productivity values estimated.

Key drivers:

Stratification and light attenuation were observed to be key drivers from a multitude of studies (Sharples et al., 2006; Capuzzo et al., 2012; Capuzzo et al., 2015; Capuzzo et al., 2017), suggesting that the key drivers observed from our research were realistic. This helps to verify that the research undertaken was reliable and therefore can be used in further research on primary production off the north-east coast.

Considerations on the methods and limitations of the research:

One limitation to this research was the equipment used for underwater light measurements. The absence of an inbuilt pressure gauge or surface PAR sensor, determining the underwater spectral measurements accurately throughout the water column was difficult. A low sample rate for depth when the dive watch was used, alongside a sampling delay for the OCR rigs, made the match-up of depth and underwater light measurements challenging. This, coupled with tidal and current forces, resulted in the OCRs experiencing drift, further increasing the challenges in assigning depth to underwater light measurements. These issues resulted in estimations of depth based on descent rate, the amount of rope let out and the dive watch readings based on a low sampling rate. This could have adversely affected the accuracy of the depth at which the OCRs collected measurements, possibly resulting in over / under estimations of light attenuation. However, the positive correlation between *in situ* K_d measurements and SPM derived K_d indicate that the methods used to derive depth and overall K_d were not completely unreliable. Perturbation of the light field is associated with wave action and surface incident flux changing due to drifting clouds (Kirk, 2000). To ensure reliable data, a handheld PAR sensor was used to offset underwater irradiance with changing surface PAR. However, the handheld PAR sensor did not have a data logger feature, therefore meaning measurements were taken every 5-seconds using a video recording taken of handheld sensors digital display. This meant fluctuations between each reading were not accounted for. In addition, matching the surface PAR to the underwater PAR posed problems in regards to complete accuracy, by reason of measurements being matched by eye using graphical outputs.

Another limitation was that only 1-replicate was taken for chlorophyll filtration and spectrophotometer samples, which meant anomalies may not have been identified. No replicates, meant averages could not be taken for each sample batch. Future studies would be designed to take triplicate samples in order to provide greater accuracy in the quantification of chlorophyll concentration. Additional time and budget would be required to allow batch sampling through a more advanced spectrophotometer to allow more than one sample to be measured at a time. The reliability of the spectrophotometer used in this study was questionable, with variations in baseline absorbance with repeated use being observed.

The use of vessels of opportunity provided good access to broad sampling sites across the study area, however, the sporadic nature of vessel cruise plans meant that determining temporal and spatial patterns of blooming events was extremely challenging. The use of multiple sample sites spanning the study area where sampling can reoccur, would help provide a greater understanding of the spatial and temporal distribution of phytoplankton. Moreover, the research collection period between March-June

was suitable for the observation of a spring bloom, but did not encompass any potential autumnal blooms which may have occurred. It also meant biological and physical parameters were not completely mapped from *in situ* measurements for the whole year which would have been key for model parameters that required data for Julian day 1.

Finally, the hydrodynamic zones outlined in this study vary significantly in regards to spatial coverage and area. This could result in zonally averaged measurements being skewed. In particular, the greater size of the offshore stratified region in comparison to other zones increases the likelihood that blooming does not occur across the whole area or at the same time. The significance of this is that zonally averaged chlorophyll data may have been under-estimated. This could provide evidence as to why the offshore stratified region was deemed to have the lowest chlorophyll concentrations when zonally averaged. In Figure 22 and 23, the satellite images show blooming throughout the northern parts of the offshore stratified region during April and May, with minimal blooming in the southern areas of the offshore stratified zone. This provides further evidence to hydrodynamic zone size hindering chlorophyll estimations.

Evaluation of the approaches used:

Satellite Observations:

Positive:

1) **Spatial Coverage:** Satellites provided broad spatial coverage, allowing for observations over the entirety of our study area, which was beneficial for the monitoring of spatial distributions of large scale phytoplankton blooms and oceanographic factors (Eg, Sea surface temperature) across the entire survey site.
2) **Access of data:** Satellite sensors allowed the enhancement of our datasets for regions that were un accessible by vessels of opportunity, or for the collection of data that fell outside our survey period, but was required for further enhancement of our datasets.
3) **Temporal Resolution**: Satellite data could be collected regularly and consistently over time, enabling the detection of long-term trends and seasonal variability in phytoplankton blooms and oceanographic factors.
4) **Tracking of phytoplankton blooms**: Satellite data was extremely useful for the tracking of blooming events, allowing *in situ* sampling to be planned to allow the capture of *in situ* data within blooming areas of the survey site.

Negatives:

1) **Limited Depth Resolution**: Satellite sensors could not directly measure phytoplankton biomass at depth, limiting the ability to capture vertical variations in phytoplankton distributions within the water column, potentially leading to the under estimation of primary production when satellite chlorophyll concentration were used. Limited depth resolution was also apparent for understanding the vertical structure of the water column with remote sensing.
2) **Cloud Cover**: Satellite observations were hindered by cloud cover and limited observations in certain weather conditions – reducing the amount of available data over the winter months when cloudier weather was present.
3) **Algorithm Sensitivity**: Interpretation of satellite-derived chlorophyll-a data requires algorithms that may be sensitive to factors such as water colour and optical properties, leading to potential inaccuracies in biomass estimates. The north-east coast is a highly turbid region (especially inshore locations) and these high turbidity readings could skew chlorophyll estimations based from satellite observations

In Situ Data Collection:

Positive:

1) **High Resolution**: In situ measurements, such as water sampling and profiling, provided high-resolution data on phytoplankton biomass and oceanographic parameters at all depths within the water column, allowing for detailed assessments of bloom dynamics and controls.
2) **Validation:** Our *In situ* data was used to validate satellite observations which could help to improve the accuracy of remote sensing algorithms. It would also allow for greater confidence in the use of remote sensing data withing the report, when *in situ* and satellite data was aligned. Outliers from satellite data could also be investigated based on *in situ* measurements collected for the same area. For example, checking if high CHL values recorded from remote sensing were true values based of *In situ* CHL extraction methods.
3) **Direct Measurements:** In situ instruments directly measured phytoplankton biomass, providing more accurate assessments of vertical and temporal variability in bloom dynamics. This aided in more accurate estimations of primary productivity.

Negatives:

1) **Limited Spatial Coverage:** In situ data collection was typically localised and not evenly spread across the survey areas. It was also resource-intensive (required chartering of vessels), making it impractical for obtaining comprehensive coverage of the survey area.

2) **Temporal Constraints:** In situ sampling was limited by weather conditions, ship availability, and budget constraints, restricting the frequency and duration of data collection. Resulting in limited *in situ* instrument deployment (11 sites where instrumentation was deployed).In addition, for a project of this size, long term *In situ* data collection was not feasible, reducing the availability of high resolution data within the survey area for a full year time scale.
3) **Sampling Bias**: In situ measurements were subject to sampling bias due to the uneven . distribution of sampling locations, potentially affecting the representativeness of data. A significant proportion of the data was collected on our behalf and were based off where local fisherman were going, so data locations were biased towards these locations. The majority of data was collected off the coast of Whitby, which limited the amount of data covering other areas of the survey site.
4) **Suitability of the Multispectral radiometer**: Although the data collected by the OCR was extremely useful in assessing the underwater light environment, the absence of a depth or pressure sensor reduced the accuracy of the findings. The use of alternative methods for depth measurement required a match ups based on depth estimations.
5) **Replicates**: Only one replicate was taken for chlorophyll extraction at each station. This therefore meant anomalous results may have been taken as true values, reducing the accuracy of CHL .

Modelling:

Positive:

1) **Phytoplankton blooming estimations:** The S2P3 and P-I models simulated the timing of blooming events accurately when compared against *in situ* data and satellite observations. It also provided a good insights into the underlying mechanisms driving bloom dynamics through the adjustment of parametrisation.
2) **Prediction**: With the success of accurate estimation of bloom timings using models, it can therefore be used to forecast phytoplankton blooming events based on specific environmental conditions observed.
3) **Investigation of controls on blooming events**: The modeling helped to verify that the key driver of phytoplankton blooming in the region was predominantly down to the timings of the onset of stratification. The model helped to verify the observations from *in situ* data and satellite observations that also indicated stratification was a key driver.
4) **Integration of Data:** The models were successfully integrated with satellite observations and *in situ* data which helped to improve the spatial and temporal coverage of blooming events

within the survey region. This enabled for a more comprehensive assessment of bloom dynamics within the region

Negatives:

1) **Complexity:** Models require parameterisation of numerous physical and biological processes, which can introduce uncertainties and complexities in model simulations.
2) **Validation:** Model outputs needed to be validated against *in* situ observational data to ensure accuracy and reliability. However, due to the lack of *in situ* measurements, only parts of the model outputs (timings and key driver of phytoplankton blooms) could be verified. However, the model outputs were verified against satellite data.
3) **Varying estimations of primary production:** Estimations varied for primary production between the models used within the study. This therefore provided an inaccurate estimation of primary production for the survey area as these values could not verified. The variability within estimations were most likely a result of limited date for water column properties, as most data used for the models were based off surface measurements.

Most reliable new information learned:

The most reliable new information that was learned overall was the observation of the timings of the phytoplankton bloom event in 2022 on the north-east coast of the UK. A three way comparison between satellite observations, *in situ* data and phytoplankton bloom modeling aligned closely, with blooming events beginning at more North latitudes in late Mrach early April. Observations from all three methods also confirmed delayed blooming at more southern latitudes (Permanently mixed region) within the survey area, whereby blooming events began in June. The timings of blooming events specifically for the north-east coast were yet to be researched prior to this study. Additionally, the key driver of phytoplankton blooming events within the survey area was yet to studied. The findings within this study confirmed that the onset of stratification was the key driver to triggering phytoplankton blooming events. This is reliable information due to this key driver being confirmed by three different data sources. Satellite data indicated that areas of the study site began blooming in areas of the shallowest mixed layer depth (indication that water was stratified). *In situ* water profiles verified that areas in more northern latitudes of the survey area were stratified in summer months (blooming was more pronounced in this region), alongside southern areas being mixed (delayed / less pronounced blooming events). Finally the S2P3 model confirmed that blooming events were triggered when water only became stratified. The study provided two new highly reliable pieces of information that can be used in the future to help understand further the impacts of phytoplankton blooming events on the north-east coast of the UK.

Future research:

1. Regular sampling off the north-east coast with the installation of mooring buoy sites with particular focus on chlorophyll fluorescence, light attenuation, full nutrient analysis and water column properties would allow greater quality control of remotely sensed data alongside model outputs. In addition, the mooring buoys would provide essential water quality data that can be used to investigate future marine catastrophic events such as the mass crustacean die off in 2021.
2. Growth-grazing incubations experiments to help understand the predator-prey interactions as well as site specific growth rates and properties. Experimental outputs could then be used for the biological parameters in the s2P3 model.
3. Plankton analysis, to understand species composition and the risk of HABs along the north-east coast.
4. Investigating the impacts of the Flamborough front and wind farms on the hydrodynamic regions, and the possible implications on phytoplankton biomass.
5. Investigating the impact of weather patterns and storm events on the timing and magnitude on phytoplankton blooming on north-east coast of the UK.

Section 5- Conclusion:

Objective 1: To use *in situ* and remotely sensed data to track and assess the magnitude of phytoplankton blooming events on the North East coastal waters of the UK in 2022.

1. *In situ* and remotely sensed data collected for the north-east coast of the UK displays seasonal trends of phytoplankton blooming events in spring and summer months. Trends observed for our study site show temporal timings of blooming on a north-south gradient, where blooming arises earliest at more northern latitudes with delayed timing in southern latitudes. From satellite imagery, phytoplankton blooms began earliest in the inshore / offshore stratified region (21st-31st March) with the permanently mixed regions phytoplankton growth period being delayed until June. Bloom intensity varied spatially and temporally, with the largest blooms observed from satellite occurring in the inshore / offshore stratified zone, where blooms covered greater areas and comprised chlorophyll concentrations of ≥ 10 mg/m^3. These values compared closely with previous chlorophyll estimations in the North Sea. Blooming events in the permanently mixed region were smaller, and had multiple isolated areas of concentrated phytoplankton biomass (chlorophyll concentration ≥ 10 mg/m^3) which covered significantly less area than the large blooms covering greater spatial distance observed in the inshore / offshore stratified zone. However, zonally averaged *in situ* measurements alongside remotely sensed chlorophyll concentrations suggested all hydrodynamic regions had peak chlorophyll concentrations in spring (April and May), but were at lower concentrations than those observed from extracting chlorophyll cocnentrations from blooms using satellite imagery. These results suggested that the inshore stratified zone had the greatest concentrations (10.53 µg/l) and the offshore stratified having the lowest (2.87 µg/l). However, these observations were of slight contradiction with satellite imagery where prolonged periods of blooming at concentration of ≥ 10 mg/m^3 were observed in the offshore stratified zone, with no clear/ significant blooming in the permanently mixed zone until June.

Objective 2: To investigate the biological and physical controls on the different spring bloom events on North East coastal waters of the UK in 2022

2. The temporal and spatial distribution of blooming events were dictated by the onset of stratification. The key drivers for stratification formation were regional differences in strength of tidal currents and, meteorological forcing, which determined whether an upper stratified water layer would be constrained within the photic depths of the sample sites. Blooming occurred

earliest in regions with pronounced stratification formation in spring, as was evident in satellite imagery for the inshore and offshore stratified zone in late March and April. These zones experienced prolonged periods of stratification which lasted approximately 169 days, according to our model outputs. However, blooming did not occur during the whole period of stratification as nutrients may have been a limiting factor within the summer months. In the permanently mixed region, there was evidence of spring-neap tidal cycles contributing to opportunities for phytoplankton growth, whereby blooming events occurred during and following the neap phase of the tidal cycle, in which the reduced current speeds during this phase facilitated stratification formation and thereby phytoplankton growth. Vertical water structure analysis using CTDs confirmed our hydrodynamic region zonation. Casts taken in the offshore stratified region provided evidence of thermoclines whereas casts taken in the permanently mixed region showed a mixed water column. Light attenuation also played a pivotal role in phytoplankton growth with strong correlation between lower K_ds and increased chlorophyll. This was particularly apparent where smaller blooms were observed in areas of reduced water clarity within the permanently mixed region, and higher intensity blooms in lower K_d zones of the inshore and offshore stratified zones. Stratification and light attenuation were interlinked as the factors/drivers that impacted the formation of stratification also increased water clarity by reducing SPM.

Objective 3: To utilise site specific meteorological data and forcing parameters into a 1-dimensional model to try simulate blooming events observed from satellite data.

3. The one-dimensional S2P3 model provided a good illustration of bloom timings. Both modelling stations' bloom timing predictions matched observational satellite measurements for each zone. Meteorological data utilised in the model were deemed to be reliable given the close correlation between SST outputs from the model, and OSTIA satellite SST observations. The model estimated NPP at station J6 (permanently mixed region) and station 13 to be 35 g C m^{-2} $year^{-1}$ and 43 g C m^{-2} $year^{-1}$ respectively which most closely resembled the least productive North Sea regions outlined by Skogen et al., (1995) and Capuzzo et al., (2017) and were observed to be situated in permanently mixed regions of the North Sea. However, our productivity estimates were still slightly underestimated compared to literature, even in the offshore stratifying waters off the coast of Northumberland. These underestimations were attributed to the following reasons:
    a) Limitations of one-dimensional model being used in areas where lateral forcing can impact productivity estimates.

b) Only one K_d estimate can be input into the S2P3 model, however light attenuation was shown to vary on a monthly basis, which could therefore limit productivity due to overestimation of K_d in some months.
c) No site-specific photophysiological parameters were input, and therefore phytoplankton assemblage phenology within the study area was not accounted for, potentially lowering productivity estimates.
d) The low-depth resolution of 2.5m intervals used , could cause key biological processes, such as sub-surface chlorophyll maximums, to be missed as observed within the study area from *in situ* CTD casts.

Objective 4: To compare primary production outputs from two different primary production models with each other and to compare the spatial and temporal model trends to in situ data.

4. Primary production estimates from the simple depth-irradiance model showed that bloom timings matched relatively closely with values generated by the S2P3 model, further verifying that predicted bloom timing were mostly accurate. However, this model predicted significantly higher productivity outputs at both modelling sites when compared to the S2P3 model. Site J6 (permanently mixed region), estimated an NPP value of 284 g C m^{-2} $year^{-1}$ with station 13 being estimated at 435 g C m^{-2} $year^{-1}$. When comparing these estimates with literature, they exceeded the productivity estimates for the most productive regions researched within the North Sea. The over-estimation of productivity values was attributed to:
    A) Photosynthetic rate and efficiency values may have been overestimated, thereby potentially resulting in greater productivity outputs.
    B) Remotely sensed chlorophyll data may have been overestimated due to sediment load obscuring actual chlorophyll concentrations. This therefore means increased chlorophyll concentrations skewed by SPM would result in increased productivity outputs.
    C) Only one K_d and chlorophyll value were used for each day, rather than an hourly measurement. This decreased the models' resolution and thereby could have resulted in over estimation of productivity.

Section 6- References:

Allen, J.I., Siddorn, J.R., Blackford, J.C. and Gilbert, F.J., (2004) 'Turbulence as a control on the microbial loop in a temperate seasonally stratified marine systems model', Journal of Sea Research, 52(1), pp. 1–20. doi:10.1016/j.seares.2003.09.004.

Alvera-Azcárate, A., Van der Zande, D., Barth, A., Troupin, C., Martin, S. and Beckers, J.M., (2021) 'Analysis of 23 years of daily cloud-free chlorophyll and suspended particulate matter in the Greater North Sea', Frontiers in Marine Science, 8. doi:10.3389/fmars.2021.707632.

Arteaga, L.A. and Rousseaux, C.S. (2023) 'Impact of pacific ocean heatwaves on phytoplankton community composition', Communications Biology, 6(1). doi:10.1038/s42003-023-04645-0.

Babin, M. (2003) 'Variations in the light absorption coefficients of phytoplankton, nonalgal particles, and dissolved organic matter in coastal waters around Europe', Journal of Geophysical Research, 108(C7). doi:10.1029/2001jc000882.

Baretta-Bekker, J.G., Baretta, J.W., Latuhihin, M.J., Desmit, X. and Prins, T.C., (2009). Description of the long-term (1991–2005) temporal and spatial distribution of phytoplankton carbon biomass in the Dutch North Sea. Journal of Sea Research, 61(1-2), pp.50-59.

Barocio-Leon, O.A., Millan-Nunez, R., Santamaría-del-Ángel, E., Gonzalez-Silvera, A., Trees, C.C. and Orellana-Cepeda, E., (2008) 'Bio-optical characteristics of a phytoplankton bloom event off Baja California Peninsula (30–31°N)', Continental Shelf Research, 28(4–5), pp. 672–681. doi:10.1016/j.csr.2007.12.002.

Behrenfeld, M.J. (2010) 'Abandoning Sverdrup's critical depth hypothesis on phytoplankton blooms', Ecology, 91(4), pp. 977–989. doi:10.1890/09-1207.1.

Blauw, A., Benincà, E., Laane, R., Greenwood, N. and Huisman, J., (2012). Dancing with the Tides: Fluctuations of Coastal. Phytoplankton Orchestrated by Different Oscillatory Modes of the Tidal Cycle. PLoS ONE, 7(11), p.e49319.

Boss, E. and Behrenfeld, M. (2010) 'In situ evaluation of the initiation of the North Atlantic Phytoplankton Bloom', Geophysical Research Letters, 37(18). doi:10.1029/2010gl044174.

Brauer, V.S., Stomp, M. and Huisman, J. (2012) 'The nutrient-load hypothesis: Patterns of resource limitation and community structure driven by competition for nutrients and light', The American Naturalist, 179(6), pp. 721–740. doi:10.1086/665650.

Brockmann, U.H., Laane, R.W.P.M. and Postma, J. (1990) 'Cycling of nutrient elements in the North Sea', Netherlands Journal of Sea Research, 26(2–4), pp. 239–264. doi:10.1016/0077-7579(90)90092-u.

Brown, L., Sanders, R., Savidge, G. and Lucas, C.H., (2003) 'The uptake of silica during the spring bloom in the Northeast Atlantic Ocean', Limnology and Oceanography, 48(5), pp. 1831–1845. doi:10.4319/lo.2003.48.5.1831.

Burson, A., Stomp, M., Akil, L., Brussaard, C. and Huisman, J., (2016). Unbalanced reduction of nutrient loads has created an offshore gradient from phosphorus to nitrogen limitation in the North Sea. Limnology and Oceanography, 61(3), pp.869-888.

Butenschön, M., Clark, J., Aldridge, J. N., Allen, J. I., Artioli, Y., Blackford, J., Bruggeman, J., Cazenave, P., Ciavatta, S., Kay, S., Lessin, G., van Leeuwen, S., van der Molen, J., de Mora, L., Polimene, L., Sailley, S.,

Stephens, N., and Torres, R.., (2021) 'S2P3-R v2.0: Computationally efficient modelling of shelf seas on regional to global scales', Geoscientific Model Development, 14(10), pp. 6177–6195. doi:10.5194/gmd-14-6177-2021.

Cannizzaro, J.P. and Carder, K.L. (2006) 'Estimating chlorophyll a concentrations from remote-sensing reflectance in optically shallow waters', Remote Sensing of Environment, 101(1), pp. 13–24. doi:10.1016/j.rse.2005.12.002.

Capuzzo, E., Painting, S.J., Forster, R.M., Greenwood, N., Stephens, D.T. and Mikkelsen, O.A., (2012) 'Variability in the sub-surface light climate at ecohydrodynamically distinct sites in the North Sea', Biogeochemistry, 113(1–3), pp. 85–103. doi:10.1007/s10533-012-9772-6.

Capuzzo, Elisa, David Stephens, Tiago Silva, Jon Barry, and Rodney M. Forster., (2015) 'Decrease in water clarity of the southern and central North Sea during the 20th century', Global Change Biology, 21(6), pp. 2206–2214. doi:10.1111/gcb.12854.

Capuzzo, E., Lynam, C.P., Barry, J., Stephens, D., Forster, R.M., Greenwood, N., McQuatters-Gollop, A., Silva, T., van Leeuwen, S.M. and Engelhard, G.H., (2017) 'A decline in primary production in the North Sea over 25 years, associated with reductions in zooplankton abundance and fish stock recruitment', Global Change Biology, 24(1). doi:10.1111/gcb.13916.

Charnock, H., Dyer, K.R., Huthnance, J.M., Liss, P. and Simpson, B.H., (2012). Understanding the North Sea System. Springer Science & Business Media.

Chassot, E., Bonhommeau, S., Dulvy, N.K., Mélin, F., Watson, R., Gascuel, D. and Le Pape, O., (2010). Global marine primary production constrains fisheries catches. Ecology letters, 13(4), pp.495-505.

Chen, M., Fan, M., Liu, R., Wang, X., Yuan, X. and Zhu, H., (2015) 'The dynamics of temperature and light on the growth of phytoplankton', Journal of Theoretical Biology, 385, pp. 8–19. doi:10.1016/j.jtbi.2015.07.039.

Cloern, J.E. (1987) "Turbidity as a control on phytoplankton biomass and productivity in estuaries," Continental Shelf Research, 7(11-12), pp. 1367–1381. Available at: https://doi.org/10.1016/0278-4343(87)90042-2.

Cloern, J.E. (1991). Tidal stirring and phytoplankton bloom dynamics in an estuary. Journal of marine research, 49(1), pp.203-221.

Cloern, J.E. and Dufford, R. (2005) "Phytoplankton community ecology: Principles applied in San Francisco Bay," Marine Ecology Progress Series, 285, pp. 11–28. Available at: https://doi.org/10.3354/meps285011.

Cole, B.E. and Cloern, J.E., (1987). An empirical model for estimating phytoplankton productivity in estuaries. Marine Ecology Progress Series, 36(1), pp.299-305.

Cross, W.F., Hood, J.M., Benstead, J.P., Huryn, A.D. and Nelson, D., (2014) 'Interactions between temperature and nutrients across levels of ecological organization', Global Change Biology, 21(3), pp. 1025–1040. doi:10.1111/gcb.12809.

Cullen, J.J. (2015) 'Subsurface chlorophyll maximum layers: Enduring enigma or mystery solved?', Annual Review of Marine Science, 7(1), pp. 207–239. doi:10.1146/annurev-marine-010213-135111.

Cushing, D.H. (1990) 'Plankton production and year-class strength in fish populations: An update of the match/mismatch hypothesis', Advances in Marine Biology, pp. 249–293. doi:10.1016/s0065-2881(08)60202-3.

Daewel, U., Akhtar, N., Christiansen, N. and Schrum, C., (2022) 'Offshore wind farms are projected to impact primary production and bottom water deoxygenation in the North Sea', Communications Earth & Environment, 3(1). doi:10.1038/s43247-022-00625-0.

Dai, Y., Yang, S., Zhao, D., Hu, C., Xu, W., Anderson, D. M., and Feng, L. (2023). Coastal phytoplankton blooms expand and intensify in the 21st century. Nature, 615(7951), 280-284.

DEFRA (2023) Panel of independent experts publish findings into Crab Deaths, GOV.UK. Available at: https://www.gov.uk/government/news/panel-of-independent-experts-publish-findings-into-crab-deaths (Accessed: 19 July 2023).

Desmit, X., Nohe, A., Borges, A.V., Prins, T., De Cauwer, K., Lagring, R., Van der Zande, D. and Sabbe, K., (2019) 'Changes in chlorophyll concentration and phenology in the North Sea in relation to de-eutrophication and sea surface warming', Limnology and Oceanography, 65(4), pp. 828–847. doi:10.1002/lno.11351.

Devlin, M., Barry, J., Mills, D., Gowen, R., Foden, J., Sivyer, D. and Tett, P., (2008). Relationships between suspended particulate material, light attenuation and Secchi depth in UK marine waters. Estuarine, Coastal and Shelf Science, 79(3), pp.429-439.

Di Pane, J., Boersma, M., Marques, R., Deschamps, M., Ecker, U. and Meunier, C.L., (2023) 'Identification of tipping years and shifts in mesozooplankton community structure using multivariate analyses: A long-term study in southern North Sea', ICES Journal of Marine Science [Preprint]. doi:10.1093/icesjms/fsad071.

Dimitry, V., Lacroix, G. and Ruddick, K., (2012). Observing and explaining the timing of spring/summer algal blooms in the Southern North Sea using ocean colour remote sensing. Royal Belgian Institute of Natural Sciences,.

Dominguez, A.A.B., Macdonald, H.S., Rickard, G. and Hammond, M.L., (2022) 'Seasonal nutrient co-limitation in a temperate shelf sea: A modelling approach', Continental Shelf Research, 249, p. 104855. doi:10.1016/j.csr.2022.104855.

Domingues, R.B., Barbosa, A.B., Sommer, U. and Galvão, H.M., (2011) 'Ammonium, nitrate and phytoplankton interactions in a freshwater tidal estuarine zone: Potential effects of cultural eutrophication', Aquatic Sciences, 73(3), pp. 331–343. doi:10.1007/s00027-011-0180-0.

Dorrell, R.M., Lloyd, C.J., Lincoln, B.J., Rippeth, T.P., Taylor, J.R., Caulfield, C.C.P., Sharples, J., Polton, J.A., Scannell, B.D., Greaves, D.M. and Hall, R.A., (2022) 'Anthropogenic mixing in seasonally stratified shelf seas by offshore wind farm infrastructure', Frontiers in Marine Science, 9. doi:10.3389/fmars.2022.830927.

Ducrotoy, J.P., Elliott, M. and de Jonge, V.N., (2000). The north sea. Marine pollution bulletin, 41(1-6), pp.5-23.

Dupont, N. and Aksnes, D.L., (2013). Centennial changes in water clarity of the Baltic Sea and the North Sea. Estuarine, Coastal and Shelf Science, 131, pp.282-289.

Eaton, D.R., Brown, J., Addison, J.T., Milligan, S.P. and Fernand, L.J., (2003) 'Edible crab (cancer pagurus) larvae surveys off the east coast of england: Implications for stock structure', Fisheries Research, 65(1–3), pp. 191–199. doi:10.1016/j.fishres.2003.09.036.

Edwards, M., Johns, D.G., Leterme, S.C., Svendsen, E. and Richardson, A.J., (2006) 'Regional climate change and harmful algal blooms in the Northeast Atlantic', Limnology and Oceanography, 51(2), pp. 820–829. doi:10.4319/lo.2006.51.2.0820.

Filippelli, G., (2008). The Global Phosphorus Cycle: Past, Present, and Future. Elements, 4(2), pp.89-95.

Finkel, Z.V., Beardall, J., Flynn, K.J., Quigg, A., Rees, T.A.V. and Raven, J.A., (2009) 'Phytoplankton in a changing world: Cell size and elemental stoichiometry', Journal of Plankton Research, 32(1), pp. 119–137. doi:10.1093/plankt/fbp098.

Franks, P., (2001). Phytoplankton blooms in a fluctuating environment: the roles of plankton response time scales and grazing. Journal of Plankton Research, 23(12), pp.1433-1441.

Floeter, J., Pohlmann, T., Harmer, A. and Möllmann, C., (2022) 'Chasing the offshore wind farm wind-wake-induced upwelling/downwelling dipole', Frontiers in Marine Science, 9. doi:10.3389/fmars.2022.884943.

Forster, RM. (2018). 'The effect of monopile-induced turbulence on local suspended sediment patterns around UK wind farms: field survey report'. An IECS report to The Crown Estate. ISBN 978-1-906410-77-3; November 2018.

Fouilland, E., Leakey, R., Jones, K., Slater, J. and Alvarez-Calleja, I., (2007) 'The response of a planktonic microbial community to experimental simulations of sudden mixing conditions in temperate coastal waters: Importance of light regime and nutrient enrichment', Journal of Experimental Marine Biology and Ecology, 351(1–2), pp. 211–225. doi:10.1016/j.jembe.2007.06.030.

Gaia Science (2024) V300A Filtration Collocation, Gaia Science. Malaysia. Available at: https://www.gaiascience.com.my/productdetails/v300a-filtration-collocation.

Gamble, J.C. (1978) 'Copepod grazing during a declining spring phytoplankton bloom in the northern North Sea', Marine Biology, 49(4), pp. 303–315. doi:10.1007/bf00455025.

Garnier, J., Beusen, A., Thieu, V., Billen, G. and Bouwman, L., (2010) 'N:P:Si nutrient export ratios and ecological consequences in coastal seas evaluated by the ICEP approach', Global Biogeochemical Cycles, 24(4). doi:10.1029/2009gb003583.

Goldman, J.C. and McGillicuddy, D.J. (2003) "Effect of large marine diatoms growing at low light on episodic new production," Limnology and Oceanography, 48(3), pp. 1176–1182. Available at: https://doi.org/10.4319/lo.2003.48.3.1176.

Greenwood, N., Forster, R.M., Créach, V., Painting, S.J., Dennis, A., Cutchey, S.J., Silva, T., Sivyer, D.B. and Jickells, T., (2011) 'Seasonal and interannual variation of the phytoplankton and copepod dynamics in Liverpool Bay', Ocean Dynamics, 62(2), pp. 307–320. doi:10.1007/s10236-011-0500-x.

Grizzetti, B., Bouraoui, F. and Aloe, A. (2011) 'Changes of nitrogen and phosphorus loads to European seas', Global Change Biology, 18(2), pp. 769–782. doi:10.1111/j.1365-2486.2011.02576.x.

Gronholz, A., Gräwe, U., Paul, A. and Schulz, M., (2017) 'Investigating the effects of a summer storm on the North Sea stratification using a regional coupled ocean-atmosphere model', Ocean Dynamics, 67(2), pp. 211–235. doi:10.1007/s10236-016-1023-2.

Groß, E., Di Pane, J., Boersma, M. and Meunier, C.L., (2022) 'River discharge-related nutrient effects on North Sea Coastal and offshore phytoplankton communities', Journal of Plankton Research, 44(6), pp. 947–960. doi:10.1093/plankt/fbac049.

Halloran, P. R., McWhorter, J. K., Arellano Nava, B., Marsh, R., and Skirving, W., (2021) 'S2P3-R v2.0: Computationally efficient modelling of shelf seas on regional to global scales', Geoscientific Model Development, 14(10), pp. 6177–6195. doi:10.5194/gmd-14-6177-2021.

Hayashida, H., Matear, R.J. and Strutton, P.G. (2020) 'Background nutrient concentration determines phytoplankton bloom response to Marine Heatwaves', Global Change Biology, 26(9), pp. 4800–4811. doi:10.1111/gcb.15255.

Holligan, P.M. (1981) 'Biological implications of fronts on the Northwest European Continental Shelf', Philosophical Transactions of the Royal Society of London. Series A, Mathematical and Physical Sciences, 302(1472), pp. 547–562. doi:10.1098/rsta.1981.0182.

Horii, T., Ueki, I. and Ando, K., 2020. Coastal upwelling events, salinity stratification, and barrier layer observed along the southwestern coast of Sumatra. Journal of Geophysical Research: Oceans, 125(12), p.e2020JC016287.

Johns, D.G. and Reid, P.C. (2001) An overview of plankton ecology in the North Sea. tech. SAHFOS.

Karlson, B., Andersen, P., Arneborg, L., Cembella, A., Eikrem, W., John, U., West, J.J., Klemm, K., Kobos, J., Lehtinen, S. and Lundholm, N., (2021) 'Harmful algal blooms and their effects in coastal seas of Northern Europe', Harmful Algae, 102, p. 101989. doi:10.1016/j.hal.2021.101989.

Kennedy, W., Pilkington, J., Wintz, P., & Fernall, D. (2022). Retrieved from https://assets.publishing.service.gov.uk/media/662761cdd29479e036a7e504/UK_Sea_Fisheries_Statistics_2022_101123___.pdf.

Kirby, R.R., Beaugrand, G. and Lindley, J.A. (2008) 'Climate-induced effects on the MEROPLANKTON and the benthic-pelagic ecology of the North Sea', Limnology and Oceanography, 53(5), pp. 1805–1815. doi:10.4319/lo.2008.53.5.1805.

Kirk, J.T.O. (2000) Light and photosynthesis in aquatic ecosystems. Cambridge England: Cambridge University Press.

Knefelkamp, B., Carstens, K. and Wiltshire, K.H., (2007). Comparison of different filter types on chlorophyll-a retention and nutrient measurements. Journal of Experimental Marine Biology and Ecology, 345(1), pp.61-70.

Kowalczuk, P., Cooper, W.J., Durako, M.J., Kahn, A.E., Gonsior, M. and Young, H., (2010) 'Characterization of dissolved organic matter fluorescence in the South Atlantic Bight with use of PARAFAC model: Relationships between fluorescence and its components, absorption coefficients and organic carbon concentrations', Marine Chemistry, 118(1–2), pp. 22–36. doi:10.1016/j.marchem.2009.10.002.

Krause-Jensen, D. and Sand-Jensen, K. (1998) 'Light attenuation and photosynthesis of aquatic plant communities', Limnology and Oceanography, 43(3), pp. 396–407. doi:10.4319/lo.1998.43.3.0396.

Lewandowska, A.M., Breithaupt, P., Hillebrand, H., Hoppe, H.G., Jürgens, K. and Sommer, U., (2012) 'Responses of primary productivity to increased temperature and phytoplankton diversity', Journal of Sea Research, 72, pp. 87–93. doi:10.1016/j.seares.2011.10.003.

Lindemann, C. and St. John, M.A. (2014) 'A seasonal diary of phytoplankton in the North Atlantic', Frontiers in Marine Science, 1. doi:10.3389/fmars.2014.00037.

Litchman, E. (2007) 'Resource competition and the ecological success of phytoplankton', Evolution of Primary Producers in the Sea, pp. 351–375. doi:10.1016/b978-012370518-1/50017-5.

Litchman, E. and Klausmeier, C.A. (2008) 'Trait-based community ecology of phytoplankton', Annual Review of Ecology, Evolution, and Systematics, 39(1), pp. 615–639. doi:10.1146/annurev.ecolsys.39.110707.173549.

Lovelock, C.E. and Duarte, C.M., (2019). Dimensions of blue carbon and emerging perspectives. Biology letters, 15(3), p.20180781.

Malone, T., Azzaro, M., Bode, A., Brown, E., Duce, R., Kamykowski, D., Kang, S., Kedong, Y.,Thorndyke, M., Wang, J., Calumpong, H. and Eghtesadi, P., (2016). Primary Production, Cycling of Nutrients, Surface Layer and Plankton. The First Global Integrated Marine Assessment, pp.119-148

Marshak, A.R. and Link, J.S. (2021) 'Primary production ultimately limits fisheries economic performance', Scientific Reports, 11(1). doi:10.1038/s41598-021-91599-0.

Martin, J. and Fitzwater, S., (1988). Iron deficiency limits phytoplankton growth in the northeast Pacific subarctic. Nature, 331(6154), pp.341-343.

Matsushita, B., Yang, W., Chang, P., Yang, F. and Fukushima, T., (2012). A simple method for distinguishing global Case-1 and Case-2 waters using SeaWiFS measurements. ISPRS journal of photogrammetry and remote sensing, 69, pp.74-87.

McCandliss, R., Jones, S., Hearn, M., Latter, R. and Jago, C., 2002. Dynamics of suspended particles in coastal waters (southern North Sea) during a spring bloom. Journal of Sea Research, 47(3-4), pp.285-302.

Moeller, H.V., Laufkötter, C., Sweeney, E.M. and Johnson, M.D., (2019) 'Light-dependent grazing can drive formation and deepening of deep chlorophyll maxima', Nature Communications, 10(1). doi:10.1038/s41467-019-09591-2.

Moll, A. (1998) 'Regional distribution of primary production in the North Sea simulated by a three-dimensional model', Journal of Marine Systems, 16(1–2), pp. 151–170. doi:10.1016/s0924-7963(97)00104-8.

Moore, C.M., Suggett, D., Holligan, P.M., Sharples, J., Abraham, E.R., Lucas, M.I., Rippeth, T.P., Fisher, N.R., Simpson, J.H. and Hydes, D.J., (2003) 'Physical controls on phytoplankton physiology and production at a shelf sea front: A fast repetition-rate fluorometer based field study', Marine Ecology Progress Series, 259, pp. 29–45. doi:10.3354/meps259029.

Muller-Karger, F.E., Varela, R., Thunell, R., Luerssen, R., Hu, C. and Walsh, J.J., (2005) 'The importance of continental margins in the global carbon cycle', Geophysical Research Letters, 32(1). doi:10.1029/2004gl021346.

Mustaffa, N., Kallajoki, L., Biederbick, J., Binder, F., Schlenker, A. and Striebel, M., (2020). Coastal Ocean Darkening Effects via Terrigenous DOM Addition on Plankton: An Indoor Mesocosm Experiment. Frontiers in Marine Science, 7.

Nathalie, H. (2016) Currents in the North Sea, Marineregions.org . Available at: https://www.marineregions.org/maps.php?album=3747&pic=115812#photogallery (Accessed: 03 August 2023).

Napoléon, C., Fiant, L., Raimbault, V., Riou, P. and Claquin, P., (2014) 'Dynamics of phytoplankton diversity structure and primary productivity in the English Channel', Marine Ecology Progress Series, 505, pp. 49–64. doi:10.3354/meps10772.

Nicholson, S., Lévy, M., Llort, J., Swart, S. and Monteiro, P., (2016). Investigation into the impact of storms on sustaining summer primary productivity in the Sub-Antarctic Ocean. Geophysical Research Letters, 43(17), pp.9192-9199.

Nielsen, T., Lokkegaard, B., Richardson, K., Pederson, F., Hansen, L., (1993) 'Structure of plankton communities in the Dogger Bank area (North Sea) during a stratified situation', Marine Ecology Progress Series, 95, pp. 115–131. doi:10.3354/meps095115.

Oehler, T., Schlüter, M. and Schückel, U. (2015) 'Seasonal dynamics of the biogenic silica cycle in surface sediments of the Helgoland Mud Area (southern North Sea)', Continental Shelf Research, 107, pp. 103–114. doi:10.1016/j.csr.2015.07.016.

Opdal, A.F., Lindemann, C. and Aksnes, D.L. (2019) 'Centennial decline in North Sea water clarity causes strong delay in phytoplankton bloom timing', Global Change Biology, 25(11), pp. 3946–3953. doi:10.1111/gcb.14810.

Pan, C.W., Chuang, Y.L., Chou, L.S., Chen, M.H. and Lin, H.J., (2016) 'Factors governing phytoplankton biomass and production in tropical estuaries of Western Taiwan', Continental Shelf Research, 118, pp. 88–99. doi:10.1016/j.csr.2016.02.015.

Pérez, G.L., Galí, M., Royer, S.J., Gerea, M., Ortega-Retuerta, E., Gasol, J.M., Marrasé, C. and Simó, R., (2021). Variability of phytoplankton light absorption in stratified waters of the NW Mediterranean Sea: The interplay between pigment composition and the packaging effect. Deep-Sea Research Part I: Oceanographic Research Papers, 169(November 2020). https://doi.org/10.1016/j.dsr.2020.103460.

Philippart, C.J., Beukema, J.J., Cadée, G.C., Dekker, R., Goedhart, P.W., van Iperen, J.M., Leopold, M.F. and Herman, P.M., (2007). Impacts of nutrient reduction on coastal communities. Ecosystems, 10, pp.96-119.

Porter, E., Mason, R. and Sanford, L., (2010). Effect of tidal resuspension on benthic–pelagic coupling in an experimental ecosystem study. Marine Ecology Progress Series, 413, pp.33-53.

Pozzobon, V., Cui, N., Moreaud, A., Michiels, E. and Levasseur, W., (2021) 'Nitrate and nitrite as mixed source of nitrogen for chlorella vulgaris: Growth, nitrogen uptake and pigment contents', Bioresource Technology, 330, p. 124995. doi:10.1016/j.biortech.2021.124995.

Quinn, J., Philip, L. and Murphy, W., (2009). Understanding the recession of the Holderness Coast, east Yorkshire, UK: a new presentation of temporal and spatial patterns. Quarterly Journal of Engineering Geology and Hydrogeology, 42(2), pp.165-178.

Rabalais, N.N., Turner, R.E., Díaz, R.J. and Justić, D., (2009). Global change and eutrophication of coastal waters. ICES Journal of Marine Science, 66(7), pp.1528-1537.

Redfield, A., (1958). The Biological control of chemical factors in the environment. American Scientist, 46(3), pp.205-221

Richardson, K. (2000) 'Subsurface phytoplankton blooms fuel pelagic production in the North Sea', Journal of Plankton Research, 22(9), pp. 1663–1671. doi:10.1093/plankt/22.9.1663.

Richardson, T.L. and Pinckney, J.L., (2004). Monitoring of the toxic dinoflagellate Karenia brevis using gyroxanthin-based detection methods. Journal of applied phycology, 16, pp.315-328.

Ritchie, R.J., (2008). Universal chlorophyll equations for estimating chlorophylls a, b, c, and d and total chlorophylls in natural assemblages of photosynthetic organisms using acetone, methanol, or ethanol solvents. Photosynthetica, 46, pp.115-126.

Roy, S., Llewellyn, C., Skarstad Egeland, E., Johnsen, G., (2011) "Update on filtration, storage and extraction solvents," in Phytoplankton pigments characterization, chemotaxonomy and applications in oceanography. Cambridge: Cambridge University Press, pp. 627–631.

Roy, S., Llewellyn, C., Skarstad Egeland, E., Johnsen, G., (2011) Phytoplankton pigments characterization, chemotaxonomy and applications in oceanography. Cambridge: Cambridge University Press.

Salmaso, N. and Tolotti, M. (2020) 'Phytoplankton and anthropogenic changes in pelagic environments', Hydrobiologia, 848(1), pp. 251–284. doi:10.1007/s10750-020-04323-w.

Sathyendranath, S., Ji, R. and Browman, H.I. (2015) 'Revisiting Sverdrup's critical depth hypothesis', ICES Journal of Marine Science, 72(6), pp. 1892–1896. doi:10.1093/icesjms/fsv110.

Sealife mortality off the North East Coast - Committees - UK parliament (2022) Sealife Mortality off the North East Coast. Available at: https://committees.parliament.uk/work/6963/sealife-mortality-off-the-north-east-coast/publications/ (Accessed: 19 July 2023).

Semmouri, I., De Schamphelaere, K.A., Mortelmans, J., Mees, J., Asselman, J. and Janssen, C.R., (2023) 'Decadal decline of dominant copepod species in the North Sea is associated with ocean warming: Importance of marine heatwaves', Marine Pollution Bulletin, 193, p. 115159. doi:10.1016/j.marpolbul.2023.115159.

Sharp, J.H. (2001) 'Marine and aquatic communities, stress from eutrophication', Encyclopedia of Biodiversity, pp. 23–31. doi:10.1016/b978-0-12-384719-5.00381-6.

Sharples, J. (1999) 'Investigating the seasonal vertical structure of phytoplankton in Shelf Seas', Marine Models, 1(1–4), pp. 3–38. doi:10.1016/s0079-6611(99)00002-6.

Sharples, J. (2007) 'Potential impacts of the spring-neap tidal cycle on shelf sea primary production', Journal of Plankton Research, 30(2), pp. 183–197. doi:10.1093/plankt/fbm088.

Sharples, J. and Tett, P. (1994) 'Modelling the effect of physical variability on the midwater chlorophyll maximum', Journal of Marine Research, 52(2), pp. 219–238. doi:10.1357/0022240943077109.

Sharples, J., Ross, O.N., Scott, B.E., Greenstreet, S.P. and Fraser, H., (2006) 'Inter-annual variability in the timing of stratification and the spring bloom in the north-western North Sea', Continental Shelf Research, 26(6), pp. 733–751. doi:10.1016/j.csr.2006.01.011.

Sharples, J., Mayor, D.J., Poulton, A.J., Rees, A.P. and Robinson, C., (2019) 'Shelf Sea Biogeochemistry: Nutrient and carbon cycling in a temperate shelf sea water column', Progress in Oceanography, 177, p. 102182. doi:10.1016/j.pocean.2019.102182.

Shaw, P. and Purdie, D. (2001) 'Phytoplankton photosynthesis-irradiance parameters in the near-shore UK coastal waters of the North Sea: Temporal variation and environmental control', Marine Ecology Progress Series, 216, pp. 83–94. doi:10.3354/meps216083.

Shimoto, A. and Matsumura, S., (1992). Primary productivity in a cold water mass and the neighbourhood area occurring off Enshunada in the late summer of 1989. Journal of Oceanography, 48(1), pp.105-11

Sigman, D. and Hain, M., (2012). The Biological Productivity of the Ocean. Nature Education Knowledge, 3(6), pp.1-6.

Simpson, J. and Sharples, J., (2012). Introduction to the Physical and Biological Oceanography of Shelf Seas

Skogen, M.D. and Moll, A., (2000). Interannual variability of the North Sea primary production: comparison from two model studies. Continental Shelf Research, 20(2), pp.129-151.

Skogen, M.D., Svendsen, E., Berntsen, J., Aksnes, D. and Ulvestad, K.B., (1995) 'Modelling the primary production in the North Sea using a coupled three-dimensional physical-chemical-biological ocean model', Estuarine, Coastal and Shelf Science, 41(5), pp. 545–565. doi:10.1016/0272-7714(95)90026-8.

Skogen, M.D., Søiland, H. and Svendsen, E. (2004) 'Effects of changing nutrient loads to the North Sea', Journal of Marine Systems, 46(1–4), pp. 23–38. doi:10.1016/j.jmarsys.2003.11.013.

Smaal, A.C., Schellekens, T., Van Stralen, M.R. and Kromkamp, J.C., (2013) 'Decrease of the carrying capacity of the Oosterschelde Estuary (SW Delta, NL) for bivalve filter feeders due to overgrazing?', Aquaculture, 404–405, pp. 28–34. doi:10.1016/j.aquaculture.2013.04.008.

Spence, M.A., Lynam, C.P., Thorpe, R.B., Heneghan, R.F. and Dolder, P.J., (2022) 'Synthesizing empirical and modelling studies to predict past and future primary production in the North Sea', Frontiers in Marine Science, 9. doi:10.3389/fmars.2022.828623.

Suggett, D.J., Moore, C.M., Oxborough, K. and Geider, R.J., (2006). Fast Repetition Rate (FRR) Chlorophyll a Fluorescence Induction Measurements. Chelsea Technologies Group, [online] p.53. Available at: <http://www.psi.cz/ftp/publications/kautsky/FRRFmethodsManual.pdf%5Cnpapers://64c875cb-35e9-49cc-86a7-69f7bda703f6/Paper/p289>.

Tett, P., Carreira, C., Mills, D.K., Van Leeuwen, S., Foden, J., Bresnan, E. and Gowen, R.J., (2008). Use of a Phytoplankton Community Index to assess the health of coastal waters. ICES Journal of Marine Science, 65(8), pp.1475-1482.

Tett, P., Gowen, R., Mills, D., Fernandes, T., Gilpin, L., Huxham, M., Kennington, K., Read, P., Service, M., Wilkinson, M. and Malcolm, S., (2007). Defining and detecting undesirable disturbance in the context of marine eutrophication. Marine Pollution Bulletin, 55(1-6), pp.282-297.

Tilstone, G.H., Land, P.E., Pardo, S., Kerimoglu, O. and Van der Zande, D., (2023) 'Threshold indicators of primary production in the north-east Atlantic for assessing environmental disturbances using 21 years of Satellite Ocean Colour', Science of The Total Environment, 854, p. 158757. doi:10.1016/j.scitotenv.2022.158757.

Townsend, D.W., Cammen, L.M., Holligan, P.M., Campbell, D.E. and Pettigrew, N.R., (1994). Causes and consequences of variability in the timing of spring phytoplankton blooms. Deep Sea Research Part I: Oceanographic Research Papers, 41(5-6), pp.747-765.

Trombetta, T., Vidussi, F., Mas, S., Parin, D., Simier, M. and Mostajir, B., (2019) 'Water temperature drives phytoplankton blooms in coastal waters', PLOS ONE, 14(4). doi:10.1371/journal.pone.0214933.

Uberoi, E., Hutton, G., ward, M., Ares, E., (2022) Uk fisheries statistics. rep. House of commons Library. Available at: https://researchbriefings.files.parliament.uk/documents/SN02788/SN02788.pdf.

Uncles, R., Stephens, J. and Harris, C., (2006). Properties of suspended sediment in the estuarine turbidity maximum of the highly turbid Humber Estuary system, UK. Ocean Dynamics, 56(3-4), pp.235-247.

van Beusekom, J., Carstensen, J., Dolch, T., Grage, A., Hofmeister, R., Lenhart, H., Kerimoglu, O., Kolbe, K., Pätsch, J., Rick, J., Rönn, L. and Ruiter, H., (2019). Wadden Sea Eutrophication: Long-Term Trends and Regional Differences. Frontiers in Marine Science, 6.

van Beusekom, J.E. and Diel-Christiansen, S., (2009). Global change and the biogeochemistry of the North Sea: the possible role of phytoplankton and phytoplankton grazing. International Journal of Earth Sciences, 98, pp.269-280.

van Haren, H., Mills, D.K. and Wetsteyn, L.P., (1998). Detailed observations of the phytoplankton spring bloom in the stratifying central North Sea. Journal of Marine Research, 56(3), pp.655-680.

van Leeuwen, S., Tett, P., Mills, D. and van der Molen, J., (2015). Stratified and nonstratified areas in the North Sea: Long-term variability and biological and policy implications. Journal of Geophysical Research: Oceans, 120(7), pp.4670-4686.

van Leeuwen, S., van der Molen, J., Ruardij, P., Fernand, L. and Jickells, T., (2012). Modelling the contribution of deep chlorophyll maxima to annual primary production in the North Sea. Biogeochemistry, 113(1-3), pp.137-152

Vernet, M., Ellingsen, I., Seuthe, L., Slagstad, D., Cape, M. and Matrai, P., (2019). Influence of Phytoplankton Advection on the Productivity Along the Atlantic Water Inflow to the Arctic Ocean. Frontiers in Marine Science, 6.

Wang, D.-Z. (2008) 'Neurotoxins from marine dinoflagellates: A brief review', Marine Drugs, 6(2), pp. 349–371. doi:10.3390/md20080016.

Wang, G., Cao, W., Yang, Y., Zhou, W., Liu, S. and Yang, D., (2010) 'Variations in light absorption properties during a phytoplankton bloom in the Pearl River Estuary', Continental Shelf Research, 30(9), pp. 1085–1094. doi:10.1016/j.csr.2010.02.010.

Wang, J., Xu, J., Yang, Y., Lyv, Y. and Luan, K., (2021) 'Seasonal and interannual variations of sea surface temperature and influencing factors in the Yangtze River Estuary', Regional Studies in Marine Science, 45, p. 101827. doi:10.1016/j.rsma.2021.101827.

Wang, Z., Liang, Y. and Kang, W. (2011) 'Utilization of dissolved organic phosphorus by different groups of phytoplankton taxa', Harmful Algae, 12, pp. 113–118. doi:10.1016/j.hal.2011.09.005.

Wasmund, N., Topp, I. and Schories, D., (2006). Optimising the storage and extraction of chlorophyll samples. Oceanologia, 48(1), pp.125–144.

Wei, J., Wang, M., Mikelsons, K. and Jiang, L., (2023) 'Chlorophyll-specific absorption coefficient of phytoplankton in world oceans: Seasonal and regional variability', Remote Sensing, 15(9), p. 2423. doi:10.3390/rs15092423.

Williamson, C.A. and Hollins, R.C. (2022) “Measured iops of jerlov water types,” Applied Optics, 61(33), p. 9951. Available at: https://doi.org/10.1364/ao.470464

Xu, X., Lemmen, C. and Wirtz, K.W. (2020) ‘Less nutrients but more phytoplankton: Long-term ecosystem dynamics of the southern North Sea’, Frontiers in Marine Science, 7. doi:10.3389/fmars.2020.00662.

Yamaguchi, H., Ishizaka, J., Siswanto, E., Son, Y.B., Yoo, S. and Kiyomoto, Y., (2013). Seasonal and spring interannual variations in satellite-observed chlorophyll-a in the Yellow and East China Seas: New datasets with reduced interference from high concentration of resuspended sediment. Continental Shelf Research, 59, pp.1-9.

Zhao, C., Daewel, U. and Schrum, C. (2019) ‘Tidal impacts on primary production in the North Sea’, Earth System Dynamics, 10(2), pp. 287–317. doi:10.5194/esd-10-287-2019.

Appendices:

Appendix 1. Example figures of the process of matching depth with underwater irradiance measurements. First graph is from site M16 and the second being M17.

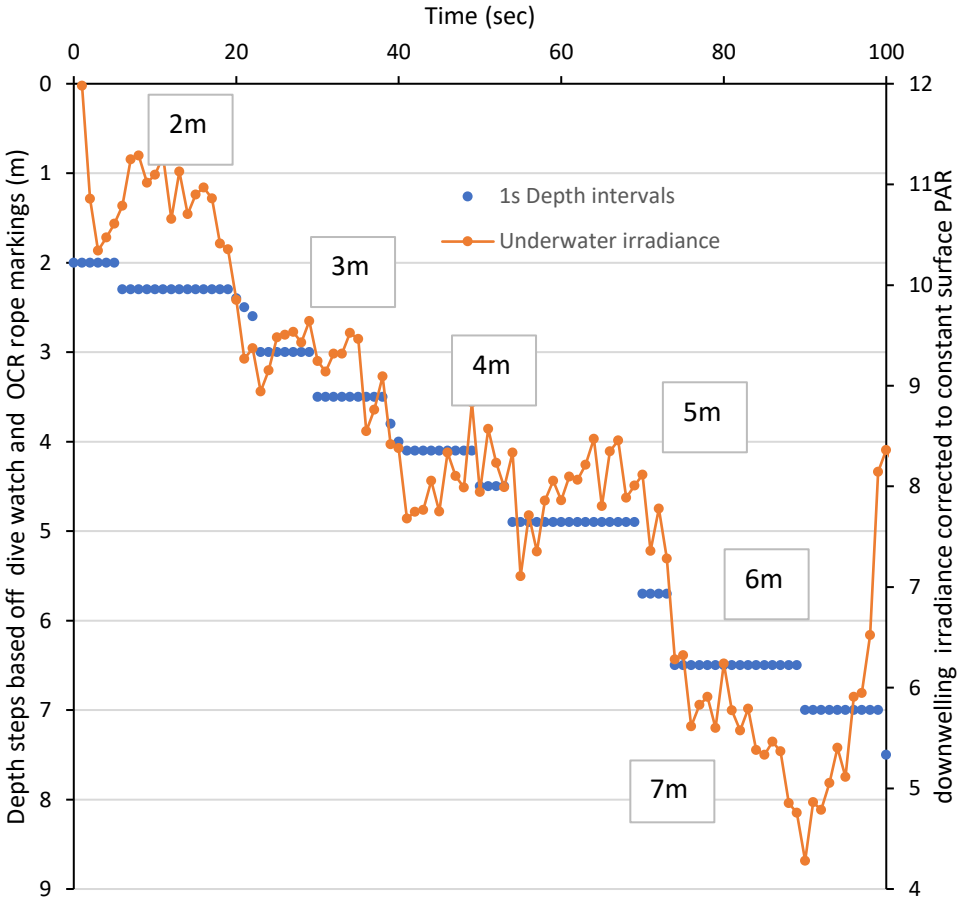

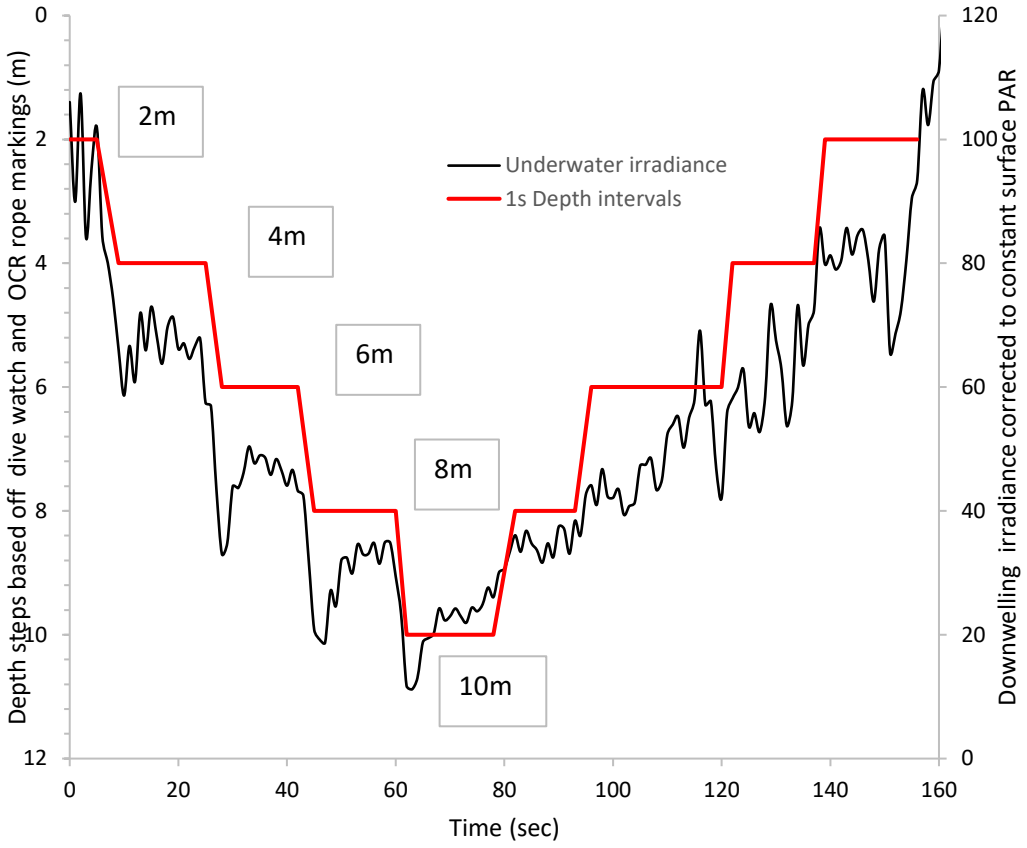

Appendix 3: Array value outputs for the LINEST function in excel

	A	B	C	D	E	F
1	m_n	m_{n-1}	···	m_2	m_1	b
2	se_n	se_{n-1}	···	se_2	se_1	se_b
3	r_2	se_y				
4	F	d_f				
5	ss_{reg}	ss_{resid}				

m	slope of line
Y	Y-intercept of line
se1,se2,...,sen	The standard error values for the coefficients m1,m2,...,mn
r2	The coefficient of determination
sey	The standard error for the y estimate.

F	The F statistic. Use the F statistic to determine whether the observed relationship between the dependent and independent variables occurs by chance.
df	The degrees of freedom
ssreg	The regression sum of squares.
ssresid	The residual sum of squares

Appendix 3: S2P3 initialisation file for model parameters for Site J6(permanently mixed region) in 2022.

Initialisation and driving parameters for S2P3 (Shelf Sea Physics and Primary Production) with dissolved oxygen model
In: Simpson & Sharples, Introduction to the Physical and Biological Oceanography of Shelf Seas
Cambridge University Press, 2012.

Physics parameters:
52.00 Total depth (m)
20 Number of depth cells
2.600 Depth cell thickness (m)
22.50 Time step (s)
53.90 Latitude (degrees, positive north)
0.00300 Bottom quadratic drag coefficient
0.100000 Maximum diffusivity and viscosity (m2 s-1)
0.000010 Background viscosity (m2 s-1)
0.000010 Background diffusivity (m2 s-1)
8.14 Initial water temperature (deg C)
0.100 Heat vertical attenuation (m-1)
0.01200 Chl effect on heat attenuation (m2 (mg Chl)-1)
0.00 Climate air temperature offset (deg C)

Light and nutrient resources:
0.260 Attenuation coefficient for PAR (m-1)
0.45 PAR as fraction of incident radiation
4.30 Initial winter nitrate (mmol m-3)
30.00 Maximum nitrate restoration rate (mmol m-2 d-1)

Tidal parameters:
M2 S2 N2 O1 K1
0.221 0.072 0.044 0.019 0.020 u amplitude (m s-1)
2.125 2.864 98.276 0.000 0.000 u phase (radians)
0.588 0.204 0.118 0.040 0.040 v amplitude (m s-1)
-1.552 -0.777 -112.530 0.000 0.000 v phase (radians)

-1.248 1.879 1.915 1.127 1.107 tidal ellipse orientation (radians)
0.173 0.154 0.104 0.000 0.000 tidal ellipse polarisation

0.619 0.214 0.125 0.044 0.045 tidal ellipse semi-major axis (m s-1)

Meteorlogical data:
2 Meteorology file type (1=model default, 2=user supplied)
https://doi.org/10.6084/m9.figshare.23686542.v2 user meteorology data file

Biology parameters:
1 Growth model (1=Modified Eppley, 2=Q10)
4.0000 Max light utilisation coefficient (mg C (mg Chl)-1 d-1 (W m-2)-1)
3.5000 Reference respiration rate (mg C (mg Chl)-1 d-1)
15.0000 Reference temperature for respiration rate (deg C)
1.0000 Q10 exponent for respiration
0.0300 Chl:carbon (mg Chl (mg C)-1)
0.0000 Near-bed seed stock of phytoplankton (mg C m-3)
0.0120 Pigment absorption cross-section (m2 (mg Chl)-1)
2.0000 Maximum nitrate uptake rate (mmol (mg Chl)-1 d-1)
1.0000 Maximum cell nutrient quota (mmol N (mg Chl)-1)
0.2000 Subsistence cell nutrient quota (mmol N (mg Chl)-1)
0.3000 Nitrate uptake half-saturation concentration (mmol m-3)
0.0000 Swimming speed (m d-1)
0.0000 Sinking speed (m d-1)
0.1200 Minimum grazing impact (d-1)
0.0000 Amplitude of seasonal grazing impact (d-1)
180 Year day on which maximum grazing impact is reached
0.1000 Biomass threshold for grazing (mg Chl m-3)

Dissolved Oxygen parameters:
1 Air-sea flux method (1=Nightingale, 2=Wanninkhof)
0 Woolf & Thorpe bubble parameterisation (1=yes, 0=no)
1.4150 Remineralisation Oxygen:Carbon (mol per mol)
9.3750 Remineralisation Oxygen:Nitrogen (mol per mol)
5.0000 benthic oxygen demand (mmol m-2 day-1)

Detritus parameters:
-1.000 slow detritus sinking speed (m day-1)
-200.000 fast detritus sinking speed (m day-1)
0.100 normalised slow detrital remineralisation rate for N (day-1)
0.100 normalised slow detrital remineralisation rate for C (day-1)
0.100 normalised fast detrital remineralisation rate for N (day-1)
0.100 normalised fast detrital remineralisation rate for C (day-1)
0.500 Proportion of grazed organic matter into detritus (0.0-1.0)
0.100 Proportion of detritus that sinks fast (0.0-1.0)

----End of initialisation data file----

Appendix 3. S2P3 initialisation file for model parameters for Site 13 (Offshore stratified region) in 2022.

Initialisation and driving parameters for S2P3 (Shelf Sea Physics and Primary Production) with dissolved oxygen model
In: Simpson & Sharples, Introduction to the Physical and Biological Oceanography of Shelf Seas Cambridge University Press, 2012.

Physics parameters:
63.00 Total depth (m)
30 Number of depth cells
2.100 Depth cell thickness (m)
12.50 Time step (s)
54.90 Latitude (degrees, positive north)
0.00300 Bottom quadratic drag coefficient
0.100000 Maximum diffusivity and viscosity (m2 s-1)
0.000010 Background viscosity (m2 s-1)
0.000010 Background diffusivity (m2 s-1)
9.09 Initial water temperature (deg C)
0.100 Heat vertical attenuation (m-1)
0.01200 Chl effect on heat attenuation (m2 (mg Chl)-1)
0.00 Climate air temperature offset (deg C)

Light and nutrient resources:
0.120 Attenuation coefficient for PAR (m-1)
0.45 PAR as fraction of incident radiation
4.20 Initial winter nitrate (mmol m-3)
30.00 Maximum nitrate restoration rate (mmol m-2 d-1)

Tidal parameters:
M2 S2 N2 O1 K1
0.212 0.068 0.041 0.018 0.018 u amplitude (m s-1)
1.807 2.570 78.210 0.000 0.000 u phase (radians)
0.325 0.112 0.068 0.021 0.028 v amplitude (m s-1)
-1.750 -1.750 -126.320 0.000 0.000 v phase (radians)

-1.011 -1.253 2.103 0.867 1.008 tidal ellipse orientation (radians)
0.191 0.521 0.145 0.000 0.000 tidal ellipse polarisation
0.381 0.117 0.078 0.028 0.033 tidal ellipse semi-major axis (m s-1)

Meteorlogical data:
2 Meteorology file type (1=model default, 2=user supplied)
https://doi.org/10.6084/m9.figshare.23686542.v2 user meteorology data file

Biology parameters:
1 Growth model (1=Modified Eppley, 2=Q10)
4.0000 Max light utilisation coefficient (mg C (mg Chl)-1 d-1 (W m-2)-1)
3.5000 Reference respiration rate (mg C (mg Chl)-1 d-1)
15.0000 Reference temperature for respiration rate (deg C)
1.0000 Q10 exponent for respiration
0.0300 Chl:carbon (mg Chl (mg C)-1)

0.0000 Near-bed seed stock of phytoplankton (mg C m-3)
0.0120 Pigment absorption cross-section (m2 (mg Chl)-1)
2.0000 Maximum nitrate uptake rate (mmol (mg Chl)-1 d-1)
1.0000 Maximum cell nutrient quota (mmol N (mg Chl)-1)
0.2000 Subsistence cell nutrient quota (mmol N (mg Chl)-1)
0.3000 Nitrate uptake half-saturation concentration (mmol m-3)
0.0000 Swimming speed (m d-1)
0.0000 Sinking speed (m d-1)
0.1200 Minimum grazing impact (d-1)
0.0000 Amplitude of seasonal grazing impact (d-1)
180 Year day on which maximum grazing impact is reached
0.1000 Biomass threshold for grazing (mg Chl m-3)

Dissolved Oxygen parameters:
1 Air-sea flux method (1=Nightingale, 2=Wanninkhof)
0 Woolf & Thorpe bubble parameterisation (1=yes, 0=no)
1.4150 Remineralisation Oxygen:Carbon (mol per mol)
9.3750 Remineralisation Oxygen:Nitrogen (mol per mol)
5.0000 benthic oxygen demand (mmol m-2 day-1)

Detritus parameters:
-1.000 slow detritus sinking speed (m day-1)
-200.000 fast detritus sinking speed (m day-1)
0.100 normalised slow detrital remineralisation rate for N (day-1)
0.100 normalised slow detrital remineralisation rate for C (day-1)
0.100 normalised fast detrital remineralisation rate for N (day-1)
0.100 normalised fast detrital remineralisation rate for C (day-1)
0.500 Proportion of grazed organic matter into detritus (0.0-1.0)
0.100 Proportion of detritus that sinks fast (0.0-1.0)

----End of initialisation data file----

Appendix 4. Field input values for the Simple excel depth-irradiance primary production model for Station J6 and 13 in the North Sea.

Excel spreadsheet can be found on figshare from the following link:

https://doi.org/10.6084/m9.figshare.23686413.v2

Appendix 5. S2P3 meteorological input dataset for station J6 and 13 in the North Sea

Excel spreadsheet can be found on figshare from the following link:

https://doi.org/10.6084/m9.figshare.23686542.v2

Appendix 6. Data source table for all data gathered and used for this project

Data	Source	Download
Chlorophyll concentrations	Copernicus Marine Products	https://doi.org/10.48670/moi-00284
Temp, sal	Copernicus Marine Products	https://doi.org/10.48670/moi-00054
SPM	Copernicus Marine Products	https://doi.org/10.48670/moi-00278
SST	Copernicus Marine Products	https://doi.org/10.48670/moi-00165
MLD	Copernicus Marine Products	https://doi.org/10.48670/moi-00059
Tidal data	Dr Simon Waldman	Dr Simon Waldman sorted and downloaded tidal data for corresponding sites
Dowsing & Tyne/Tees SmartBuoy	CEFAS data hub	http://data.cefas.co.uk/#/View/3051
Scarborough, Whitby, Hornsea SmartBuoy	NATIONAL NETWORK OF REGIONAL COASTAL MONITORING PROGRAMMES	National Coastal Monitoring - Scarborough
Photosynthetically Available Radiation, R. Frouin	NASA Earth data 'Giovanni'	https://giovanni.gsfc.nasa.gov/giovanni/#service=ArAvTs&starttime=2022-01-01T00:00:00Z&endtime=2022-12-31T23:59:59Z&bbox=-0.033,53.9326,0.2802,54.2072&data=MODISA_L3m_PAR_Mo_4km_R2022_0_par&dataKeyword=Surface%20PAR&portal=GIOVANNI&format=json
Bathymetry	GEBCO	GEBCO - The General Bathymetric Chart of the Oceans
Metrological data	ECMYF (ERA5)	ECMWF Reanalysis v5 | ECMWF
Nutrients	Environment Agency	https://environment.data.gov.uk/water-quality/view/landing
Additional In situ chlorophyll	Environment Agency	https://environment.data.gov.uk/water-quality/view/landing